# Optical Changes during Normal Emmetropization, Lens-induced Myopia and its Recovery in the Young Chick Eye

by

Zheng Shao

A thesis
presented to the University of Waterloo
in fulfillment of the
thesis requirement for the degree of
Master of Science
in
Physics and Vision Science

Waterloo, Ontario, Canada, 2015

# AUTHOR'S DECLARATION

This thesis consists of material all of which I authored or co-authored: see Statement of Contributions included in the thesis. This is a true copy of the thesis, including any required final revisions, as accepted by my examiners.

I understand that my thesis may be made electronically available to the public.

## Statement of Contributions

This thesis has been written in a manuscript format. I would like to acknowledge the names of my co-authors who contributed to the research described in this thesis, these include:

- Kaitlin Bunghardt,
- Marsha L Kisilak,
- Dr. Elizabeth L. Irving, and
- Dr. Melanie CW Campbell.

Please reference the beginning of each Chapter for details for contributions of authors.

# Abstract

In human eyes, the at-birth hyperopoic defocus gradually decreases to mild hyperopia or emmetropia at around age 6. Studies on refractive development suggest somewhat complex mechanisms at work between eye power and length. Myopia occurs as a result of failure of normal emmetroipzation. Myopia is linked with various ocular pathologies and is now considered an independent risk factor of a range of ocular diseases. Therefore, myopia research is essential. The substantially increasing prevalence of myopia has particularly attracted researchers' attention. Any improvement in the understanding of the mechanisms of normal emmeropization and myopia development has the potential to introduce interventions that can limit or prevent myopia incidence and/or progression.

The eye power calculation presented is simpler than other approaches and provides an accurate power variation during normal emmetropization without the need for *ex vivo* measurements. Eye power calculation during normal growth showed a decrease in eye power and that the small difference between the rate of change in eye power and that of dioptric eye length, gives a decrease in MOR. When we modify the eye power calculation with one additional assumption, it can to be applied to myopic eyes. During emmetropization to hyperopoic defocus (LIM) and its recovery, eye power calculations based on different additional assumptions confirm a change in the optics, either in the positions of cardinal points or in the focal length, depending on the assumptions used. Changes in curvatures of the ocular surfaces remain to be assessed.

Emmetropization is an active mechanism; it appears to be driven by values of angular blur due to defocus which are above the level of the cone photoreceptor resolution during emmetropization. Angular blur reaches a level similar to cone spacing at the completion of emmetropization. Rates of change in optical axial length (OAL), corneal radius and the lens power are proportional to angular

blur, causing blur to reduce significantly. Angular blur varies linearly with MOR and its rate of change. After emmetropization, the constant angular blur and slightly increasing linear blur suggest that eye growth might be relatively uniform. The links between rates of change in OAL, corneal radius and the lens power during and after emmetropizaton may be related to a common signaling molecule or via passive mechanisms.

During LIM and recovery from it, VCD is a main contributor to changes in mean ocular refraction. However, the relative change in the front of the eye (represented by anterior cornea to back lens distance) is proportional to the relative change in OAL and is important to overall OAL changes compared to the control eye.

The change in eye power in relation to the change in eye length is important to normal emmetropization. The optics also changes during LIM and the recovery from it. In addition, in normal growth, a direct link between the changes in ocular parameters and retinal blur is shown. Since many of these results are consistent with findings during emmetropization in children, the link between the changes in ocular parameters and retinal blur may be important to understanding normal development and development of myopia in human.

# Acknowledgements

It has been my good fortune to have the advice and guidance of many talented people. I would like to take this opportunity to express my utmost gratitude to:

My incredible supervisor, Dr. Melanie Campbell, whose patience, intelligence, diligence and erudition profoundly had an everlasting impact on me both academically and personally.

My kindhearted committee members, Dr. Elizabeth Irving, whose earnest and sagacity enlightened my thoughts, and Dr. Donna Strickland, whose humorous and cheerful spirits softened my impressions on authority figures to foster better communication skills.

My excellent colleagues, Ian Andrews, Kaitlin Bunghardt, Si Chen, Laura Emptage, Heqing Huang, Marsha Kisilak, Reza Khanbabaie, Rachel Redekop, Namrata Shah, Olivia Stanley, and Kevin Tuck (alphabetically ordered by last name), whose friendliness and assistance eased my nerves and sailed along with this project.

My easygoing English tutors, Navjot Rai and Zara Wong, and friend, Fang Liu, whose encouragement and persuasion urged me on to knock at the door to this journey, and my grammatical-stickler ESL instructor, Mrs. Pat Skinner, whose maddening attention to writing drove me to finally learn to punctuate prose.

My elegant friend, Carol Cameron, and her little buddy, Huey, whose selfless time and care sheltered my loneliness and longing for a nearby family.

My invincible partner, Yexiang Zhang, whose persistence and carefulness prompted me to meld intellectual prowess with determination and inspiration.

Last but not least, those people who established and regulated the following awards/scholarships, International Masters Student Award, Marie Curie Graduate Student Award, Graduate Research Studentship, Science Graduate Experience Award, enabled me to stay; Dr. Shoufa Lin and associates, whose efforts of initializing the China 2+2 program that brought me here to Canada; and my fellow classmates, whose companionship motivated me throughout the past years.

*This is the end of a two-year journey but the beginnings of an even more fruitful one.*

# Dedication

"Faith is the bird that feels the light and sings when the dawn is still dark."

— Rabindranath Tagore

*I lovingly dedicate this thesis to my mom,*

*for finding me the light,*

*whenever it was far away,*

*and*

*to my family,*

*for reminding me the lyrics,*

*no matter what had happened.*

# Table of Contents

# List of Figures

# List of Tables

# Chapter 1

# Introduction

## 1.1 Emmetropization and Myopia

Myopia occurs as a result of failure of normal emmetropization, a regulatory process that guides an eye to balance its axial length and power. Massive attention has been put into myopia research for decades because of the substantially increasing prevalence of myopia and the links between myopia and ocular pathologies, such as glaucoma, retinal detachment,[1] and age-related macular degeneration (AMD).[2] Any improvement in the understanding of the mechanisms which cause a breakdown of normal emmetropization and resulting myopia development has potential benefits of introducing interventions that can limit or prevent myopia incidence and/or progression.[3]

### 1.1.1 Optical Changes during Normal Emmetrpoization

An emmetropic eye (Figure 1-1a) enables a clear image to be produced at the photoreceptor layer. In this case, the eye is considered to have no refractive error. Otherwise, an eye will have a mean ocular refraction (MOR) and to be either hyperopic (Figure 1-1b) or myopic (Figure 1-1c), resulting in an image plane either behind or in front of the photoreceptor layer. Humans are born with a broad variation of defocus (refractive error is normally distributed in the range of -12 Diopters (D) to +12 D[4] with an approximate average hyperopia of 1.00 D to 2.50 D with a standard deviation (SD) of 1.50 D to 2.50 D; reviewed in a book edited by Spaide and colleagues)[2]. During the first year of postnatal development, as normal emmetropization proceeds, axial length increases significantly, and both the cornea and the crystalline lens lose powers by

flattening. Changes in powers and axial length are coordinated to achieve emmetropia.[5] In human eyes, a substantial reduction of hyperopia occurs between birth and the third year of life.[6] After the age of three, there are still increases in axial length and the anterior chamber depth, with a significant reduction in the crystalline lens power, but there is limited change in the corneal power.[2, 7] Emmetropization is finished at about age six for humans, as originally shown by Hirsch and Weymouth in 1947.[8, 9] Additionally, the refractive error distribution in the adult eye has a much narrower distribution than the infant with a peak located close to emmetropoia, having a SD about ±1.00 D.[10] The fact that all the components of refractions (cornea, anterior chamber, and crystalline lens) are normally distributed but the refractive error is concentrated in the neighborhood of emmetropia, giving a leptokurtotic shape, suggests the existence of an active mechanism (emmetropization) controlling the development of the eye and minimizing its refractive state.[4]

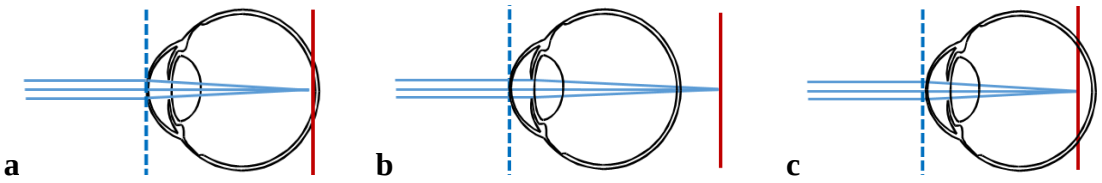


**Figure 1-1 Refraction of rays from a distant axial object point for (a) emmetropic eye, (b) hyperopic eye and (c) myopic eye.**

Linear retinal blur occurs at the photoreceptor layer for hyperopic or myopic eyes because the image is focused behind or in front of the photoreceptor layer, having positive (b) or negative (c) mean spherical refractive error (mean ocular refraction, MOR).

Emmetropization might be the result of both passive and active processes (reviewed by Brown and colleagues).[11] Passive mechanisms could include a proportional enlargement of the eye, causing a reduction in the power of the dioptric system in proportion to the increasing axial length which would cause decreasing MOR. However, this proportional expansion gives an MOR reduction which is not sufficient enough to explain the rapid decrease in the refractive error seen in human and animal eyes during normal growth.[5, 12] Some people suggest that the growth in the eye might involve different parts growing at different rates.[9] Thus, an active mechanism must involve a fine-tuning of eye power and length controlled by the feedback of the image formation on retina with the consequent coincidence of the focal point of the eye and the photoreceptor layer. An active contribution can be hypothesized given that the rate of decrease of refractive error in infants is proportional to the magnitude of the initial refractive error within a certain range,[10, 13] suggesting that the change toward emmetropia may be visually guided.[14] Animal experiments (including those performed on the chick model) have confirmed that emmetropization is an active process regulated by the defocus of the retinal image (see Section 1.1.3 below).

### 1.1.2 Myopia Development in Human Eyes

Beyond the initial emmetropization (birth to age 6), the ocular components of the human eye continue to grow, and the eye usually maintains emmetropia (except when a condition like cataract which effects the components). Myopia results because of a breakdown in the emmetropization process. It usually develops over the school years and presents low to moderate myopic refractive errors with a magnitude up to 6 D without associated ocular pathology. This type of myopia typically develops when the eye has

completed the infantile, rapid-growth stage and has reached approximately 95% of its normal adult axial length,[2] resulting in a longer axial length than the focal length of the eye[2] and a lower power of the crystalline lens.[7] In comparison with average emmetropic eyes, the vitreous chamber shows the largest change.

Several environmental risk factors for myopia have been discussed. "Nature versus nurture" was first coined by Galton in 1875.[15] The risk of developing myopia is greater when both parents are myopic than when one parent is myopia.[16-18] In turn if one parent is myopic, the risk is higher than when neither parent is myopia.[18, 19] Near work was proposed to be associated with myopia in several cross-sectional studies;[19-21] however, the results are inconsistent in other cross-sectional studies[22, 23] and longitudinal studies.[17, 21] Interest has shifted to the association between time outdoors (lifestyle, light exposure) and myopia, which is well documented in both cross-sectional and longitudinal studies (reviewed by the book edited by Spaide and colleagues)[2]. Recent studies confirm that time spend outdoors was negatively associated with myopia incidence in both younger and older school children in Australian,[24] primary school children in Beijing[25] and Taiwan,[26] even in young adults.[27] Considerable interest is now focused on the moderate protective effects of time outdoors, with a plausible explanation that bright lighting condition outdoors stimulate the release of dopamine from the retina, which then acts as an inhibitor of axial elongation.[28, 29]

As longer axial length is commonly observed in myopic eyes, axial length variation has been examined to monitor the development of myopia. However, axial length varies with height,[30] and eyes with longer axial length can still be emmetropic if eye power is lower than average. Alternatively, it has been suggested that the ratio of axial length to cornea

radius of curvature (AL/CR) is a better index[31-33] to predict the refractive state rather than axial length variation only. The AL/CR ratio has no gender difference and gets larger in myopic eyes, with a mean of 3.18 at baseline in the COMET study of myopic children,[34] compared to emmetropic eyes,[33] with a value of about 3.00.[35] More importantly, around age 6, similar to the narrow distribution of the refractive error, the distribution of the AL/CR ratio is also narrow, suggesting that an important part of the changes up to this age involve matching the axial length of the eye to the corneal power. However, the underlying distribution of AL and CR remains normal.[34] Also, research has been extended to study the crystalline lens development during myopia. Significant lens thinning,[7, 36, 37] and lower lens power[7] has been reported within myopic eyes. Understanding the underlying biological mechanisms of eye growth and refractive error development would be helpful.

### 1.1.3 Emmetropization and Myopia Studies in the Chick Model

Several animal models have been developed to study the mechanisms underlying emmetropization and refractive error development. The understanding that emmetroipzation is an active, visually-guided mechanism[38] which compensates the innate refractive errors was established with the help of the chick model.[39-45] The chick is ideal because of its affordability, rapid growth rate and its ability to survive without a mother.[46, 47]

Studies of the chick model have supported the idea that the visual environment imposes a powerful influence on refractive errors through controlling eye growth during the post hatching developmental period. Research on myopia in chicks involves the induction of myopia through form deprivation (form deprivation myopia, FDM; an open loop

condition) or through negative defocusing lenses (lens-induced myopia, LIM; a closed loop condition; Figure 1-2 and Figure 1-3).

**Figure 1-2 A goggled chick.**

The right eye of the chick is goggled with a lens, and the left eye of the chick is the control eye.

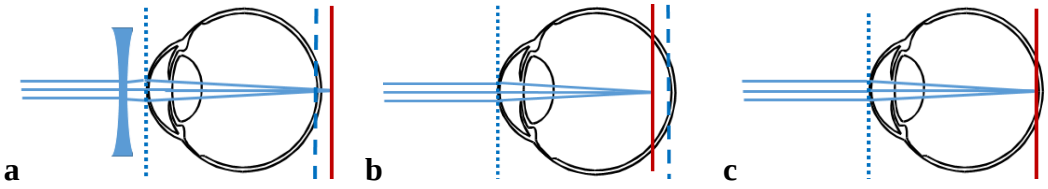


**Figure 1-3 (a) A negative lens is put in front of a normal eye causing the focus to move behind the eye. (b) The eye then grows to better match the retinal position to the focal point. Lens-induced myopia results on lens removal. (c) Recovery from lens induction of myopia though changes in power and eye length.**

The red plane indicates where a distant object is focused; and the blue dashed plane is the photoreceptor layer. In (c), these two planes overlap because the eye recovers from the induced myopia and becomes emmetropic.

#### 1.1.3.1 Experimental Myopia

Axial length elongation is observed in both cases,[48] with similarities at the molecular and cellular levels in terms of some retinal expression transcripts[49] and dopamine release.[50] However, it remains a controversial topic as these similarities may have different underlying mechanisms.[48, 49] During form deprivation myopia, images on the retina are obscured by a diffuser or lid suture, and, as no image can be brought into focus by the excessive ocular elongation which results, there is no definite endpoint. When the diffuser is removed, the eye is myopic, but it can return to normal given time. Manipulation of the early refractive development of the chick eye through a positive or negative defocusing lens provides a closed loop condition. This allows the eye to neutralize the refractive error in order to compensate the defocus. If a negative lens is used, hyperopic defocus results, and the eye is myopic after goggle removal (Figure 1-3b).[42, 51-53] Given sufficient time, the magnitude of myopic defocus in the chick eye is equal to the power of the inducing lens.[51] Remarkably, it has shown that chicks are able to compensate for a large range of refractive errors in response to defocusing lenses to as much as -30 D[51, 52] when application of lenses occurred at an earlier age.[54] Conversely, placing a positive defocusing lens onto the chick eye will cause myopic defocus, resulting in hyperopia through a decrease in the rate of axial elongation from that seen in normal growth.[55, 56] However, the eye responds faster to the myopic defocus (positive lenses) than to hyperopic defocus (negative lenses).[57]

Notably, chick eyes are able to recover from induced hyperopia by positive lenses[57] and induced myopia by negative lenses[57] or diffusers.[58] However, the rates of recovery differ from the rates of induction, and the mechanisms are thought to differ.[2, 59] Remarkably,

after disconnecting the eye from the brain (for example, by optic nerve section) the chick eye can still develop form-deprivation myopia[60] or compensate for positive or negative lenses.[57] Recovery from form-deprivation myopia occurs with less accuracy,[61] and recovery from positive and negative lenses is shifted to a new end-point.[57]

#### 1.1.3.2 Possible Mechanism of Experimental Myopia

Unlike in the human case, it is widely believed that excessive axial elongation, through changes in the vitreous chamber depth (posterior lens to anterior retina), fully explains the refractive changes when LIM is established[54, 62, 63] and following the recovery from such modification[64] in animal experiments. Control of eye growth is considered to primarily occur within the eye, driven by the defocus, involving an interaction of molecules between the retina and sclera (retinoic acid and the levels of mRNA; or increased expression of gene ZENK).[65] As well as eye length changes that occur during LIM and its recovery, the vitreous chamber depth is also modulated, by major changes in the thickness of the choroid, swelling in response to myopic defocus and thinning in response to hyperopic defocus in both chicks[66] and humans.[57, 67]

### 1.1.4 Motivations

Much attention has been given to the examination of eye length growth at the endpoint of emmetropization. Considering that the MOR is caused by the mismatch between the focal point of the eye's optics and the photoreceptor position (Figure 1-4), it is likely that the optics in the eye (cornea and/or crystalline lens) change during normal emmetropization and development of lens induction of myopia and its recovery. Cornea radius can be measured *in vivo* using keratometry, and anterior chamber depth (ACD, anterior cornea to

anterior lens) and lens thickness (LT) may be determined from biometry. However, accuracies are limited given the highly curved surfaces in the small chick eye. Furthermore, investigations of the contribution of the optical components are limited because studies of crystalline lens require complex calculation using the Gullstrand thick lens equation,[4] where lens radii and refractive indices need to be obtained *ex vivo*,[43, 45, 68] since lens radii and refractive indices are needed. Therefore, observation of longitudinal changes within the optics is not possible. Also, the optical power is affected by every inaccuracy or uncertainty during dimension and curvature measurements, and cross-sectional data are affected by individual variation.

Within experimental uncertainty, literature data suggests that the power of the crystalline lens in chicks during early growth remains unchanged with age,[43, 69] but there are also reports of changes in the range of accommodation of the lens.[70] In humans, decrease in the power of the crystalline lens has been reported.[7, 13, 71-73] Recently, our lab has shown that shorter-term diurnal changes in MOR in chicks result from changes in both optical axial length (OAL; anterior cornea to anterior retina) and eye power during normal growth.[40] Also, it has been shown that, whereas the difference in OAL between treated and control eyes decreases by 50% in the second week compared to the difference during first week, the difference in corneal radius between eyes increases,[74] hence supporting the hypothesis that power changes during myopia development.

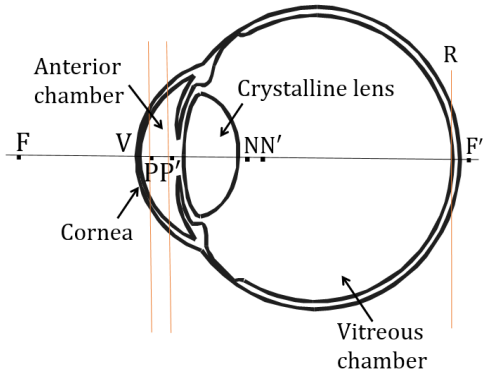


**Figure 1-4 A schematic human eye showing ocular components and relative positions of optical parameters (diagram originally created by Kisilak).**

V is the vertex of the eye. F, F′ are focal points; P, P′ are principal points; N, N′ are nodal points. R is the photoreceptor layer, located within the retina. Axial length (AL) is defined as the distance from the vertex to the photoreceptor layer. 1st focal length is the distance from P to F, which is equal to the posterior nodal distance (from N′ to F′); 2nd focal length is defined as the distance from P′ to F′.

Here we will show that eye power can be inferred from MOR and OAL. By definition, the dioptric distance of the eye's far point (MOR; in the unit of D) is the difference between the image vergence needed for sharp retinal imagery and the power of the eye (in the unit of D or $m^{-1}$)[4]

$$\mathrm{MOR} = \mathrm{K}' - \mathrm{F_e}\,. \qquad 1\text{-}1$$

The image vergence, K′, is the inverse of the optical length (k′; from the second principal plane, P′, to the photoreceptor layer, R; Figure 1-4) multiplied by the refractive index of the vitreous chamber, n′,[4]

$$\mathrm{K}' = \frac{\mathrm{n}'}{\mathrm{k}'}\,. \qquad 1\text{-}2$$

I will show that the k′ can be derived from an *in vivo* OAL measurement, a method that can be potentially applied to study the longitudinal relative eye power changes compared to changes in length in normal growth and during induction of and recovery from myopia.

The growth of components of the eye is influenced by the visual experience; in terms of retinal processing, retinal blur due to MOR is believed to be important in the control of eye growth. Absolute changes in retinal angular blur (EB, equivalent blur)[42] or linear retinal blur (LRB), geometrical approximations of the change in the angular and linear half-widths of the point spread function, PSF,[12] can be easily calculated as a function of age or lens treatment from the optical length, focal length and pupil size of the eye.[12, 42] Possible mechanisms of growth modulation by retinal blur can then be studied.

Therefore, **I wish to study how eye power and eye length are related (using longitudinal data of MOR and OAL) and regulated by retinal blur due to defocus during normal emmetropization; and how they change differently during lens induction of myopia (with negative lenses, LIM) and its recovery. I am also interested in ocular changes which contribute to changes in eye power.**

### 1.2 Thesis overview

This first chapter provides the introduction and the motivation of the study of emmetropization and myopia using the chick model. Chapter 2 describes the techniques being used in this thesis and relating to the construction of the chick schematic eye model. Chapters 3, 4, and 5 were written as independent manuscripts. Chapter 3 discusses the possibility of using a proposed mathematical calculation of eye power and retinal

blurs to study the changes in eye power during normal growth, with results also pertaining to the end point of emmetropization and that emmetropization appears to be driven by the reduction of angular blur due to defocus. Chapter 4 discusses the contributions of powers (including eye power, corneal power and lens power) to the reductions in retinal blurs in more detail and shows a strong connection to the active mechanism of emmetropization during normal growth. Chapter 5 presents the dimensional changes (including OAL, cornea to back lens distance, LT, and VCD) during lens-induced myopia and its recovery and discusses the possible change in eye power based on modified eye power calculations. Assumptions in the calculations are based in part on the dimensional measurements. Chapter 6 discusses the use of an optical technique (optical coherence tomography) to measure chick eye dimensions more accurately and compares the results with ultrasound measurements. Chapter 7 presents general discussions and conclusions. Supplemental discussion and figures are provided through Appendices A to B.

# Chapter 2

# Review of Techniques

## 2.1 Introduction

Emmetropization is the process of reducing the refractive error at birth to achieve emmetropia, which is characterized by a match between the focal length of the optics and the optical length of the eye. Assessing biometry data (about structural changes) of the ocular components during development of the normal eye or the eye undergoing treatments leading to refractive error is critical in terms of understanding how emmetropization is achieved or breaks down in the development of myopia. **This chapter reviews the commonly used techniques for measuring refractive errors and dimensions (also being used in other chapters of this thesis), focusing on the selective *in vivo* methods for longitudinal studies within small chick eyes.**

Schematic eye models describe the geometrical and structural properties of the ocular components, which intrinsically reflect the optical quality of the eye. Schematic eye models of the chick eye (see example, Figure 2-1) has been developed for young (between days 0 to 15)[39, 43] and for 30 day-old[45] chicks, together with optical parameters reported at other ages.[42, 45, 53, 60, 75-81] Image properties can be calculated through ray-tracing. Fundamental optical characteristics can be studied to determine the relative importance of each component to the overall optical quality. Furthermore, extensive predictions can be made to postulate the potential contribution of unknown factors (for example, the distribution of refractive index in the lens). Constructing optical models of the chick eye requires measurement of the refractive state, axial dimensions, curvatures,

and refractive indices of the ocular media (cornea, aqueous and vitreous, also the crystalline lens if possible). Various techniques are used for measuring or inferring different parameters.

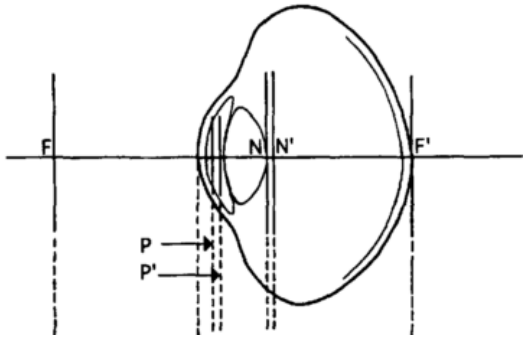


**Figure 2-1 A sketch for the paraxial chick schematic eye model on day 0 (adapted from Irving and colleagues with permission).**[43]

Constructed based on measurements of radii of curvatures, distances between surfaces, and refractive indices. An equivalent refractive index of the crystalline lens, defined as the homogeneous index of the lens with the same external geometry and focal length as the crystalline lens, was used.[82]

### 2.1.1 *In vivo* Measurements

#### 2.1.1.1 Refractive Error, Corneal Curvature and Dimensions

Refractive error (mean ocular refraction, MOR) and dimensions can be measured *in vivo*. Refractive state is measured by retinoscopy (see Section 2.2.1) or Hartmann-Shack (H-S) wavefront sensing technique (see Section 2.2.2). Anterior corneal curvature is most commonly measured by keratometry[39, 43, 45, 58, 60, 78, 80] with a precision of 0.01 mm[43] to 0.02 mm,[60] and the cornea over the measured region is considered spherical. Corneal

thickness, anterior chamber depth, lens thickness, vitreous chamber depth, and optical axial length (OAL; anterior cornea to anterior retina) (see Figure 1-4 and figure caption for Figure 3-1) are measured with ultrasonography. Additional aids, such as anesthesia and lid retractors, can also be helpful. However, they have side effects on the animal and the dioptric properties[39, 83] so as far as possible we avoid them.

#### 2.1.1.2 Experimental Conditions

Cycloplegia (which paralyses accommodation) with[58, 60, 61] or without anesthesia[43, 45, 51, 53] can be used during *in vivo* measurements, sometimes with lid retractors[39] to keep the eye open during measurements with anesthesia. It has been pointed out that cycloplegic refractions are slightly more hyperopic (on average 1.3 D more hyperopic).[45] However, non-cycloplegic refraction is considered advantageous in that natural accommodation tonus, a possibly important factor for normal eye growth, is conserved.[53] Some scientists make refractive measurements without any additional aids[40, 42, 52, 77] and studies have shown that growth rate[39] and optical qualities[83] are affected after repeated anesthetic use and that lid retractors change the optics.[83]

In addition, it has been shown that both MOR and OAL have significant diurnal variations with a period of around 24 hours and 12 hours, respectively,[40, 84] so measurements should be taken approximately around the same time on each experimental day to avoid the influence of diurnal variation.

### 2.1.2 *Ex vivo* Measurements

#### 2.1.2.1 Radii of Curvatures and Dimensions

Anterior[43, 45] and posterior[39, 43] radii of curvature of the crystalline lens are often measured *ex vivo* within frozen sections, based on the best circular fits for the paraxial region. They can also be measured *in vivo* using phakometry. Corneal thickness, anterior chamber depth, lens thickness, vitreous chamber depth, and axial length can also be measured in frozen sections[43, 45, 63] or by ultrasonography (ultrasound biomicroscopy UBM[75] or A-scan ultrasound)[43, 58] either *in vivo*[43] or within excised eyes.[43, 58, 75] In this thesis, the radii of curvatures and dimensional data, either measured *in vivo* using ultrasound or OCT; or within frozen sections or with ultrasound *ex vivo* from the literature are used.[43, 45]

#### 2.1.2.2 Refractive Indices

Refractive indices are currently measured *ex vivo*. Refractive indices of cornea, aqueous and vitreous are measured using an Abbe refractometer within excised eyes.[43, 45] These three refractive indices are found to be stable throughout the life of a chicken.[45] The refractive index of the cornea has been measured as 1.369[43, 68] or 1.373[45], which is smaller than the mean refractive index of the human cornea (1.376).[4] Refractive indices of the aqueous and vitreous chamber are consistently found to be 1.335.[43, 45]

However, the crystalline lens exhibits a gradient refractive index,[85] and the complex index profile is difficult to measure or interpret. In the construction of schematic eye model, the equivalent refractive index of the lens is usually calculated by matching the focal length (measured optically)[69] of the excised lenses with the measured lenticular radii and lens thickness. Alternatively, the gradient index profile can be characterized by

a large number of iso-indicial shells with the highest measured index of 1.3947 in the lens core and a lower measured index of 1.3738 in the periphery measured with both Abbe and Pulfrich refractometers.[68] In optical coherence tomography, another index, termed the average refractive index of the lens, is used go from the optical path length of light shining through the lens to the physical thickness and surface curvatures. It can also be determined by dividing the measured optical path length in the center of the lens by the actual central lens thickness from the shadow photography images of the same lens.[86]

#### 2.1.2.3 Advantages and Disadvantages of *ex vivo* Measurements

*Ex vivo* measurements give better ocular structural information under specific experimental manipulations for comparisons because the measurement conditions are more stable and the influence of repeated cycloplegia, anethesia and lid retractors can be avoided. However, because animals are sacrificed, it is impossible to include a large sample size or to make longitudinal measurements, to closely observe the normal ocular development or consecutive changes after applying experimental manipulations. Therefore, longitudinal *in vivo* studies are recommended.

## 2.2 Refractive Error Measurements

Eyes with refractive errors are divided into two main categories: spherical ametropia and astigmatism.[4] If only spherical ametropia is present, the eye's refractive system can be approximated as symmetrical about is optical axis, with all rays intersecting at a single point in front of or behind the retinal plane of the system. Thus, myopia or hyperopia occurs. More generally, negative or positive lenses with power equal to the spherical

equivalent refractive error (S-C/2, where S is the sphere and C is the cylinder correction needed)[4] can be used to move the focus plane (corresponding to the circle of lease confusion) onto the retina. Astigmatism is the result of rays from different meridians being focused at different locations because the power of the eye is asymmetric. Therefore, the rays of the light will pass through one of two planes (both containing the optical axis) through the eye such that the power in one meridian of the optics is minimum, with an angle $\theta$, range from $0°$ to $180°$, and maximum on the other (perpendicular to the maximal meridian); a point source will form 2 line foci. Between these two lines, there is a circular blur image known as the circle of least confusion. The power for the cylindrical lens is C, equal to the difference in power between the maximal and minimal meridians. The power of the sphere, S is the power of the maximum meridian.

The mean ocular refraction (MOR) is the spherical lens power placed at the principal plane of the eye which places the circle of least confusion on the retina. MOR can be calculated from spherical defocus and the absolute value of the cylinder.

$$\mathrm{MOR} = \mathrm{S} - \frac{\mathrm{C}}{2} \qquad 2\text{-}1$$

The refractive error can be measured by retinoscopy or a Hartmann-Shack (H-S) wavefront sensing system.

### 2.2.1 Retinoscopy

Retinoscopy measures the MOR with an accuracy of 0.7 D in the chick eye within two weeks of age[87] or 0.3 D at about four weeks of age.[58] Measurements are performed in scotopic room illumination. A white light is shone into the eyes close to the optical axis,

and the observer subjectively interprets the direction of the light reflex to be with, against, or neutral relative to movement of the source. The "with" motion, showed by a relatively clear, well-defined yellowish/orange moving reflex, means the eye is hyperopic. The "against" motion, interpreted by a vague, one-sided shadow moving across pupil in the opposite direction to the retinoscope, suggests the eye is myopia. Plus or minus lenses are then placed between the observer and the measured eye until a neutral reflex, characterized as a bright, stationary reflex that engulfs the eye, is determined. The correction is then adjusted for the observer's working distance.

When doing the measurement, with the parallel reflex band of the retinoscopy streak, the meridian with the minimal power is first identified. Then, along the perpendicular meridian (the maximal meridian), similar scoping is performed; the sphere power of the lens that makes the reflex motion neutral is S, and the angle is θ. The difference between the maximal and minimal power needed is the recorded cylinder power, C. The recorded refraction in negative cylinder form is then given as

$$\text{Prescription reads as } S - C \times \theta. \qquad 2\text{-}2$$

Therefore, MOR can be calculated from Eqn. 2-1.

### 2.2.2 Hartmann-Shack (H-S) Wavefront Sensing

Alternatively, refractive error can be measured objectively by a Hartmann-Shack (H-S) system in the chick[42] or human[88] eye. In our lab, a customized H-S system was built for measuring aberrations in the growing chick eye during normal growth and lens-induced myopia (LIM).[42] For chicks within first two weeks of age, this customized-designed H-S system is considered more accurate than the retinoscopy (0.7 D) with an accuracy of 0.5

D.[87] For the measurement a dimly lit environment is used for greater sensitivity and a larger pupil size.[87] In a H-S apparatus (Figure 2-2), a small laser beam (633 nm) is focused to a small disc on the retina and diffusely reflected back out, filling the pupil. Distorted by the optical components of the eye, the emerging wavefront is sampled and focused by a lenslet array, with the resulting image (consisting of one spot for each lenslet, see Figure 2-2) captured by a CCD camera. The spot displacements, Δx and Δy are proportional to the derivatives of the wavefront aberrations, $W(x, y)$:

$$\frac{\partial W(x,y)}{\partial x} = -\frac{\Delta x}{f} \text{ and } \frac{\partial W(x,y)}{\partial y} = -\frac{\Delta y}{f} \qquad 2\text{-}3$$

where f is the focal length of the lenslet array. The corresponding slope vector, **s** contains Δx- and Δy-shifts for each spot.

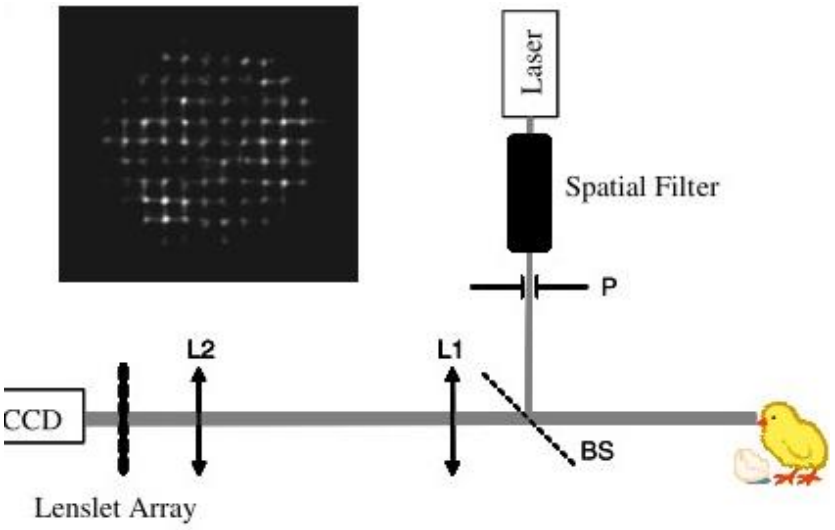


**Figure 2-2 Schematic of a customized Hartmann-Shack system the chick (adopted from Kisilak and colleagues).**[42]

L1 and L2 are lenses, BS is a beam splitter, and P is a pinhole.

The wavefront aberration, $W(x,y)$, is described by an orthogonal set of functions, called Zernike polynomials, Z, where each orthogonal term specifies a certain mode of aberrations,[89] all weighted by an optimal set of coefficients, $\vec{c}$. The polynomials are ordered by a double index scheme, consisting of a normalization factor, a radial-dependent component and an azimuthal-dependent component.[90] The optimal set of coefficients are from minimizing the root mean square of the difference between the estimated wavefront from the Zernike coefficients, $\mathbf{Zc}$, and the measured wavefront. To accomplish this minimization,[91]

$$\vec{c} = \begin{bmatrix} c_1 \\ c_2 \\ \vdots \\ c_n \end{bmatrix} = (DD^T)^{-1}D\vec{s} \qquad 2\text{-}4$$

where

$$D = \begin{bmatrix} \frac{\partial Z_1(x,y)_1}{\partial x_1} & \frac{\partial Z_1(x,y)_2}{\partial x_2} & \cdots & \frac{\partial Z_1(x,y)_m}{\partial x_m} & \frac{\partial Z_1(x,y)_1}{\partial y_1} & \cdots & \frac{\partial Z_1(x,y)_m}{\partial y_m} \\ \frac{\partial Z_2(x,y)_1}{\partial x_1} & \frac{\partial Z_2(x,y)_2}{\partial x_2} & \cdots & \frac{\partial Z_2(x,y)_m}{\partial x_m} & \frac{\partial Z_2(x,y)_1}{\partial y_1} & \cdots & \frac{\partial Z_2(x,y)_m}{\partial y_m} \\ \vdots & \vdots & \ddots & \vdots & \vdots & \ddots & \vdots \\ \frac{\partial Z_n(x,y)_1}{\partial x_1} & \frac{\partial Z_n(x,y)_2}{\partial x_2} & \cdots & \frac{\partial Z_n(x,y)_m}{\partial x_m} & \frac{\partial Z_n(x,y)_1}{\partial y_1} & \cdots & \frac{\partial Z_n(x,y)_m}{\partial y_m} \end{bmatrix} \qquad 2\text{-}5$$

and $D^T$ is the transpose matrix, and the order of Zernike terms in D indicates the order of the output of Zernike coefficients. The MOR is calculated from the defocus term ($Z_2^{-2} = Z_4$),[92]

$$\text{MOR} = \frac{-4\sqrt{3}Z_2^{-2}}{r^2} \qquad 2\text{-}6$$

where r is the radius of the entrance pupil in the eye. In this thesis, the aberrations were fit with 4th order Zernike polynomials, and measurements were averaged across frames for each bird on each day. Images, with larger pupils, corresponding to an unaccommodated state, were chosen. Because the aberrations change with pupil size,[88] in order to study underlying changes in the central optics which impact MOR, a constant pupil size is used across birds and ages during the experiment.

### 2.2.3 A Small Discussion of Retinoscopy and H-S technique

Retinoscopy and the H-S technique are considered interchangeable methods for measuring MOR in the chick eye with a 1 D offset,[42] possibly caused by a combination of chromatic aberration and the small eye artifact[93] during measurement of retinoscopy.

If we consider there is chromatic aberration in the eye, and that light reflects from the photoreceptor layer in the retina between the light used for retinoscopy (white centered at green) and the red light used in H-S measurement of refraction and that the second principal point is stationary with wavelength,[4] then

$$\mathrm{MOR_{red}} - \mathrm{MOR_{green}} = \left[\mathrm{K'_{red}} - \mathrm{K'_{green}}\right] - \Delta \mathrm{F_{e_{red-green}}} \qquad 2\text{-}7$$

$$= \left[\frac{\mathrm{n'_{red}}}{\mathrm{k'_{red}}} - \frac{\mathrm{n'_{green}}}{\mathrm{k'_{green}}}\right] - \Delta \mathrm{F_{e_{red-green}}}$$

where $\mathrm{n'_{red}}$ and $\mathrm{n'_{green}}$ are the refractive indices of the vitreous chamber depth at 500 nm and 650 nm; $\mathrm{K'_{red}}$ and $\mathrm{K'_{green}}$ are dioptric lengths, and $\mathrm{k'_{red}}$ and $\mathrm{k'_{green}}$, the optical lengths measured at 500 nm or 650 nm are equal; and $\Delta \mathrm{F_{e_{red-green}}}$ is the chromatic difference of the power, which is smaller than -3 D in the chick eye.[44] The difference in

MOR will be less than the chromatic difference of power. Thus due to chromatic aberration, a hyperopic shift of the H-S relative to retinoscopy would be expected.

The small eye artefact for white light which shifts the MOR more hyperopic than the actual refraction was originally postulated to arise because the reflection of retinoscopy light (centered at 550 nm, green light) occurs at the retinal/vitreous interface, in front of the photoreceptor layer a distance about 135 μm for mammals in front of the latter.[93] However, it is also known that red light reflects from deeper in the retina than green light, so that the artefact of retinoscopy for white light is expected to be reduced and potentially to be wavelength dependent.[4] The effect of the postulated position of the retinal reflection would introduce a myopic shift of the H-S refraction relative to the retinoscopy refraction, opposite in sign and likely smaller than he hyperopic shift due to chromatic aberration. Thus the small hyperopic shift of the H-S refraction relative to retinoscopy is expected.

### 2.3 *In vivo* Dimensional Measurements

Paraxial schematic eye models can indicate how changes in a single dimension, for example, eye length (without other concurrent changes) would change MOR. To elucidate mechanisms underlying normal emmetropization and myopia, monitoring dimensional changes during experimental myopia induction in various animal models is important. A-scan ultrasound is considered a gold standard for *in vivo* measurement. Small animal eyes create difficulties in accurately measuring individual optical components with precision. More recently, the possibility of using an optical method to measure the small eye has been explored.

### 2.3.1 A-scan Ultrasonography

Sound travels within solid or liquid materials in a wave pattern. In A-scan biometry, a parallel sound beam is emitted from the transducer probe at a frequency of between 10 and 30 MHz, and echoes bounce back into the probe by reflection from different interfaces. Sound waves travel at different velocities (faster through solids than through liquids) within media of different densities. In the eye, reflected beams can be detected using a 10 MHz probe at the aqueous/anterior lens surface, the posterior lens/vitreous surface, the vitreous/retinal surface and other surfaces posterior to this (see Figure A-1). Echoes received by the probe are converted by the biometer to signals above the baseline. The distance between two interfaces can then be determined by multiplying one half of the time difference ($\Delta t$) between echoes by the speed ($v$) of sound within the medium.

$$\text{Distance between two interfaces} = v \times \frac{\Delta t}{2}. \qquad 2\text{-}8$$

The resolution of ultrasound is characterized by the system's ability to differentiate two interfaces that lie in the close proximity. The greater the difference in refractive index of the two media at each interface, the stronger the echo is, thus the higher the signal. Higher frequencies give better resolution but less penetration (because they are absorbed more than lower frequencies). Misalignment will reduce the strength of the signal from the echo or cause missing signals, leading to unreliable measurements. Identification of misaligned A-scan diagrams is discussed in Appendix A.

During ultrasound measurement, either contact or immersion techniques can be used. In the contact mode, the probe is directly placed on the corneal vertex to let the sound beam travel along the optical axis, but corneal compression by the probe is likely,

especially in chick with a softer cornea. Alternatively, the immersion technique avoids contact with the cornea. The probe is immersed into a shell filled with saline solution or onto a water pad placed on the lids. By doing this, the probe and cornea are no longer in contact, thus anterior and posterior corneal spikes can be obtained. However, three different immersion instruments failed to give adequate peaks when used by us on alert chicks.

### 2.3.2 The Optical Approach

The distances between surfaces in the eye and potentially their shapes can be measured using optical systems, such as partial coherence interferometry (PCI), optical low coherence interferometry (OLCI), and optical coherence tomography (OCT). All refer to the same basic set-up, a Michelson interferometer using low coherence illumination. In an optical measurement system, optical path length and intensity of the coherently reflected infrared light (instead of a sound beam) from internal tissue interfaces are recorded by comparing it to light that has traveled a known reference path length.[94] In a time domain system, the path length of the light is measured using an interferometric technique.

In a Michelson interferometric set-up (Figure 2-3), the incoming light emitted by an extended source is divided into two perpendicular beams by a beam-splitter. The two beams are reflected by mirrors M1 (sample interface) and M2 (movable reference mirror) and then return through the beam splitter to the detector. The two beams interfere with each other, and the interference patterns are captured by the detector. If a coherent light source is used, interference fringes will be observed only at precise optical path differences; but if low-coherence or short pulse light is used, the interference pattern will

occur when two optical path lengths match within the coherence length of the light.[94] In a time domain system (as the Visante anterior segment OCT being used in Chapter 6), by changing the position of M2, constructive and destructive patterns are obtained. In systems designed for ophthalmology or vision science, the light beam propagating into the eye gets reflected from the major surfaces. The optical path differences between reflections from different surfaces and the reference beam can be measured by detecting the interference while scanning the reference path length (by moving M2).

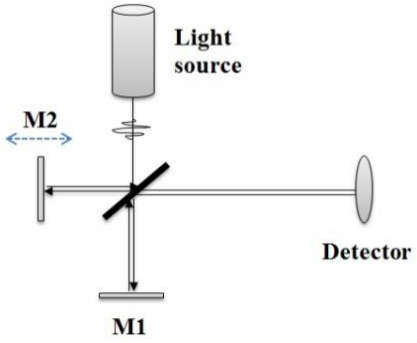


**Figure 2-3 A schematic of a Michelson interferometric set-up.**

Despite of the fact that the same principle is used among PCI, OLCI and OCT, they are distinguished by some differences. PCI and OLCI have almost the same set-up, the difference is that OLCI with an near-infrared source has a broader bandwidth, thus a rather short coherence length (about 10 μm)[95], compared to a longer coherence length of about 160 μm in PCI. The axial resolution is determined by the coherence length,[94] since interference only occurs when the path length is matched within the coherence length, which is the spatial width of the autocorrelation of the interference signal from the two

fields (inversely related to the bandwidth). For a source with a Gaussian spectral distribution, the axial resolution (Δz, an equivalent of the coherence length) is defined as[94]

$$\Delta z = (\frac{2\mathrm{In}2}{\pi})(\frac{\lambda^2}{\Delta\lambda}) \quad 2\text{-}9$$

where λ is the center wavelength of the source and Δλ is the full widths at half maximum of the source autocorrelation function which approximates the spectral bandwidth. Being one-dimensional ranging techniques, PCI and OLCI share the same limitations. This is where OCT is superior, offering the capacity to reconstruct cross-sectional or three dimensional images. In OCT, cross-sectional images can be generated by performing a series of axial scans at varies transverse positions. In contrast to time-domain techniques, using a photodiode to measure intensity after moving the reference arm, Fourier-domain OCT can detect the intensity from all the path differences simultaneously. Instead of having a scanning mirror which matches the optical path length difference and a detector recording the position of this movable mirror, Fourier-domain OCT has a stationary reference mirror with a spectrometer or a light source with a scanning wavelength to record the interference signal as a function of the wavelength of the light reflected from ocular surfaces.

The optical OCT approach is becoming popular because it is non-invasive (no direct contact with the eye is required) and has higher resolution than ultrasound. Comparison with conventional ultrasound techniques within human eyes,[96-99] as well as animal models,[95, 100-104] has shown that optical methods have potential in multiple applications, notably in ophthalmology for diagnostic measurements. In addition, most biologic tissues

are highly scattering and it is easier to focus light than sound (giving better transverse resolution).[94]

# Chapter 3

# Calculation of Total Eye Power and Retinal Blur during Normal Emmetropization in the Chick Eye

*This chapter is partially based on the abstract by Shao et al., presented in part at the annual meeting of the Association for Research in Vision and Ophthalmology, Fort Lauderdale, Florida, May 2012. This chapter has been submitted for publication. Olivia Stanley and Kevin Tuck helped the author of the thesis prepare for the oral presentation for the conference by providing suggestion during rehearsals.*

*The co-authors are Dr. Elizabeth Irving, Marsha Kisilak, and Dr. Melanie Campbell. Detailed declaration of contributions is as follows:*

*Dr. Campbell first proposed a possible eye power calculating using refractive error and optical axial length data, advised on and checked calculations throughout the work. Kisilak provided the idea of a relative principal plane position which was constant with age. They also had previously developed the image metrics used (equivalent blur and linear retinal blur) in collaboration with Dr. Jennifer Hunter. Dr. Irving provided background understanding and published normal chick eye parameters (of refractive error and optical axial length) during first two weeks of development for initial analysis. Kisilak provided previously unpublished normal pupil radius data between days 0 and 15.* ***The author of the thesis*** *first applied the eye power calculation to the normal chick eye parameters (provided by Dr. Irving) during the first two weeks of age. Then the author of the thesis examined this eye power calculation by comparing the outcomes with other reported literature values and further discussed the constant ratio of the distance between second nodal point and the anterior retina to optical axial length used in the calculation. Also, the author of the thesis did some literature search for normal development data beyond two weeks of age to enable a more complete presentation of normal emmetropization between days 0 and 75. Moreover, the author of the thesis calculated the equivalent and linear retinal blurs due to defocus using literature and experiment pupil data during days 0 and 35. The concept of defining the end of the period of emmetropization from the near constancy of equivalent blur was developed by Dr. Campbell. The author of the thesis wrote up the manuscript (including the literature*

*review) after discussion with Dr. Campbell about interpretation of data and figures. Dr. Campbell provided critical revision of and polished the article. Other co-authors read and commented on the manuscript.*

*This research is supported by the Natural Sciences and Engineering Research Council (NSERC).*

**ABSTRACT**

**PURPOSE.** An eye power calculation is developed and tested and used to study the co-variance of optical length and eye power and their contributions to emmetropization and retinal image quality during normal growth in chick eyes.

**METHODS.** Novel equations were used to calculate eye power. From literature values of chick eye parameters, MOR and optical axial length (OAL; anterior cornea to anterior retina) were fitted as a function of age. Dioptric eye length (K′) and eye power were derived up to day 75. Pupil size data were used to calculate the angular and linear retinal blurs (EB and LRB) on the retina due to defocus.

**RESULTS.** An exponential fit of eye power vs age to day 15 also defined its variation to day 75. During emmetropization, OAL increases while MOR decreases. Eye power decreases exponentially with age reaching and maintaining a value very close to K′ from day 35 onward. This gives a stable value of MOR beyond day 35. EB and LRB decrease almost exponentially until day 35. After about day 35, MOR changes little, EB remains almost constant while LRB increases slowly, in agreement with predictions of a uniformly expanding eye model.

**CONCLUSIONS.** The eye power calculation presented is simpler than other approaches and provides an accurate power variation during normal emmetropization without the need for extensive dimensional data. Concurrent variations in eye power combine with eye length changes to produce the smaller changes in MOR during emmetropization. We define the time point at which MOR and angular retinal blur (EB) become stable as the completion of emmetropization. Emmetropization appears to be driven by an active

reduction of EB. After emmetropization is complete, the measured ocular parameters are consistent with uniform expansion.

**Keywords** Ocular development • Emmetropization • Eye power • Chick • Growth

## 3.1 Introduction

The eye is said to be emmetropic when the image is located close to the photoreceptor layer. Otherwise, the eye is hyperopic or myopic with a spherical refractive error which contributes to the mean ocular refraction (MOR). This MOR produces a defocus blur on the retina. Most species begin life with a hyperopic refractive error,[65] which gradually reduces towards emmetropia as the eye grows by an active process called emmetropization.[11] During emmetropization, the optical blur on the retina from aberrations other than defocus also reduces.[42] This response to the direction of defocus of the eye is a fine-tuned growth regulation mechanism guided by the mismatch between eye length and optical power.[1, 64, 65] Emmetropization is complete around age 6 for humans as originally shown by Hirsch and Weymouth in 1947,[8] but hyperopia or myopia may develop at older ages.[4, 105, 1064, 105] Their development involves a breakdown in correctly identifying and compensating for defocus as the eye grows. Therefore, understanding the process by which optical power and eye length are regulated during normal growth and subsequently during myopia development when emmetropization fails, is crucial.

The chick is a popular animal model in which to study eye growth during normal emmetropization and the development of induced refractive error. Its growth changes are rapid, and chicks feed independently after hatching. In chicks, both refractive error and ocular dimensions change more rapidly during the first 2 weeks post-hatching[38, 39, 42, 43, 63] but changes have been reported beyond this time[38] until day 75.[45] Schematic eye models (see for example, Figure 3-1) developed for chicks at different ages[39, 43, 45] help explain changes during emmetropization and lay the ground work for explaining changes with

refractive errors induced by lenses placed in front of the eye. It is widely believed that axial length changes fully explain the refractive error seen when the endpoint of induced myopia is reached[45, 63] and after full recovery from such modification.[64] However, the contribution of optical power relative to that of eye length during emmetropization and response to lens manipulations is not often examined.[45] In addition, our lab has recently shown that changes in both eye length and power lead to short-term diurnal changes in refractive error.[40]

Eye power is often calculated cross-sectionally on different birds at different times by combining many dimensions, often measured post-mortem, which increases the uncertainty of the calculated power. Recently, a customized Bennett's equation for calculating lens power in chick eyes from *in vivo* measurements of refraction, keratometry and biometry was proposed[107] from which eye power could also be calculated. Here, we wish to derive eye power from two measurements, refractive error and eye length, using a new, simplified method which could be used longitudinally in living eyes. We will test the method on cross-sectional data. We wish to study ocular power changes and the defocus blur on the retina as a function of age during emmetropization in normal growth. We will then present a new definition of the endpoint of emmetropization and insights gained into this active process.

## 3.2 Methods

### 3.2.1 Experimental Data

Eye power was derived from spherical equivalent refraction (mean ocular refraction, MOR) and ocular dimensions (see section 3.2.2 below) reported in the literature.[39, 43, 45] During normal growth for three different strains, White Leghorn, sub-strain Ross 308;[39] White Rock cross; and White Leghorn,[43] Cornell-K[45] chicks were used. MOR data points for birds up to and including day 14[39, 43] were measured from the original figures in the papers and for birds from day 10 onward[45] were determined from the regression cited by Iribarren and colleagues.[107] Additional data from Schaeffel and Howland[53] are also discussed. Data were not corrected for the artefact of retinoscopy. Optical axial length (OAL) values, anterior cornea to anterior retinal surface,[40] were read from the figures or determined from the regression given in the original papers.[43, 45] In the work by Irving and colleagues,[43] MOR was measured by retinoscopy without anesthesia (a combination of longitudinal and cross-sectional data), and OAL was measured with A-scan ultrasound on 52 birds (cross-sectional data). In the paper by Schaeffel and Howland,[53] MOR was measured by cycloplegic Hartinger refractometry and OAL by ultrasound with anesthesia. Avila and McFadden's[39] MOR was measured by retinoscopy cross-sectionally under anesthesia. Here, OAL was determined after subtracting their measured retinal thickness[39] from their reported anterior cornea to posterior retina distances. Other dimensions (for example, the locations for second focal point, F′, and second nodal point, N′)[39] were determined from the figures. In addition, pupil radius data before day 14 (Ross Ross chicks, from a published experiment[52] where pupil radius was not reported) and

from day 14 to day 35 (White Leghorn chicks)[84] were combined and fitted with an exponential function.

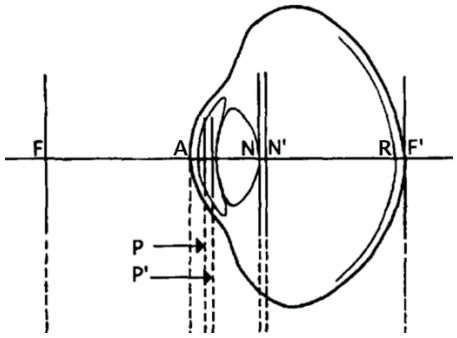


**Figure 3-1 A schematic eye drawing with relative positions of the cardinal points of the eye (adopted from Irving and colleagues).**[43]

F, F′ are focal points, P, P′ are principal points, and N, N′ are nodal points, making up the cardinal points of the eye. R is the photoreceptor layer, located within the retinal thickness. $\overline{P'R}$ (k′) is the optical length. Axial length (AL) is the distance from the anterior cornea to the back of the sclera.[40] Optical axial length (OAL) is the distance from the anterior cornea to anterior retinal surface (the vitreous/retinal interface, R′, not labeled in the figure),[40] which is shorter than AL.

### 3.2.2 Equations for Eye Power and Retinal Blur due to Defocus

Dioptric length (K′) is defined as

$$K' = \frac{n'}{k'} \qquad 3\text{-}1$$

where n′ is the refractive index of the vitreous, and k′ is the optical length ($\overline{P'R}$ , Figure 3-1). According to Bennett and Rabbetts,[4] MOR can be expressed in terms of K′ and eye power ($F_e$) as

$$MOR = K' - F_e. \quad 3\text{-}2$$

From Eqn.s 3-1 and 3-2, the power of the eye can be expressed as

$$F_e = \frac{n'}{k'} - MOR. \quad 3\text{-}3$$

In schematic eyes, power is calculated from the powers of cornea and lens along with the distances between their principle points. Here we use Eqn. 3-3 to calculate eye power from k′ and MOR. k′ can't be measured directly but can be derived as a function of age from the positions of the cardinal points and retina (Figure 3-1) such that

$$k' = \frac{n'}{n} \times (\overline{N'R} + \overline{RF'}) - \overline{RF'}, \quad 3\text{-}4$$

where n=1 and n′=1.335[43, 45] are the refractive indices for the air and the vitreous, R is the position of the photoreceptor layer, F′ is the second focal point, and N′ is the second nodal point. Because the defocus, $(\frac{n'}{n} - 1) \times \overline{RF'}$ in the normal eye is small compared to $\frac{n'}{n} \times \overline{N'R}$, k′ can be approximated as

$$k' \approx \frac{n'}{n} \times \overline{N'R}. \quad 3\text{-}5$$

Note that k′ is measured to the photoreceptor layer. Since there is no consistently reported distance of the anterior retina to the photoreceptor layer for chick, we used OAL in calculating k′.

Using data of Irving and colleagues,[43] for a normal growing eye, the distance from N′ to anterior retinal surface ($\overline{N'R'}$) to OAL ratio was found to be constant within 3.5% (0.66) with age as were the ratios calculated from Avila and McFadden (0.66)[39] and Schaeffel and Howland (0.66 if the data are fitted with a constraint of zero intercept, also see Figure 5-A2 in Appendix-5.6.3).[45] Therefore, for simplicity we assume 0.66 for all populations as a function of age,

$$\frac{\overline{N'R'}}{OAL} \approx \gamma = 0.66, \tag{3-6}$$

substituting Eqn. 3-5, then

$$k' \approx \gamma \times \frac{n'}{n} \times OAL = 0.88 \times OAL. \tag{3-7}$$

k′ is substituted into Eqn. 3-3 so that

$$F_e \approx \frac{n}{0.66 \times OAL} - MOR. \tag{3-8}$$

The size of the blur circle on the retina due to defocus, the linear retinal blur (LRB)[12] produced by the refractive error, is the product of equivalent blur (EB)[42] and the first focal length of the eye (f),

$$LRB = EB \times f = \frac{EB}{F_e}, \tag{3-9}$$

where EB, an angular measure of the retinal blur is defined as[42]

$$EB = \frac{4\left(3^{\frac{1}{2}}\right) RMSA}{r} = \left|\frac{4\left(3^{\frac{1}{2}}\right) Z_5}{r}\right|, \tag{3-10}$$

where RMSA is the root mean square aberration, $Z_5$ is the Zernike coefficient for spherical defocus, and r is the radius of the eye's entrance pupil. Because MOR is related to $Z_5$,[92]

$$EB = MOR \times r, \tag{3-11}$$

from Eqn.s 3-9 and 3-10, the radius of LRB can be written in terms of MOR, r, and $F_e$,

$$LRB = \frac{|MOR| \times r}{F_e}. \tag{3-12}$$

Dioptric length (K′) and eye power were derived as a function of age from the data in Section 3.2.1 using Eqn. 3-8 and the resulting data points were then best fitted with a function. In addition, for Avila and McFadden's data,[39] K′ and eye power were also derived from the exact cardinal positions of the eye's optics. To examine effects of ignoring the small $\overline{R'F'}$ distance, results for eye power (Eqn. 3-3) with k′ calculated from Eqn. 3-7 were then compared to the exact results using Eqn. 3-4. The angular and linear blurs (equivalent blur, EB; and linear retinal blur, LRB) on the retina due to defocus were derived from the fits to MOR, eye power and pupil radius as a function of age using Eqn.s 3-11 and 3-12.

### 3.3 Results

MOR data for birds up to and including day 14[43] and after day 8 and up to day 75[45] were combined into data set 1 because these reported MOR values can be well fit by a single curve (Figure 3-2a) along with a second curve for another data set 2.[39] Figure 3-2 also shows the variations of OAL, K′ and eye power.

OAL (Figure 3-2b) initially increases rapidly with age and then more slowly as the emmetropization progresses. Meanwhile, dioptric length (Figure 3-2c) and eye power (Figure 3-2d) decrease exponentially by approximately 100 D over the entire period, by very slightly different amounts, causing the MOR to decrease rapidly from nearly 6.55 D to 0.80 D. This exponential decrease in MOR for data from 0 to 75 days (Figure 3-2a) is due to the difference between the slower exponential functions for K′ (the reduction of K′ with a time for a 50% change, t50=26 days, Figure 3-2c; also see Figure 3-2e) and eye power (t50=28 days, Figure 3-2d; also see Figure 3-2e).

Pupil radius (Figure 3-3a) initially increases rapidly with age and then levels off. EB and LRB decrease approximately exponentially with age (Figure 3-3b and c) to minimum values of about 3.4 arcmins and 8.2 microns, respectively, well above the blur radius at the diffraction limit. After day 35, MOR and EB remain almost constant as the eye continues to grow, LRB increases slowly.

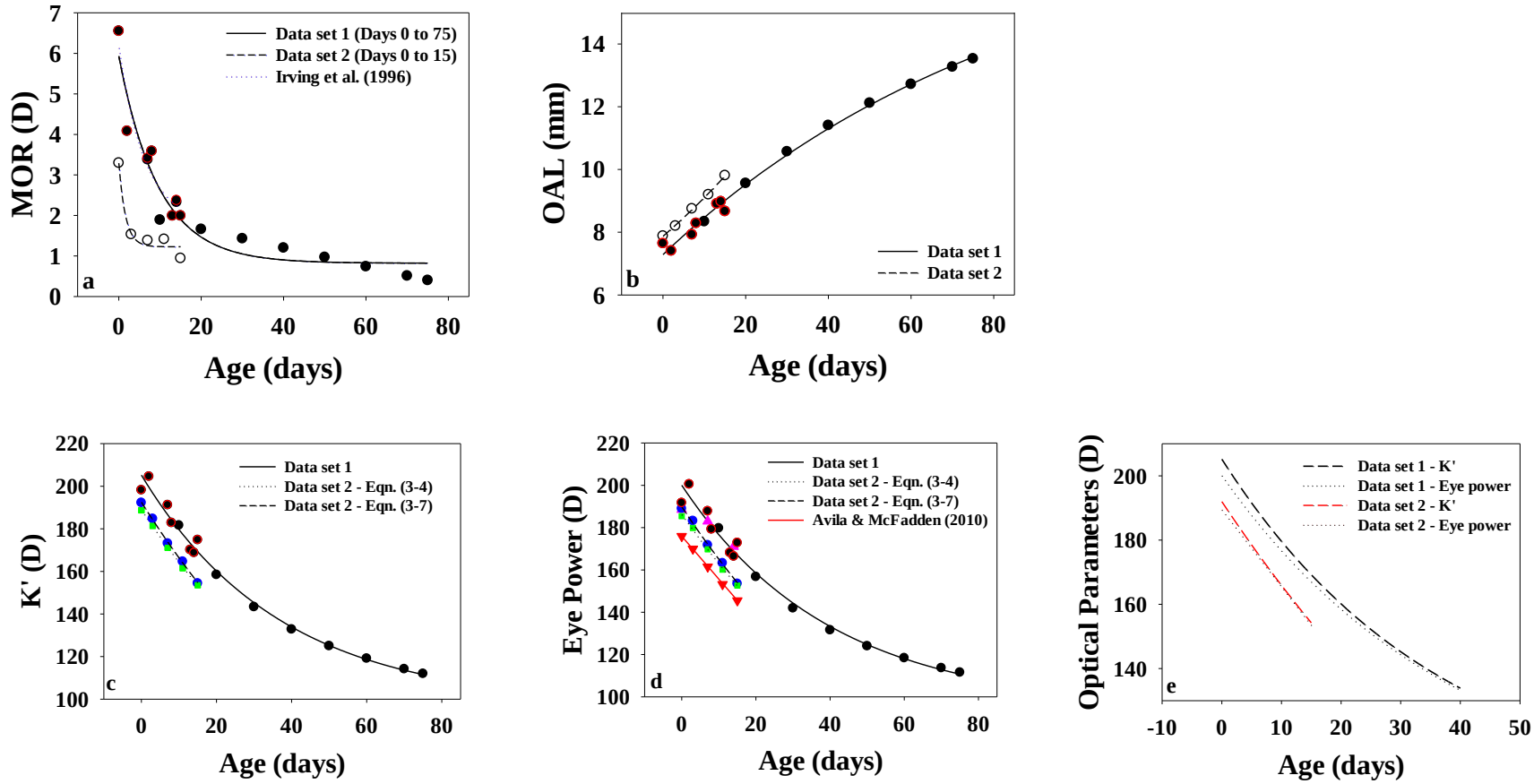


**Figure 3-2 Optical parameters vary with age including (a) MOR, (b) optical axial length, (c) dioptric length, (d) eye power, and (e) fits for dioptric length and eye power from (c) and (d).**

MOR and OAL data were determined from the original papers[39, 43, 45] at each time point and were not corrected for the small eye artefact of retinoscopy. (a) The dotted curve represents the exponential fit for a subset of the data reported by Irving and colleagues.[43] K′ (c) and eye power (d) were calculated at each data point from OAL (b). The resulting data points and data for MOR (a) and OAL (b) were best fit by exponential functions, with constants shown in Table 3-1.

Solid curves fit data set 1 (MOR (a) and OAL (b)) and derived quantities (K′ (c) and eye power (d)) from day 0 to day 75 (before day 15: red-edged filed circles;[43] beginning from day 10: black filled circles).[45] Data set 2 from Avila and McFadden[39] and derived quantities are fit by dashed curves. For data set 2, different colored symbols represent different methods of calculation: green squares and open blue circles represent K′ (c) and power (d) from k′ using Eqn. 3-4 or 3-7, respectively. The green squares and blue circles are almost identical in value.

In figure (d), upright pink and inverted red triangles are cross-sectional eye power data reported by Irving and colleagues,[43] and by Avila and McFadden.[39] The red solid line represents the linear eye power regression reported by Avila and McFadden.[39]

In figure (e), the plot of power (solid from d) and K′ (solid from c) are truncated at day 40 to make the differences between the curves for data derived from data set 1 (black curves) and data set 2 (red curves) more visible.

**Table 3-1 Best fit regression functions for optical parameters in Figure 3-2, t is age in days (all $p<0.05$).**

| Parameters | Data set 1 (Days 0 to 75, combined data)[43, 45] | Data set 2 (Days 0 to 15)[39] | |
|---|---|---|---|
| **MOR (D)** | MOR = 0.8 + 5.1×exp(-0.10× t) | MOR = 1.2 + 2.1× exp(-0.6 × t) | |
| **OAL (mm)** | OAL = 7.29 + 10.9 × [1-exp(-0.0115× t)] | OAL = 7.87 × exp(0.0146× t) | |
| **Dioptric length (D)** | K′ = 97 + 108 × exp(-0.027× t) | Eqn. 3-4 | K′ = 188.8 × exp(-0.0139 × t) |
| | | Eqn. 3-13 | K′ = 192.5 × exp(-0.0146 × t) |
| **Power of the eye (D)** | Power = 94 + 105 × exp(-0.025 × t) | Eqn. 3-4 | Power = 186.2 × exp(-0.0133 × t) |
| | | Eqn. 3-14 | Power = 189.4 - 2.40× t |
| **Pupil Radius (mm)[52, 84]** | Radius = 0.92 + 0.30 × [1 - exp(-0.15 × age)]; between days 0 to 35 | | |

During days 0 to 15 (Data set 2), OAL can also be fitted with a linear regression; however, the F statistic is better for the exponential fit. Eye power calculated from k′ derived using Eqn. 3-7 is best fit with a linear function as reported for power by Avila and McFadden;[39] however, using Eqn. 3-4, the F statistics is better for the exponential fit. The precision with which the values are listed was determined from the standard deviations.

The best fits to MOR in data set 1 can also be fitted with an exponential function without a constant term as reported by other authors.[39, 42] Similar to the results reported here, data given up to day 25 by Schaeffel and Howland[53] for MOR can be fitted with an exponential function.

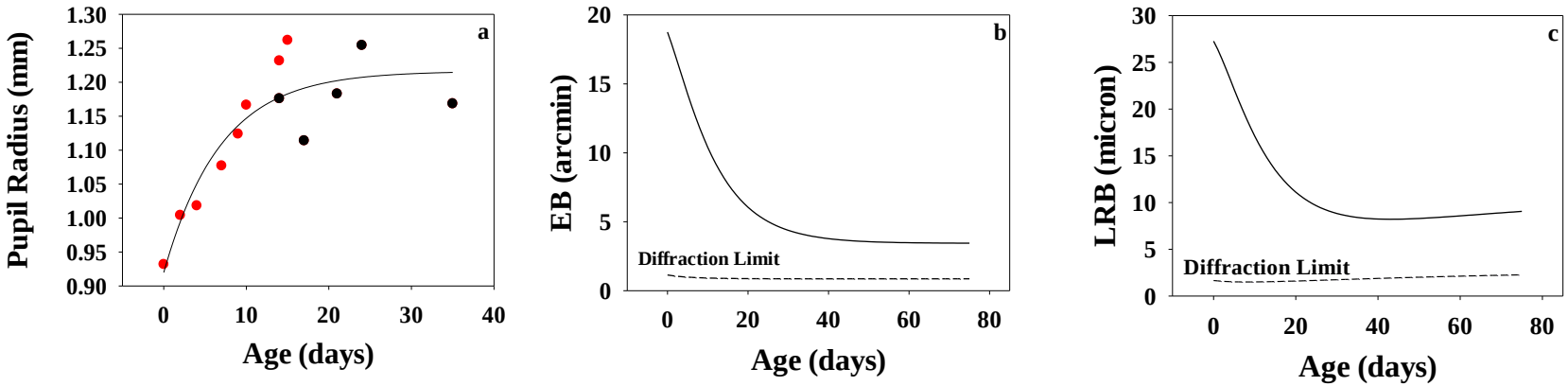


**Figure 3-3 (a) Pupil radius (between days 0 to 35), (b) angular blur radius due to defocus (equivalent blur EB), and (c) blur radius on the retina due to defocus (linear retinal blur, LRB) as a function of age.**

Data for pupil radius as a function of age for control eyes is unpublished data of Kisilak and colleagues (red symbols) taking as part of a published study[52] and Tian and Wildsoet (black symbols)[84] which are fitted with an exponential function (Table 3-1). To the best of our knowledge, pupil radius has not been measured beyond day 35.

Curves for EB and LRB were calculated from the regressions of MOR, eye power and pupil radius using Eqn.s 3-11 and 3-12 (and assuming the same fit to pupil radius after day 35). Both show approximately exponential decreases with age until after day 35 when LRB increases slowly.

## 3.4 Discussion

### 3.4.1 Emmetropization

As previously noted for chick[38, 42, 58] and young human eyes,[13] our results show an active emmetropization which cannot be explained by uniform eye growth. The endpoint of emmetropiztion has implicitly been assumed to occur when the eye becomes emmetropic. Our results indicate that emmetropization is complete when MOR is almost constant with a rate of change very close to zero (Figure 3-4) (which occurs in chick starting from day 35). At this point, the rates of change of power and K′ are close (Figure 3-4) and the values are very similar. Angular blur changes litter after day 35 (Figure 3-3b). Linear blur reaches a minimum value on day 43 (Figure 3-3c). As in the literature,[39, 42, 43] rapid emmetropization occurred during first two weeks of age with the refractive error decreasing from hyperopic to nearly emmetropic. At the time of emmetropization, the measured MOR in chick has not reached zero (~1.0 D). Animal studies suggest that emmetropia should be the endpoint of emmetropization,[65] and that slightly hyeropic MOR is due to the small eye artefact.[39, 93] However, it has also been suggested that the preferred endpoint for refractive development in humans might be mild hyperopia.[108] The small eye artefact[93] was not corrected and would be 1.3 D if the distance from the vitreous/retinal interface to the photoreceptor layer is 0.135 mm as given by Glickstein and Millodot.[93] It might also indicate that the blur due to defocus is at or below the amount that can be sensed by the retina during emmetropization. At emmetropization the EB of approximately 4.4 arcmins is very similar to the inter-cone

spacing of ~3.8 arcmins on day 21 (the last day measured) (unpublished data).[109] Prior to day 35 when the eye is emmetropizing, the EB is larger than the inter-cone spacing (e.g. on day 21, EB = 5.8 arcmins, cone spacing is 3.8 arcmins).

An exponential function fits angular blur due to defocus between days 0 and 35. The t50 (17 days) is slightly smaller than, that of angular blur due to higher-order aberrations (HOA) (22 days).[12] This similarity suggests either that optical changes during the emmetropization of defocus blur produce a reduction in blur due to HOA at a similar rate or that both defocus and HOA blurs emmetropize proportional to EB until EB is reduced sufficiently.[12]

It is not possible from this data to say which of length or power may be actively responding to defocus blur. If only the variation in OAL occurred without concurrent power changes, the eye would become myopic with growth.

If the endpoint of normal emmetropization is mild hyperopia when the retinal blur decreases to close to the cone spacing, when the treated eye recovers from the induced myopia, the endpoint might expected to be mild myopia when blur is first matched to the cone sampling. However, the treated eye recovers to mild hyperopia to match the control eye (see Chapter 5). This might be due to a homeostatic control mechanism,[65] or it might be that the existence of directional signals in the defocus blur of the chick eye (astigmatism, diurnal fluctuations and higher order aberrations) enables the determination of the sign of defocus (as originally proposed by Hunter and colleagues; reviewed by Wallman and Winawer).[65] Given a myopic defocus, the eye could continue to emmetropize until the amount was just detectable with opposite sign of defocus.

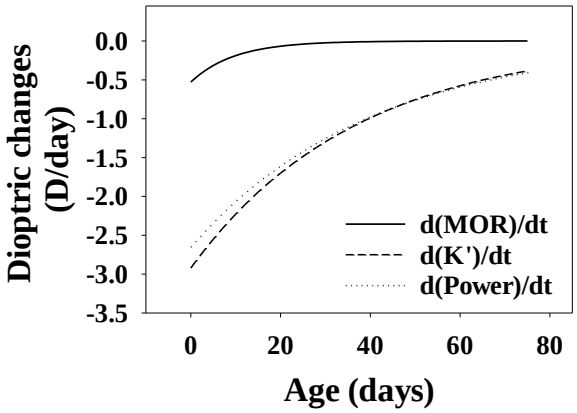


**Figure 3-4 Dioptric changes (derivatives of MOR, K′ and eye power with respect to time) as a function of age.**

Rates of change of MOR, K′ and eye power are shown as solid, dashed and dotted curves, respectively.

### 3.4.2 Eye Growth after Completion of Emmetropization

Beyond the age when emmetropization is complete, the eye continues to grow albeit more slowly and with indistinguishable rates of change of eye power and dioptric length (Figure 3-4), and the rate of change in MOR is almost zero. The angular blur on the retina is almost constant (Figure 3-3b), but the linear blur derived from regressions of MOR, pupil radius, and eye power suggests that it may increase slowly (Figure 3-3c) in agreement with the predictions by Hunter and colleagues in an approximately uniformly expanding eye model.[12] If this slight increase in LRB is real, it is very likely that the eye may grow approximately

uniformly after the completion of normal emmetropoization. In support of this, from day 35 onwards, the continuing small decrease in MOR agrees with the prediction of uniform expansion calculated from OAL increase. Furthermore, it is important to note that the eye may still emmetropize beyond the age at which normal emmetropiozation is complete[38, 45] if angular blur is increased by imposed defocus. The increase in LRB seen in normal growth, after day 35 would be similar to that due to the increase expected if defocus were imposed by (a mild) treatment. However, an increase in angular blur would only come from defocus not normal growth, supporting the hypothesis (in the previous section) that angular blur drives emmetropization.

### 3.4.3 *In vivo* Calculated Eye Power with Age

As found here, a decrease in eye power with age (Figure 3-2d) has been previously reported for chicks by the authors from whom the data was taken[39, 43] and others.[107] However, we show an exponential decrease in power over a large age range. K′ and eye power decrease with very similar t50s (of 26 days and 28 days, respectively). The small mismatch between their rates of change gives the rapid exponential decrease in MOR (t50=6.9 days).

We have tested an approximate eye power calculation which could be calculated longitudinally in living eyes from optical length of the eye and MOR (using justified approximations in Eqn. 3-8). Our approach is in contrast to most previous work where eye power was calculated from cross-sectional measurements of corneal and crystalline lens curvatures and ocular component thicknesses,[39, 43, 107] a procedure that introduces multiple additive uncertainties (as discussed by Rozema and colleagues).[110]

The values from our approximate eye power calculation (using Eqn. 3-8) is very close to the values reported for White Rock cross chicks,[43] differing by a maximum of 2.7% on day 14. Our values are less than 7.5% larger for the White Leghorn, sub-strain Ross 308[39] than the eye power data originally reported. The effect of freezing the eye in their studies may explain some of our difference from Avila and McFadden's result.[39] A further difference likely arises from the equivalent refractive index of the crystalline lens, which they adjusted so that the paraxial focus was located on the photoreceptor plane whereas our method does not constrain the focal point.

Recently, Iribarren and colleagues[107] customized the A and B constants in Bennett's equation[107] for chick eyes,[45] which could be used to determine eye power. When the eye power is calculated, it is less than 7% smaller than our calculated eye power using different literature data.[39, 43] If we use the same literature data,[45] the differences are less than 0.5%, suggesting that our calculation is consistent within measurement error.

### 3.4.4 Assumptions in the Eye Power Calculation

There are two assumptions made in our derivation of eye power. One assumption is that the ratio, $\gamma$ (Eqn. 3-6), is approximately constant with age. Secondly, we assume that in a normally growing eye, the nodal point to retina distance ($\overline{N'R'}$) is very close to the posterior nodal distance.[12]

For the first assumption, up to two weeks of age, literature data on chicks do not show an age dependence ($p>0.05$) in $\gamma$, and gives a mean of 0.66 for normal White Rock cross[43] and

White Leghorn, sub-strain Ross 308[39] chicks. For older chicks (beyond day 15), Schaeffel and Howland[45] reported an approximately constant ratio of 0.63 "within various age groups" (when discussing birds aged from day 14 to 86). However a value of 0.66 without an intercept fits Schaeffel and Howland's[45] data well. If the eye powers of different strains were calculated with differing values of $\gamma$, they would differ by less than 6.1%. The predicted trends of the optical parameters are not sensitive to the ratio value. Therefore, a constant $\gamma$=0.66 is a good approximation. For the second assumption that $\overline{F'R'}$ is small, the distance between F′ to R′ is less than 2.6% of OAL on day 0 when the hyperopic defocus and $\overline{F'R'}$ are at their maxima, giving a change in eye power value of 1.7% compared to an exact calculation.[43]

Data from Avila and McFadden[39] were used to test the effects of these two assumptions. The difference in eye power values between the exact calculation (Eqn. 3-4) of k′ and the calculation with the two assumptions (Eqn. 3-8) is less than 2% which supports the assumptions made.

### 3.4.5 Advantages of the Proposed Eye Power Calculation

There are two major advantages of the proposed eye power calculation. Firstly, it only requires eye length and MOR which can be accurately measured *in vivo* in awake birds without cycloplegia or anesthetic. Results are affected less than by combining larger numbers of measurements as in the *in vivo* Bennett methods,[107] which requires additional keratometry and lens thickness measurements. Similar to retinoscopy, keratometry in the chick eye faces

the challenge of accommodation by the cornea. Lens thickness is quite difficult to measure within alert birds using ultrasound. If anesthesia is applied, lid retractors will potentially affect image quality.[83]

Secondly, our proposed eye power calculation is not dependent on assumptions made to simplify the complex refractive index profile of the crystalline lens, which in turn will affect the power values. The equivalent refractive index of the chick lens has been reported to change with age[107] and varies between reports from 1.395 to 1.486.[39, 43, 45] However, the only refractive index needed for our eye power calculation is the vitreous, with a consistent value reported in the literature.[43, 45]

### 3.4.6 Limitations of *ex vivo* Eye Power Calculation and Effects of the Small Eye Artefact

As well as the *in vivo* methods discussed in the previous section, eye power can be derived from *ex vivo* cornea and lens powers, using dimensions and refractive indices as in schematic eye models.[39, 43, 45, 107] Corneal power can be calculated based on corneal radius or corneal curvature, which if not taken from *in vivo* measurements (of corneal curvature), can be measured in frozen sections (for corneal radius).[45] The calculation of lens power, based on Gullstrand's lens formula requires knowledge of lens surface curvatures often acquired from frozen sections.[39, 43, 107] However, lens thickness and radii of curvatures changes with freezing[39, 43] and needs to be corrected.[107] In addition, instead of considering the gradient refractive index of the lens, schematic eye models usually assume a constant equivalent refractive index. A distribution of refractive index in the lens has also been inferred by

measuring the lens between prisms.[45] Equivalent refractive index has been determined through modeling to match the measured dimensions with refractive errors[39] or from focal length measurements of the isolated lens.[43, 69]

Modeling requires information on refractive error, and an assumption as to what surface light is reflected from during refractive error measurement.[93] The small eye artefact in which the reflection originates anterior to the photoreceptors remains controversial in the chick eye.[39, 43] Avila and McFadden[3943] calculated the lens refractive index apparently assuming that light is reflected from the photoreceptor layer. As a result, they would calculate a smaller refractive index than for a focus at the front of the retina, leading to a lower reported eye power. Irving and colleagues[43] measured the equivalent refractive index of the isolated lens and from this calculated a small eye artefact for the chick.

### 3.4.7 Differences between Strains

Despite the potential differences in body weight[59, 111111] between the different strains from which data were taken (some birds are bred as commercial layers;[39, 45, 112] and some are bred as broilers),[43] it has been reported that there is little variation in ocular development.[39] However, we found some potential strain differences.

MOR for all birds shows a rapid exponential decrease during emmetropization with differences between the data sets in the absolute values.[39, 43, 45] In Figure 3-2a, we combined MOR data for White Rock cross chicks up to and including day 14[43] and from day 10 onwards for Cornell-K chicks.[45] MOR data from the two strains are consistent, and can be

fitted with a single exponential function. On average, MOR data for White Leghorn layers, sub-strain Ross 308[39] are systematically less hyperopic (open circles in Figure 3-2a) than White Ross cross (broilers)[43] and White Leghorn layers, sub-strain Cornell K chicks[45] with differing exponential fits. However, the standard deviations of the data points overlap on days 0 and 15.

Broilers tend to grow faster than commercial layers.[111] Nevertheless, the standard deviation of pupil size for Ross Ross chicks overlaps with that for White Leghorn chicks[84] on day 14 and the two data sets can be pooled and fitted significantly with a single exponential function.

### 3.5 Conclusions

An eye power calculation from optical length and MOR, longitudinally in living eyes is tested, which has the potential to diminish the multiple additive uncertainties obtained during cross-sectional measurements. In the long term, it may be possible to extend this calculation to myopic eyes by taking into consideration the distance from the second focal point to the photoreceptor layer, which can be calculated from MOR.

During normal emmetropization, covering a longer observation period (beyond two weeks of age), MOR decreased exponentially, as was found during the shorter period range of first two weeks. This rapid exponential decrease in MOR in normal growth comes from a small mismatch between the rates of change of optical power and dioptric length. The completion

of emmetropization can be defined as the point at which the rate of changes in MOR and angular blur approach zero, at which point MOR is slightly hyperopic. This is followed by slower growth with a gradual decrease in the rates of change in ocular parameters (e.g., pupil radius, length and power). The constant angular blur and slightly increasing linear blur suggest the eye growth might be relatively uniformly after completion of emmetropization. Emmetropization appears to be driven by values of angular blur which are above the level of the cone photoreceptor resolution during emmetropization, reaching a level when its radius of angular blur is similar to cone spacing at the completion of emmetropization.

# Chapter 4

# Powers and Eye Length during Emmetropization and their Relationship to Retinal Blur in the Chick Eye

*This chapter is currently being modified for submission to a journal.*

*The co-author is Dr. Melanie Campbell. Detailed declaration of contributions is as follows:*

*Dr. Campbell and Kisilak had previously developed, in collaboration with Dr. Jennifer Hunter, the image metrics (equivalent blur and linear retinal blur) used in this chapter. The idea for the chapter, to compare the rates of change of ocular properties to retinal blur was developed jointly by Dr. Campbel and the author of the thesis. The author of the thesis decided to analyze the contributions of cornea and lens powers to emmetropization in chick, developed the methodology for this and compared it to findings for human.*

***The author of the thesis*** *plotted the rate of change in optical parameters as a function of either equivalent or linear retinal blur due to defocus based on the results in Chapter 3. To better compare the relationship between eye power and length, the author of the thesis analyzed power component data from the literature for the same experimental period as the data in Chapter 3. The author of the thesis obtained corneal radius data from the literature and calculated corneal power. Also, the author of the thesis applied the customized version of Bennett's equation for the chick eyes (published by Iribarren). The author of the thesis postulated possible new mechanism for emmetropization. The author of the thesis wrote up the manuscript after discussion with Dr. Campbell about interpretation of data and figures, the importance of equivalent blur guiding emmetropization, and the possible relationships between optical axial length, corneal radius and lens power based on common signaling control. Dr. Campbell provided critical revision of and polished the article.*

*This research is supported by the Natural Sciences and Engineering Research Council (NSERC).*

**ABSTRACT**

**PURPOSE:** Emmetropization is an active process involving feedback from the retina. To examine changes in ocular properties during emmetropization in the normal chick eye and which changes are proportional to retinal blur due to defocus to better understand the feedback loops in emmetropization.

**METHODS:** Mean ocular refraction (MOR), dioptric length (K′), and eye power and their rates of change were taken from previous work (Chapter 3) and were plotted as a function of MOR, rate of change in optical axial length (OAL; anterior cornea to anterior retina) and angular and linear retinal blurs due to defocus (EB and LRB). The relationships of literature values of corneal radius, corneal and lens powers to other ocular parameters and retinal blurs were examined during and after emmetropization.

**RESULTS:** As emmetropiozation proceeds, rate of change in MOR, which linearly varies with MOR and retinal blurs (EB and LRB), decreases exponentially with age and OAL. During emmetropization, rate of change in OAL decreases linearly with MOR ($p=0.007$), rate of change in MOR ($p<0.0001$) as well as with decreasing retinal blurs (EB $p=0.009$ and LRB $p=0.03$). Similarly, during emmetropoization, the rate of increase in corneal radius varies linearly with retinal blurs (EB $p=0.009$ and LRB $p=0.02$); the rate of change in lens power is proportional to the rate of change in OAL, MOR, rate of change in MOR and retinal blurs ($p<0.0001$). After emmetropization, the above relationships change.

**CONCLUSIONS:** Emmetropization appears to be actively driven by angular blur due to defocus, causing proportional changes in OAL, corneal radius, and lens power which vary in

an almost linear fashion with EB. This in turn causes a linear change with MOR and its rate of change.

**Keywords** Ocular development • Emmetropizatoin • Power • Chick • Growth

## 4.1 Introduction

Refractive error occurs when the optics of the eye is unable to focus distance object onto the photoreceptor layer without accommodation. Emmetropization is the process when after birth hyperopic refractive errors gradually reduce in magnitude with a dramatic decrease in their variability,[38] resulting from a combination of both passive and active processes.[5, 11, 58] It is known that passive emmetropization, occurring because proportional enlargement of the eye reduces the power of the dioptric system, is insufficient to account for the refractive changes observed.[12, 58] Alternately, emmetropization is an active, vision-dependent growth-regulation mechanism[14] involving a retinal mediated[11, 65] visual guidance of ocular growth. We have postulated that regulation occurs through the processing of defocus blur on the retina.[113] However, the precise mechanisms coordinating the structural and optical development of the eye during the time course of emmetropization are not understood.

In human infants, that the change in axial length growth over a period of time is larger with a larger initial hyperopic MOR (mean sphere or mean ocular refraction) is a key factor during emmetropization. Axial length changes are thought to be important,[13] but reductions in the power in cornea and crystalline lens have been reported as insignificant factors.[13] Studies in children beyond the endpoint of emmetropization around age 6 show that axial length continues to increase, and corneal power continues to change slowly,[114, 115] but changes in the crystalline lens, for example lens thickening and decrease in power,[7, 13, 71, 72] being proportional to axial elongation, are potentially important for the determination of final refractive state. According to Morgan and colleagues, the detailed process of the control in

the reduction of lens power has so far not been studied experimentally.[49] Therefore, understanding how a balance between optical parameter and eye length develops could enable a better understanding of the mechanisms which drive/control emmetropization.

The chick eye is a popular model to study normal emmetropization and refractive error development.[38-40, 43, 45, 52, 58] Recently, Avila and McFadden[39] proposed that emmetropization in chick is potentially the result of rapid growth of the lens of the eye and inhibition/inactivity in ocular growth, followed by ocular growth which stabilized the refractive error. In other words, the relationships between eye length and powers (of cornea and lens) result in the decrease in refractive error. Previously (in Chapter 3), we defined the endpoint of emmetropization (between day 30 and 35) as when the rate of change in the refractive error becomes very small, and the refraction is almost stable.[113] At the same time angular blur due to defocus (EB) stabilizes, suggesting that EB might be actively contributing to emmetropization.[113] Here, we examine changes in ocular properties during emmetropization in normal chick eyes using literature data,[43, 45] including unpublished data from our lab[52] to determine which changes are proportional to the retinal blur due to defocus.

## 4.2 Methods

Literature values of chicken eye length and measurements of eye defocus, MOR, were used.[43, 45] Eye power was previously calculated from the MOR and optical axial length (OAL; anterior cornea to anterior retina) using a novel method (Chapter 3).[113] OAL, dioptric length

(K′), and angular and linear blurs on the retina (EB and LRB) were also taken from previous work (Chapter 3).[113] They were based on literature data.[43, 45, 52, 84]

Corneal radius data for birds on days 0, 2, 7, 8, 13, and 14,[43] measured by ophthalmometer without anesthesia, were taken from the original figures in the papers, and for birds on days 14, 35, 42, and 75,[45] measured by photokeratometry, were determined from the regressions as reported.[45] Corneal power was derived from the corneal radius of curvature[43, 45] by considering a single surface corneal model[45] with an aqueous refractive index of 1.335.[39, 43] In addition, lens power were calculated using the customized Bennett equation for chicks[30] (which calculates lens power from as the final factor which determines the eye's refractive error, given all other ocular dimensions) using literature data.[30, 43, 45] Optical parameters involved in the calculation [including corneal radius (CR), anterior chamber depth (ACD), lens thickness (LT), vitreous chamber depth (VCD), anterior and posterior lens radii, and OAL] for days 0, 7, and 14 were given in Irving and colleagues,[43] and for days 14, 35, 42, and 75 were extrapolated from figures and regressions.[30, 45] As indicated by Iribarren and colleagues,[30] when dimensional data were all obtained within frozen sections, lens radii, ACD, LT, and VCD were corrected for lens freezing. Note that no corrections[30] for the dimensions and lens radii were performed here for the data by Irving and colleagues,[43] since they reported ultrasound measurements for ACD, LT, and VCD, in contrast to Schaeffel and Howland.[45] However, corrections of lens radii only affect the total lens power by less than 0.1 D.

To study the covariance of ocular parameters and their relationships to retinal blurs during normal growth, the fits for optical parameters (MOR, OAL, K′, and eye power) and their rates of change (derivatives as a function of age), as well as retinal blurs (EB or LRB) due to defocus (taken from Chapter 3), as a function of age were sampled on each day. Rates of change in optical parameters were then plotted as a function of other parameters or retinal blurs. Corneal radius, corneal power and lens power were plotted and fitted as a function of age; rates of change in these parameters were plotted as a function of age, retinal blurs, and rate of change in OAL.

Paired values of the rates of change in OAL and corneal radius at the time points (on days 0, 2, 7, 14, 15, 35, 42, and 75), at which MOR, pupil radius, and OAL were measured, were fitted with a linear function of various parameters or retinal blurs.

**4.3 Results**

Rates of change in MOR as well as K′ and eye power decrease nonlinearly in magnitude as emmetropization proceeds (Figure 4-1) with age[113] (Figure 4-1a). During emmetropoization, rate of change in MOR is proportional to MOR (Figure 4-1b) and also to EB (Figure 4-1c; $p<0.0001$) and LRB (Figure 4-1d; all $p<0.0001$). Rate of change in MOR reaches to a stable rate of almost zero at about days 30 to 35. We have previously defined this as the time when emmetropization is complete.[113] After this time, rates of change in K′ and eye power are

almost identical (Figure 4-1a). Rates of decrease in MOR, K′ and eye power all decrease nonlinearly with decreasing rate of change in OAL (Figure 4-1e).

With age, OAL increases more slowly (Figure 4-2). Curves are the derivative of OAL regression with respect to age, obtained in Chapter 3, versus other properties over the full time course (Figure 4-2). Within the first 30 days, linear fits were performed to these curves. Values of the rate of change in OAL were fitted as a function of MOR, EB and LRB at the same times, calculated from the experimental measured values on days 0, 2, 7, 14 and 15. The decrease in the rate of change in OAL was found to be linearly related to the decreasing MOR ($p=0.007$, Figure 4-2a), EB ($p=0.009$, Figure 4-2c) and LRB ($p=0.025$, Figure 4-2d) until emmetropization is complete. The rate of change in OAL decreases approximately linearly with the rate of change in MOR, but only until day 30 ($p<0.0001$, Figure 4-2b). After day 35, different relationships were seen, including a different slope for the rate of change in OAL with MOR ($p=0.02$, Figure 4-2a).

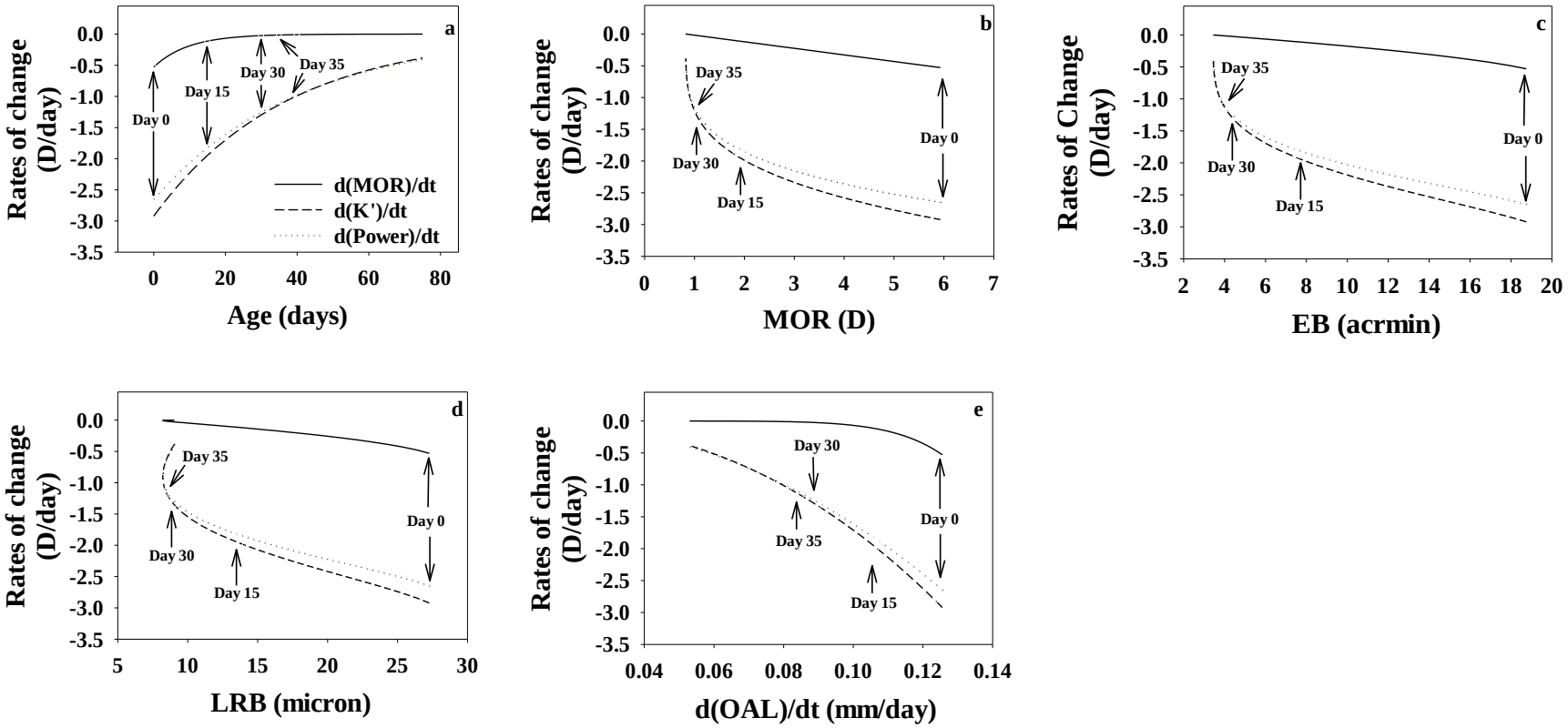


**Figure 4-1 Rates of change in (derivatives with respect to time of) MOR, K′ and eye power as a function of: (a) age, (b) MOR, (c) EB, (d) LRB, and (e) rate of change in OAL.**

Rates of change of MOR, K′ and eye power are shown as solid, dashed and dotted curves, respectively. Arrows indicate the age on curves.

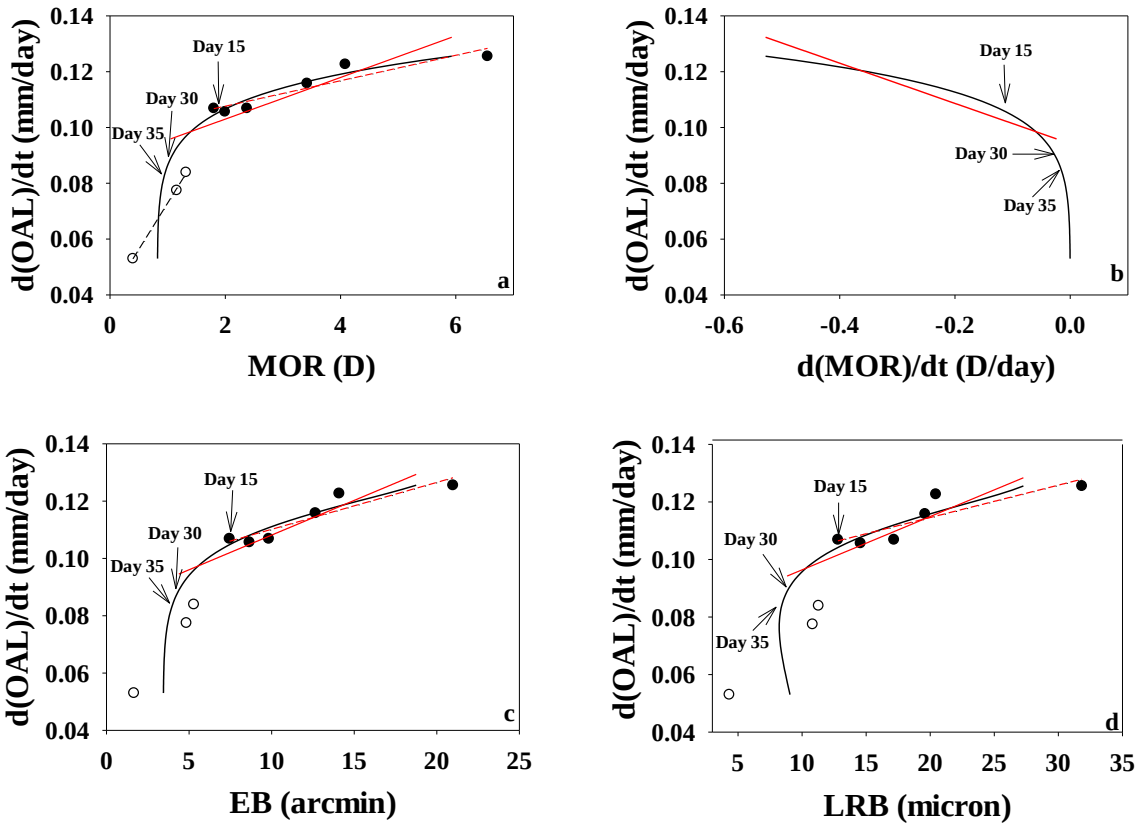


**Figure 4-2 Rate of change in OAL as a function of (a) MOR, (b) rate of change in MOR, (c) EB, and (d) LRB.**

The paired values are the rate of change in OAL with MOR (a), EB (c) and LRB (d) at the time points at which MOR,[43, 45] pupil radius,[52, 84] and OAL[43, 45] were measured.

The curves come from the fit to MOR as a function of age, calculated EB and LRB, and the derivatives of the fits to OAL and MOR in Chapter 3, sampled at each day. OAL and MOR were taken from regressions to literature data as a function of age; their rates of change are the derivatives of the regressions. Arrows indicate the age on the solid black curve.

Red solid line is the fit to the curve between days 0 and 30. Red dashed line is the fit to the points on days 0, 2, 7, 14 and 15 (a, c and d). The first open circles represents values on day 35, and the other two are days 42 and 75. Black dashed line is the fit to the points after day 35 (a); the fits in (c) and (d) are not significant. The paired values were determined from the derivative of the fit to OAL as a function of age in the previous paper (Chapter 3).[113]

Corneal radius increases exponentially (Table 4-1 and Figure 4-3a) with age. Optical axial length to corneal radius ratio (OAL/CR) increases linearly with age from 2.6150 to 2.9402 with a slope of 0.0043/day (p=0.0003) (Figure 4-3b). During emmetropoization (up to day 15), the rate of change in corneal radius varies linearly with both EB (p=0.009, Figure 4-4a) and LRB (p=0.02, Figure 4-4b). After emmetropization, there tends to be a different relationship between the rates of change in corneal radius and retinal blurs, but the slopes to the few data points are not significant. The linear relationship between rates of change in corneal radius and OAL exists both during and after emmetropization (Figure 4-3c, $p<0.0001$, $r^2 = 0.9967$).

**Table 4-1 Regression functions and associated coefficients that describe the development of cornea and lens; t is age in days (all p<0.0003).**

| Parameters | Days 0 to 75[43, 45] |
|---|---|
| **Corneal radius (mm)** | Cornea radius = 2.80 + 2.50 × [1 - exp(-0.018 × t)] |
| **Corneal power (D)** | Corneal power = 67 + 52 × exp(-0.030 × t) |
| **Lens power (D)** | Lens power = 93 – 1.00 × t + 0.0061× $t^2$ |

The lens power can also be fitted with an exponential function; however the F statistic is better for the polynomial.

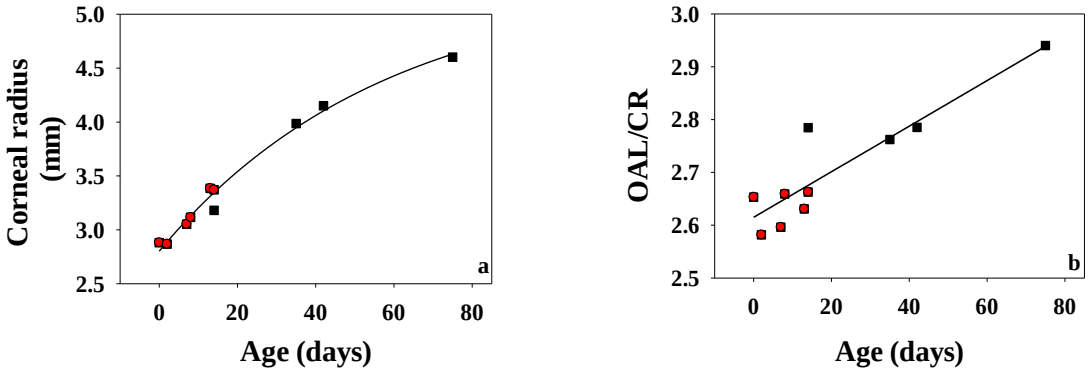


**Figure 4-3 (a) Corneal radius (CR) and (b) optical axial length to corneal radius ratio (OAL/CR) as a function of age.**

Corneal radius (a) and OAL/CR ratio (b) before and including day 14[43] are red-filled squares and from day 14 onwards are black squares.[45]

Corneal radius was fitted with an exponential function with age ($p<0.0001$). OAL/CR ratio was fitted with a linear function with age ($p=0.0003$).

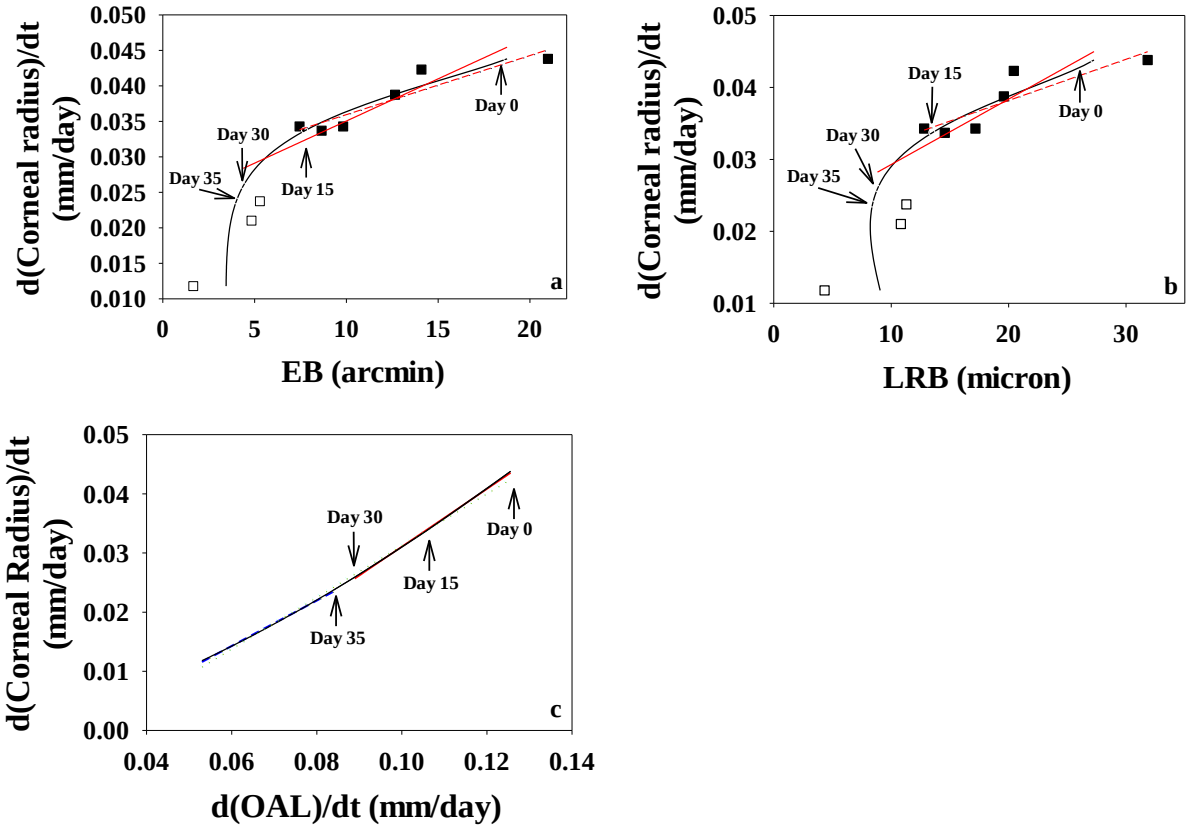


**Figure 4-4 Rate of change in corneal radius as a function of (a) EB, (b) LRB, and (c) rate of change in OAL.**

The paired values are the rate of change in corneal radius with EB (a) and LRB (b) at the time points at which MOR,[43, 45] pupil radius,[52, 84] and OAL[43, 45] were measured.

Black curves come from the derivative of the fit to corneal radius as a function of age, sampled at each day versus EB and LRB as a function of age (from Chapter 3) ((a) and (b)) and the derivative of the fit to OAL (c). In (a) and (b), red solid line is the fit to the curve between days 0 and 30; and the red dashed line is the fit to the closed-square points before and including day 15. In (c), red and blue solid lines are the fit to the curve before day 30 and after day 35, respectively; turquoise dotted line is the fit to the overall curve. All three fits are similar and overlay the original black curve.

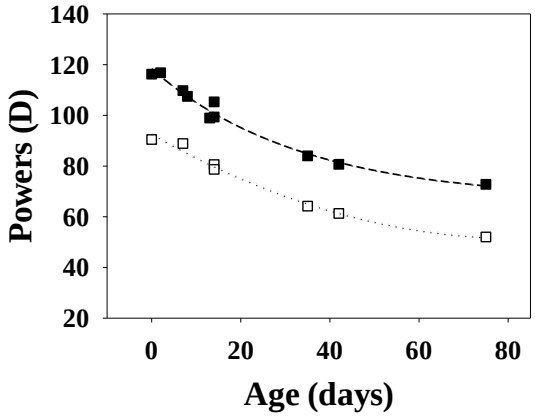


**Figure 4-5 Corneal power and lens power as a function of age.**

Corneal power (closed squares; dashed curve) was calculated and fitted with an exponential function with age ($p<0.0001$; Table 4-1).

Lens power (open squares) was calculated. The data is fitted with polynomials with age (dotted curve; $p=0.0002$; Table 4-1).

Both corneal power and lens power decrease with age (Figure 4-5). The rates of change in total eye power, corneal power and lens power all become less negative with age (Figure 4-6a). During emmetropization, the rate of change in corneal power is bigger than that in the lens power lens power between days 0 and 30. Meanwhile, the rate of change in lens power is almost linearly proportional to MOR (Figure 4-6b, $p<0.0001$, $r^2=0.8625$), rate of change in MOR (Figure 4-6c), and both angular (Figure 4-6d, $p<0.0001$, $r^2=0.9171$) and linear (Figure 4-6e, $p<0.0001$, $r^2=0.9303$) blurs between days 0 and 30, and the rate of change in OAL (Figure 4-6f) over the whole time. The rate of change of cornea power is linear with blur and

linear with the rate of change of OAL up to about day 25. After the emmetropization is complete (after day 30 or 35), the rates of change in corneal and lens power become very similar. Later (around day 60), both rate of change in corneal and lens powers become nearly zero (Figure 4-6).

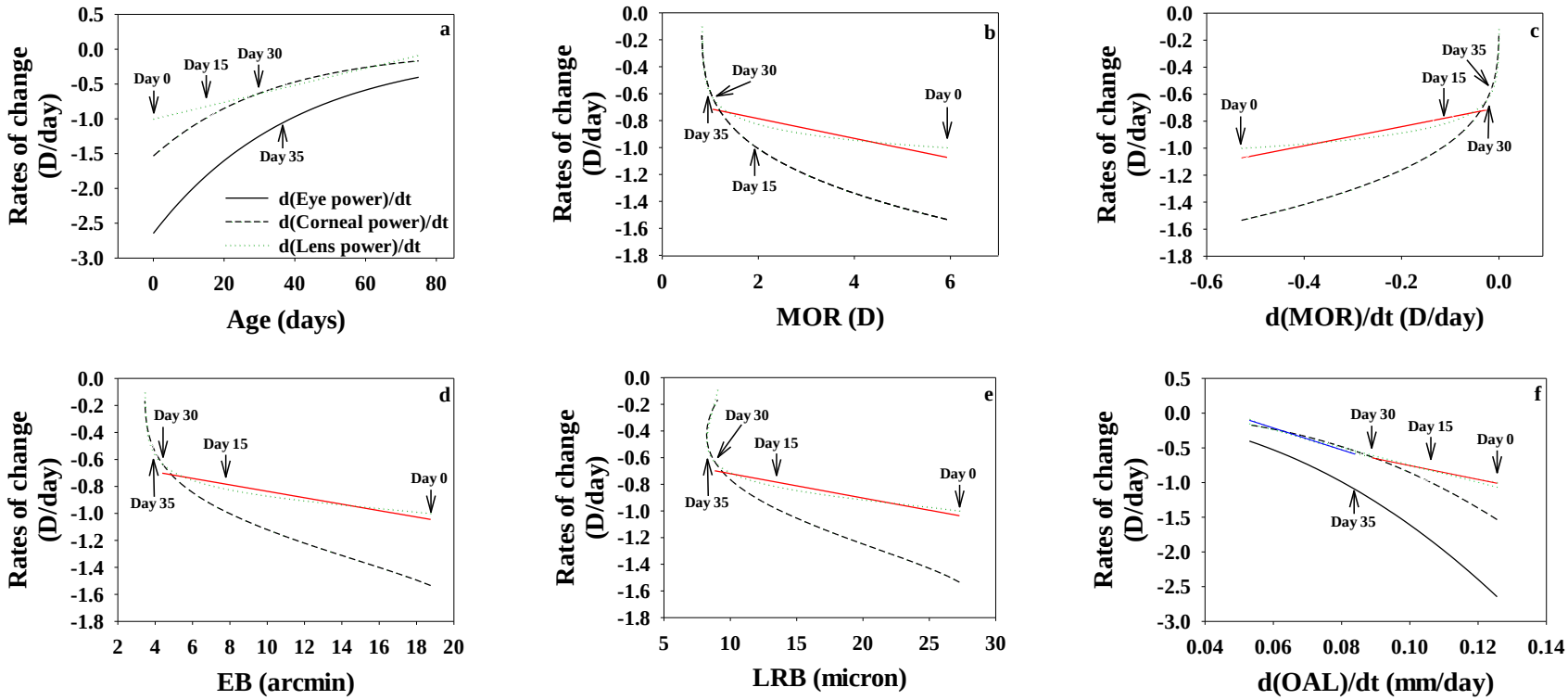


**Figure 4-6 Rates of change in eye power, corneal and lens powers as a function of (a) age; rates of change in corneal and lens powers as a function of (b) MOR, (c) rate of change in MOR, (d) EB, (e) LRB, and (f) rate of change in OAL.**

Rates of change of eye power, corneal power and lens power are shown as black solid, dashed and dotted curves, respectively. Red solid lines are the linear fits for the rate of change in lens power versus different parameters between days 0 and 30 (b to e). In (f), red and blue solid lines are fit to the curve before day 30 and after day 35, respectively; the turquoise line is the fit to the overall curve. All linear fits overlap and overlay with the data (dotted curve).

## 4.4 Discussion

### 4.4.1 Blurs on the Retina

Retinal image quality represented by EB and LRB, due to both higher-order aberrations (HOA)[12, 42] and defocus,[113] improves during emmetropization. The times for a 50% change, t50s, for EB due to defocus and higher-order aberrations are 17 and 22 days, respectively. Therefore, overall angular and linear blurs in chick decrease with age during emmetropization.[12] We have hypothesized that blur on the retina is the initial signal to emmetropization.[113] As retinal blurs due to MOR are believed to stimulate molecular signals which in turn modulate eye growth,[65] we examined the relationship of the optical parameters to angular and linear blurs (Figure 4-1c and d; Figure 4-2c and d; Figure 4-4a and b; and Figure 4-6d and e).

As previously shown,[113] during emmetropization, MOR, angular and linear blurs (EB and LRB) decrease with age until the endpoint of emmetropization around day 30 to 35[113] when MOR and EB become relatively constant. Consistent with theories of active emmetropization,[5, 11] we find the change in MOR is proportional to MOR (Figure 4-1b), resulting from the exponential dependence of MOR on time. However, because the size of the blur on the retina is dominated by its dependence on MOR:[42]

$$EB = MOR \times r, \qquad 3\text{-}11$$

a linear relationship between EB and MOR, is due to the relatively smaller percentage change in pupil size (24%) between days 0 and 35 compared to MOR (84%). This produces a

rate of change in MOR in proportional to EB (Figure 4-1c), the angular blur on the retina. In turn, the rate of change of MOR is almost linear with linear retina blur (LRB) because eye power varies less rapidly than MOR,

$$\mathrm{LRB} = \frac{|\mathrm{MOR}| \times \mathrm{r}}{\mathrm{F_e}}. \qquad 3\text{-}12$$

The t50's of EB and LRB are 17 days and 23 days, respectively. They are not very different as expected.

We previously reported evidence that angular blur (EB) actively controls emmetropization.[113] In this case, the angular or the linear blur would be expected to be linked to optical parameter changes. During emmetropization (between days 0 and 15), a linear relationship was found between the rate of change in OAL with either EB (p=0.009, $r^2$=0.8499, Figure 4-2c) or LRB (p=0.025, $r^2$=0.7526, Figure 4-2d), of which EB shows the stronger linear relationship. These observations support that emmetropization is driven by an active response of the retina,[14, 38] to angular blur due to defocus. The linear proportionality of the rate of change of OAL to retinal blur suggests that a signaling molecule produces a rate of eye lengthening which increases proportionally to the amount of retinal blur. Previously it has been postulated to be proportional to MOR in lens-induced myopia,[65] but we hypothesis that the mechanism of the response involves retinal blur.

Similar linearity can be observed between the rate of change in cornea radius with either EB (Figure 4-4a, p=0.009, $r^2$=0.8536) or LRB (Figure 4-4b, p=0.024, $r^2$=0.7568) during emmetropization, also with EB having a stronger relationship.

### 4.4.2 Mechanisms of Growth during Emmetropization

#### 4.4.2.1 Passive Emmetropization

It is known that a scaled model of uniform ocular expansion approximately predicts the changing paraxial properties in chicks but is insufficient to predict the actual rapid decrease in MOR and aberration blurs on the retina.[12] For example, when the data are fit to the same type of exponential function between days 0 to 35, K′ and eye power have similar t50s of 61 days and 65 days, respectively,[113] similar to that for lens power (t50=67 days), slightly smaller than that for corneal power (t50=71 days). But all are much slower than the rate of change in MOR (t50=12 days) which arises due to the small difference in the t50's of K′ and eye power (see Chapter 3). For dimensions, between days 0 and 35, the time needed for OAL to change by 50% (t50=34 days) is similar to that for focal length (t50=38 days), but somewhat smaller than that for corneal radius of curvature (t50=43 days) as expected. OAL increases by 22% between days 0 and 14, with a percentage change in focal length (19%) and pupil size (28%) giving a relatively small variation of the f-number (around 8%).[12] Therefore, a model of uniform ocular expansion is a good initial approximation of paraxial power, cornea, and K′ changes during normal growth.[12] Additional small differences in the rates of change of component powers and K′ are responsible for active emmetropization beyond the effects of uniform scaling (see the following section).

#### 4.4.2.2 Active Emmetropization

EB on the retina appears to modulate the rate of change of eye length which is in turn connected to the rates of change of cornea and crystalline lens power. The linear relationship between the rate of change in OAL with angular blur is the strongest support of an active mechanism during emmetropization as this implies that the OAL changes at a rate proportional to the angular blur on the retina (EB) until the EB approaches the spacing of the cones (Chapter 3), at which point the rate of change of OAL decreases rapidly, and EB is almost constant. The rate of the eye's elongation (representing as the rate of change in OAL) was also found to be almost linear with MOR (Figure 4-2a) and the rate of change in MOR (Figure 4-2b) during emmetropization (between days 0 and 30) in chick eyes, a result similar to human eyes, measured by Mutti and colleagues and argued to represent active emmetropization.[13]

The linear relationships between the rates of change of corneal radius and OAL with EB suggests a connection between changes in corneal radius and OAL which are very significantly linearly dependent (Figure 4-3c) both during and after emmetropization. Thus, corneal growth (anterior chamber) could be passively connected to growth of OAL (posterior chamber) through the common equator giving ocular expansion, driven by the rate of change of OAL or the connection could be active. The growth rate of the cornea is less than that of the OAL (Figure 4-4c) and the relative growth rates also differ somewhat (Figure 4-7c), leading to the small change observed in OAL/CR ratio with age (Figure 4-2b).

In addition, the rate of loss of lens power varies proportionally with EB ($p<0.0001$, $r^2$ =0.9171, Figure 4-6d) and LRB ($p<0.0001$, $r^2$=0.9303, Figure 4-6e) during emmetropization. This might be due to its linear relationship with the rate of change in OAL (Figure 4-6f) which persists even after emmetropization and OAL's linear proportionality to EB. Alternatively, it is possible that angular blur actively regulates the change in OAL, corneal radius and lens power through common signaling molecules, so that the changes in OAL, corneal radius, and lens power are linked (with linear covariances) during emmetropization. The link after emmetropization is complete might either indicate a persistence of a signal which decays over time or a lens response to molecules released which promote continued growth but which are not modulated by retinal blur.

Because eye length and eye power contribute to the decrease in MOR, the following relationship holds:

$$\frac{\Delta \mathrm{MOR}}{\Delta \mathrm{OAL}} = \frac{\Delta K'}{\Delta \mathrm{OAL}} - \left[ \frac{\Delta(\text{Corneal power})}{\Delta \mathrm{OAL}} + \frac{\Delta(\text{Lens power})}{\Delta \mathrm{OAL}} - \frac{\Delta\left[\frac{d}{n} \times (\text{Corneal power}) \times (\text{Lens power})\right]}{\Delta \mathrm{OAL}} \right]. \quad 4\text{-}1$$

The change in MOR per unit of OAL elongation is the result of dioptric length, corneal power and lens power changes, also the change in the interaction term, per unit of OAL change. The net emmetropization from an initial hyperopic refraction results in a negative

term on the left hand side of the equation which results because of the faster change in K′ with respect to OAL than the total eye power (the sum of the final three terms) (Chapter 3). We could also derive these relationships by considering the change of each as a function of the change in OAL (Figure 4-1e and Figure 4-6f). For instance, between days 0 and 1, 1 mm increase in OAL is associated with a -4.2 D total change in MOR; a -24 D, -12.6 D, and -8.3 D change in dioptric length, corneal power and lens power, respectively, which means that the third term in the square brackets decreases 1.1 D per mm of OAL change. Thus as discussed previously (Chapter 3), emmetropization occurs because the change in K′ (24 D) is larger than the change in power (19.8 D). Between days 14 and 15, and days 30 and 31, as emmetropization proceeds, a 1 mm increase in OAL is associated with a smaller change in MOR of -1.1 D and -0.2 D, respectively; similar decreases in the rate of change is seen in K′ (Figure 4-1e) and corneal and lens powers (Figure 4-6f), but with a smaller difference in K′ and power terms (Table 4-2). The power components' contributions are smaller, but very important in terms of reducing the contribution of K′, which gives the emmetropization.

**Table 4-2 Change in optical parameters due to per unit of OAL elongation at three time points**

| Change in Optical Parameters (D/mm) at Different Time | $\frac{\Delta MOR}{\Delta OAL}$ | $\frac{\Delta K'}{\Delta OAL}$ | $\frac{\Delta(\text{Corneal power})}{\Delta OAL}$ | $\frac{\Delta(\text{Lens power})}{\Delta OAL}$ | Interaction term |
|---|---|---|---|---|---|
| **Between days 0 and 1** | -4.2 | -24.0 | -12.6 | -8.3 | -1.1 |
| **Between days 14 and 15** | -1.1 | -17.9 | -9.0 | -7.5 | +0.3 |
| **Between days 30 and 31** | -0.2 | -14.2 | -7.0 | -6.9 | +0.1 |

The interaction term is the final term in Eqn. 4-1.

As is well known, the rate of emmetropization is larger than it would be with passive scaling of the eye over time.[12, 58] In human, it is found to be proportional to the change in OAL.[13] Changes in corneal and lens power were also found to be proportional to the change in OAL.[12] Here in the chick eye, lens power is smaller than corneal power, but the relative rate of change in lens power was found to vary linearly with the relative change in K′ with a slope not significantly different from 1.0 (Figure 4-7a), significantly larger than the relative change in corneal power (0.85, Figure 4-7b). In agreement with this, the corneal radius changes proportionally with the change in OAL with a slope of 0.74, significantly smaller than 1.0 (Figure 4-7c). Thus the rate of emmetropization, faster than in uniform expansion, arises primarily because the cornea changes more slowly than in a uniformly expanding eye.

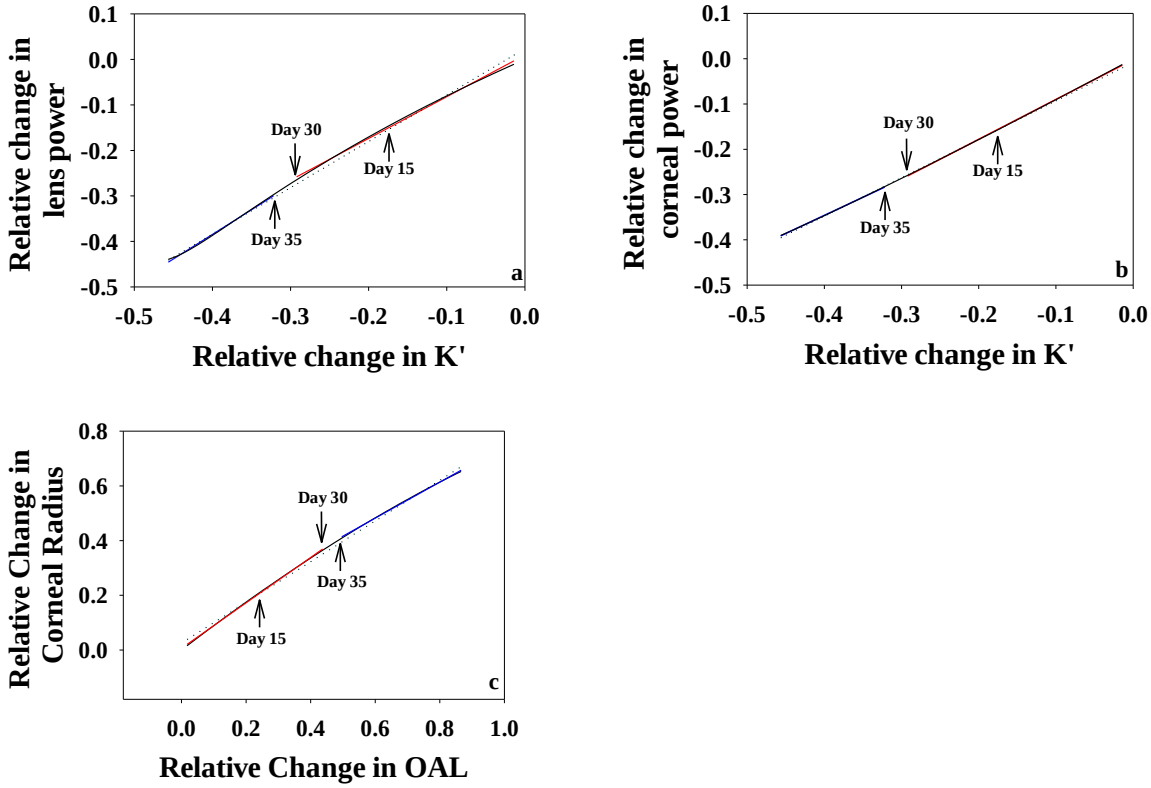


**Figure 4-7 Relative changes in (a) lens power and (b) corneal power as a function of relative change in K′. (c) Relative change in corneal radius as a function of relative change in OAL.**

The black curves come from the fits to lens and corneal power, corneal radius and OAL as a function of age, sampled at each day. Arrows indicate the age on the solid black curve.

Red and blue solid lines are the fit to the curve before day 30 and after day 35, respectively; turquoise dotted line is the fit to the overall curve. All three fits are similar and overlay the original black curves. The slopes over the whole range are 1.00, 0.85, and 0.74 in (a), (b), and (c), respectively.

#### 4.4.2.2.1 Corneal Radius and OAL with EB

Like the rates of change of OAL, the rate of change of corneal radius is also proportional to the blur on the retina during emmetropization, suggesting a similar response to active signaling by the retina, likely involving a signaling molecule. The retina, being the sensorimotor apparatus, might be able to start the signal process from the amacrine cells and control the eye growth through an alternation of dopamine production/concentration or a change in ZENK mRNA expression, two molecular impacts that had been seen in refractive error experiments in chicks, resulting in modulation of the choroid and sclera.[65] Considered the reciprocal nature between melatonin and dopamine due to diurnal variation, the fact that a melatonin receptor subtype has been revealed in the chick cornea and retina might link the alternation of the growth of the cornea and axial length during normal development.[116] Similar dopamine control has been seen to change lens optical power in the fish eye,[117] which suggests a link between lens and OAL as well (see Section 4.4.2.2.2).

Considering the likelihood of a relationship between changes in OAL and corneal radius during growth, we first explore the changes in cornea. The linear relationship between the rate of change in corneal radius and angular blur may arise from the linear relationship between rates of change in corneal radius and OAL. The rate of change in corneal radius has a highly significant linear variation with rate of change of OAL both before and after the completion of emmetropization ($p<0.0001$, Figure 4-3c). That their linearity persists after emmetropization is complete when their responses are no longer proportional to retinal blur suggests a linked expansion of both the anterior and posterior chambers. In agreement with

this, the linear regression of OAL/CR ratio indicates a small increase with age, which differs slightly from what was reported by Iribarren and colleagues[30] using data from day 10 data onwards (originally reported by Schaeffel and Howland),[45] likely due to their lack of points before day 20.

#### 4.4.2.2.2 Lens Power and OAL with EB

The rate of elongation of OAL (dotted curve in Figure 4-6f) has an almost linear relationship with the loss of lens power both before and after emmetropization ($p<0.0001$), over a range that extends beyond the linearly between loss of lens power and retinal blurs. The relative changes in OAL and lens power are also linearly related both before and after emmetropization. In addition, the relative change in lens power suggests a uniform expansion corresponding to the elongation of the eye, giving a slope of 1.0 with respect to the relative change in K′ (Figure 4-7a). Therefore, there might be a possible relationship between lens power and the rate of change in OAL in the sense that they could be mutually coordinated during and after emmetropization.

In human, equatorial stretch in the crystalline lens might be a factor relating axial length to the absolute decrease in the power of the lens, a theory originally proposed by van Alphen.[118] In human, loss of lens power has been found in parallel to the axial elongation progress during development.[119] However, in chick, we saw no evidence of lens thinning (Chapter 5) and our calculated lens power decreases consistent with uniform expansion during normal development.

A response to an active signal originating in the retina, likely involving a signaling molecule might also alter the crystalline lens. While the OAL increases during emmetropization in a way to minimize the angular blur, the lens has optical plasticity in the regulatory processes optimizing visual function,[117] the optics of the lens is potentially influenced by released neuroactive substances from the dopaminergic system in the retina[120] – a possible mechanism that might explain the simultaneous linearity in the loss of lens power with both retinal blur due to defocus and the rate of change in OAL during emmetropization. As in the case of the cornea, we postulate the continuing presence of a lower level of signaling molecules during growth beyond the completion of emmetropization. Visual input seems to play an important role in the development of the lens (as seen in the fish eye),[121] and dopamine has been seen to change the lens optical power.[117] One possible result of molecular signals originating at the retina might be a fast and accurate change in the refractive index distribution within the lens and thus a change in the lens power.

### 4.4.3 After Emmetropization

After emmetropization is complete around day 35, OAL lengthens more slowly, resulting in changes in K′. Eye power changes similarly to K′ to maintain a small EB (Figure 4-1c), and LRB may increase slightly (Figure 4-1d). A linear relationship of the rate of change in OAL with EB is no longer observed (Figure 4-2c). The continuing proportional relationships between the rate of change in corneal radius and loss of lens power with the rate of change in OAL suggest that growth of these elements remains linked after emmetropization is complete, maintaining a constant EB.

### 4.4.4 Comparisons with Human Eyes

In chick, corneal and lens powers decrease with the increase in OAL during emmetropization. Also, the rate of change in OAL is proportional to MOR, rate of change in MOR, as well as angular and linear retinal blurs (EB and LRB), supporting the active emmetropization mechanism. Similarly, in human, when substantial emmetropization occurs between 3 and 9 months of age, Mutti and colleagues[17] concluded that there was active emmetropoization after reporting a correlation between the reduction in MOR and the initial MOR. We expect that this relationship arises from the influence of retinal blur (which is dependent on MOR) on the rates of growth of the ocular components including axial length. With an increase in axial length, lens and corneal powers decreased[9, 13, 122] as we observe here in chick. We found in chick a rate of loss of lens power, proportional to the increased axial elongation not only during emmetropization but also after, similar to that found in early human development.[7, 13] In early human development,[13] the lens power decreased at a somewhat faster rate than in uniform expansion to produce a reduction in MOR during emmetropization but we find, in chick, that lens power is consistent with uniform expansion. In both human[13] and chick eyes, the change in corneal power is slower than predicted by the uniform expansion.

## 4.5 Conclusions

Emmetropization is an active process, supported by the observation that angular blur due to defocus causes proportional rates of change in OAL, corneal radius and lens power until blur

reduces sufficiently and emmetropization is complete. The results here support that the eye grows in such a way as to improve angular blur until it is close to cone spacing. Growth appears to be regulated by a signal whose strength is proportional to angular blur and which alters the rate of axial elongation. The rates of change of the radius of the cornea and the power of the lens in turn are proportional to the rate of change of axial elongation throughout growth. These relationships produce rates of change in MOR with an increase optical axial length that are very close to the measured rates. The links between rates of change of optical axial length and cornea radius of curvature and lens power may be via passive mechanisms or they may relate to a common signaling molecule which could, for example, modify the refractive index distribution within the crystalline lens. Many of these results are consistent with findings during emmetropization in children, but here we show that the changes are actively linked to retinal blur.

# Chapter 5

# Eye Power and Dimensions during Lens Induced Myopia (LIM) and Recovery in the Chick

*This chapter is partially based on the abstract by Shao et al., presented in part at the annual meeting of the Association for Research in Vision and Ophthalmology, Orlando, Florida, May 2014.*

*The experiment related to this chapter was performed with the assistance of Kisilak and Bunghardt who advised on experimental methods. Bunghardt guided the author of the thesis with animal handling while Kisilak controlled the computer for data acquisition of Hartmann-Shack (H-S) measurements and dimensional measurements using the ACCUTOME A-scan ultrasound. Dr. Campbell, Bunghardt, Kisilak and the author of the thesis were involved in the choice of A-scan instrument and discussed its testing. The approach for modifying the calculation of eye power for eyes with large refractive errors was discussed between Dr. Campbell and the author of the thesis, the idea of measuring the anterior chamber dimensions and relating these to the approximations needed in the calculations came from Dr. Campbell.*

***The author of the thesis*** *selected H-S images before Kisilak helped to analyze the images using software already developed for the purpose of quantifying refractive error from H-S patterns. The author of the thesis analyzed the dimensional data and developed selection criteria for image and peak selection for the ultrasound measurements. The author of the thesis used a customized program (developed by Ian Andrews) which shows a scaled-up view of ultrasound diagram to obtain dimensional data. The author of the thesis analyzed the data (plotted the figures, performed t-tests and ANOVA) after excluding data from birds which did not emmetropize to the negative goggle. Furthermore, the author of the thesis modified the equations for eye power derived in Chapter 3 so that that they could be applied to myopic eyes with one assumption of cardinal point position. The author of the thesis tested the eye power variation under different possible assumptions based on discussions with Dr. Campbell. Dr. Campbell*

*provided feedback on the analysis and organization of the chapter and critical revision after the author of the thesis finished writing the first draft.*

**ABSTRACT**

**PURPOSE.** To obtain longitudinal dimensional data during lens-induced myopia (LIM) and its recovery: optical axial length (OAL), corneal to back lens distance (CBL), lens thickness (LT), and vitreous chamber depth (VCD); and to discuss possible methods of calculating eye power and predicting changes in eye power during LIM and its recovery.

**METHODS.** Six Ross Ross chicks were unilaterally treated with a -15 D goggle from the day of hatching to day 7 and then it was removed. Measurements continued to day 10. Retinoscopy estimates, Hartmann-Shack (H-S) measurements and A-scan ultrasound were performed. Eye power was calculated based on different assumptions. Paired t-tests, linear fits and ANOVAs were performed to compare treated and control eyes and dimensions on a given day to the day prior to treatment.

**RESULTS.** The relative change in the front of the eye is proportional to the relative change in OAL, with a slope not different from 1 except for a slightly larger slope for treated eyes during LIM. This experimental finding motivated the assumptions in the eye power calculation. During LIM, 60% of the emmetropization to the -15 D goggle was established on day 7, with significant difference in OAL, CBL, LT and VCD between eyes. 57% of OAL increase between goggled and control eye was due to VCD and 43% to CBL. Eye power in treated eyes changed similarly to control eyes during LIM but showed significant difference on day 4 between eyes under various assumptions; one assumption showed additional significant differences on days 7. Recovery of refractive error occurred rapidly within two days of goggle removal. One assumption gave a significant difference between eye power on

day 8. Meanwhile, within treated eyes, OAL and VCD decreased significantly between days 7 and 9, as did eye power by a small amount. Decreases were significant by eye for assumption 2 and 3. Beyond day 9, there was no significant difference in dimensions or eye power between eyes.

**CONCLUSIONS.** The change in VCD is a contributor to emmetropization to hyperopic defocus; the front of the eye also shows changes. Emmetropization following goggle removal is more rapid than to the goggle. Changes in curvatures of the ocular surfaces remain to be assessed in LIM and its recovery in order to determine which eye power calculation is closer to the reality.

**Keywords** Ocular development • Lens-induced myopia (LIM) • Recovery • Chick • Growth

## 5.1 Introduction

Studies have confirmed that optically altering visual experience early in life by either positive or negative lenses can be compensated through changes in eye growth (reviewed by Wallman and Winawer).[65] Regulation of eye length during short-term exposure to retinal image defocus has been recently observed in human, with small but bi-directional optical axial length (OAL) changes in response to the direction of defocus.[67] For long-term exposure to hyperopic defocus to the retina, animal models of lens-induced myopia (LIM) have been established in chicks,[51, 54] guinea pigs,[123] macaque monkeys[124] and fish.[125] Among these animal models, the chick is a popular myopia model because of its rapid ocular growth. Chick eyes are able to compensate for the widest range of defocus,[51] and chicks recover from LIM when the goggle is removed.[42, 48] The chick eye refocuses defocused images, primarily via changes in axial elongation,[53, 54, 64, 66] due to an increase in the size of vitreous chamber,[57] in order to move the retina plane to the location of the focal plane, determined by the refractive power of the cornea and lens. Changes in power during LIM are not well studied as the contributions of optical components remain insignificant (for example corneal power) due to the huge variability[51] or have not been discussed (lens power).[45] When the lens used to induce myopia is removed, axial length elongation pauses while the optics of the eye continues to mature, letting the focal plane gradually move towards the retina in order to reduce the induced myopia.[126]

Much attention has been given to changes in OAL in myopic eyes compared to normal. However, it has been reported that, in human, for those who develop myopia later in life,

compensatory optical changes in dimensions, such as in the cornea and the crystalline lens, likely take place from infancy up to time of myopia onset.[127] Also, a breakdown of lens compensation during myopia[108] has been reported for both Northern Europe[71] and East Asian[7] children. The results suggest that the rate of loss of lens power in the development of refractive error needs to be assessed in more detail, considering the correlation found between axial length and lens power.[7] In chicks, during normal growth (Chapter 3)[128] and diurnal variation of mean ocular refraction (MOR),[40] we have previously shown that changes in MOR are due to both changes in optical length and optical power. The role of the optics of the eye in matching the retinal plane to the image plane during LIM and its recovery will be investigated here including whether and how the optical changes contribute to emmetropization during LIM and its recovery.

In a longitudinal study, dimensional data were obtained in chicks for both control eyes and eyes during induction of myopia and recovery from LIM. We calculate eye power via a method modified from Chapter 3 for the larger MOR in treated eyes by making and testing different assumptions. We then test the assumption that eye power within treated eyes does not change compared to control eyes.

## 5.2 Methods

### 5.2.1 Experimental Data

Two sets of 6 Ross Ross chicks (Gallus gallus domesticus) of mixed sex were measured on different occasions. On one set, measurements were made of optical axial length (OAL; anterior cornea to anterior retina) and other dimension (CBL, cornea to back lens; lens thickness, LT; and vitreous chamber depth, VCD). All were measured by A-scan Plus Connect, Accutome, Malvern, PA which has a reported clinical precision of 0.1 mm. MOR was measured on days 0, 1, 2, 3, 4, 6, 7, 8, 9, and 10. On the second set, OAL (by our old A-scan, Oculometer 4000, Radionics Medical Inc, Scarborough, Ontario) and MOR on days 0, 2, 4, 7, 8, 9, and 10 were measured. Chicks were obtained from a local hatchery (Maple Leaf Poultry, New Hamburg, ON, Canada) on the day of hatching. All chicks developed naturally under a fluorescent light cycle of 14-hour light/10-hour dark during the experiment. A -15D goggle was placed on one chicks' eye from the day of hatching to day 7 then removed; measurements continued up to day 10. Prior to goggling, retinoscopy (white light), Hartmann-Shack measurement (633 nm), and A-scan Plus Connect ultrasonography were performed, close to the optical axis. Refractive error and dimensional measurements were performed when goggles were removed for a short time between 8:00 and 11:00 am to avoid diurnal variation in optical parameters.[40] Birds were lightly restrained during measurements without the use of anesthesia and lid retractors to avoid changes in the optics[83] and effects of repeated anesthesia on growth.[39] All experiments received ethics clearance from the

University of Waterloo Animal Care Committee and adhered to the ARVO Statement for the Use of Animals in Ophthalmic and Vision Research.

A customized program was developed to show a scaled-up view of the reflections, with the origin at the position of the probe, and peaks showing for anterior and posterior lens, and vitreous/retinal surfaces of the eye. Images indicating severe tilts are excluded (see Appendix A for selection criteria). Dimensions were obtained through averaging measurements from at least three images (of sufficiently good quality) of the five scans taken of each eye for individual birds.

Data for MOR and dimensions were averaged across eyes at each measurement time and were plotted as a function of age and treatment without correction for the small eye artefact.[93] Paired t-tests, regressions and ANOVAs were performed and were deemed significant for $p \leq 0.05$.

### 5.2.2 Assumptions for Eye Power Calculations

Considering that the chick eyes responds to imposed defocus rapidly with compensatory increased growth, largely through modulation of vitreous chamber depth,[2, 54, 57] we first tested **Assumption (1)** that the optics of the eye is not a function of the treatment, meaning there is no change in any cardinal point positions nor eye power, with all compensation is due to changes in OAL with no power change.

Eye power is defined as

$$F_e = \frac{n'}{k'} - MOR. \qquad 3\text{-}3$$

where the dioptric length, K′, can be determined from the optical length (k′; distance from 2nd principal point, P′, to the photoreceptor layer).[4] If we assume (**Assumption 2**) that the optics of the eye changes but that P′ is in the same position in the treated eye as in the control eye, the difference in k′ between eyes comes from the difference in OAL.

$$k'_t = \overline{P'R'}_t = \overline{P'R'}_c + (OAL_t - OAL_c), \qquad 5\text{-}1$$

where subscripts t and c stand for treated and control eyes.

Previously (in Chapter 3) for normal eyes,[113] we have shown that eye power can be calculated from MOR and OAL by assuming the distance from the 2nd nodal point (N′) to the anterior retina (R′) is a fixed proportion of OAL (the first assumption in Section 3.4.4), and the distance from the 2nd focal point (F′) to R′ is very small compared to OAL (the second assumption in Section 3.4.4). The first assumption about the ratio of N′R′ distance to OAL is not thoroughly verified within young myopic eyes. The reported relationship between N′R′ distance and OAL for experimental birds is for day 26 only.[53] Obviously, the second assumption no longer holds when the eye becomes myopic. Here, we modified the eye power calculation so that it can be applied to myopic eyes (see Appendix-5.6.2), where the distance $\overline{F'R'}$ is a function of MOR and $\overline{N'R'}$. An assumption is needed when determining the distance $\overline{N'R'}$ from measured dimensional data. Because the relationship between $\overline{N'R'}$ and eye length (see Appendix-5.6.3), we assume a 0.66 ratio of $\overline{N'R'}$ distance to OAL in both control and treated eyes (**Assumption 3**). In addition, we find (see Results) that the change in CBL

relative to the baseline on day 0 (LIM) or day 7 (recovery) is proportional to the relative change in OAL (Figure 5-2a) and that a linear relationship may exist between vertex to N′ distance and CBL (Figure 5-2b) These results motivated another possible assumption for eye power calculation. In **Assumption 4**, we assume the vertex to N′ distance is correlated with CBL and/or OAL (more details in Appendix B).

For each assumption, longitudinal eye power data was calculated for days 0, 2, 4, 7, 8, 9, and 10.

## 5.3 Results

### 5.3.1 MOR and Dimension Changes

During LIM, while MOR in the control eye decreased exponentially during normal emmetropization, the MOR in the treated eye becomes -7.4 D by day 7 (Figure 5-1a), showing an emmetropization to the -15 D goggle by about 60%. MOR differed by eyes starting from day 1 (t-test, $p=0.006$). A univariate ANOVA (SPSS; IBM, Armonk, NY) showed a significant difference in OAL (Figure 5-1b) by eye ($p=0.004$), by day ($p<0.001$) and by eye×day ($p<0.001$). For CBL (Figure 5-1c) and VCD (Figure 5-1e), there was a significant difference by eye ($p<0.001$) and by day ($p<0.001$) but no significant difference with eye×day. On day 7, significant differences in OAL, CBL, LT, and VCD were present between eyes. 57% of OAL increase between goggled and control eye was due to VCD and 43% to CBL. LT (Figure 5-1d) shows significant differences by day ($p<0.001$) and by

eye×day ($p=0.003$). Here, MOR and OAL are presented without correcting the small eye artefact.

After goggle removal, the control eye continued to emmetropize; meanwhile, MOR in the treated eye emmetropized rapidly to a value not different from the control eye within two days. During recovery between control and treated eyes, there were significant differences in CBL and LT by day and by eye, in VCD by eye×day ($p=0.005$), and in OAL by eye ($p<0.001$) with significant differences in MOR and LT between eyes on day 8. Between days 7 and 9, both OAL (t-test, $p=0.024$) and VCD (t-test, $p=0.016$) in the treated eye decreased significantly, but OAL (t-test, $p=0.004$) and VCD (t-test, $p=0.013$) in the control eye continued to increase significantly. Starting on day 8, paired t-tests suggested no difference between eyes. No significant difference in OAL between eyes was found starting from day 8. Recovery was complete by day 9, and MOR and all other dimensions converged in both eyes with no significant differences between eyes.

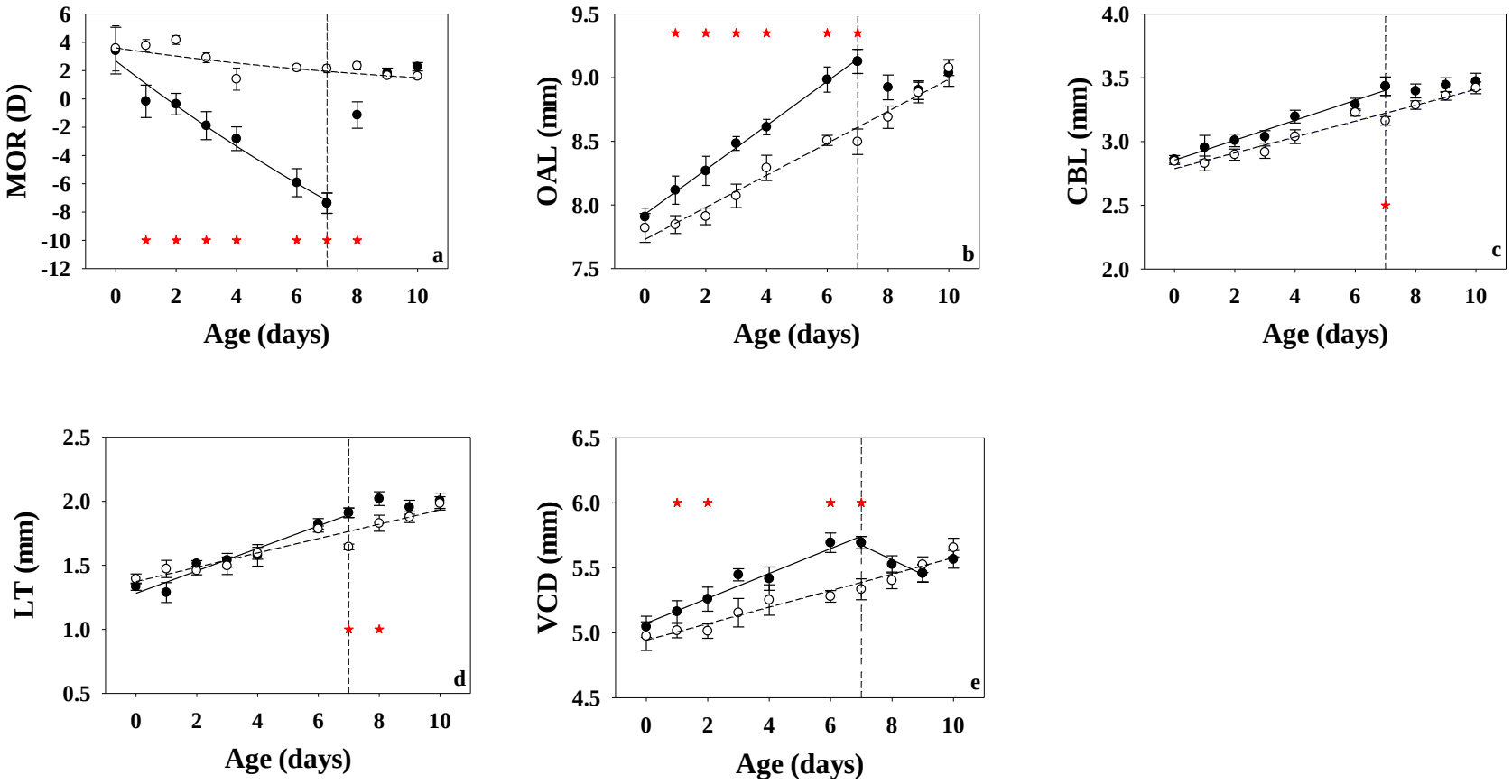


**Figure 5-1 (a) MOR, (b) optical axial length (OAL), (c) corneal to back lens distance (CBL), (d) lens thickness (LT), and (e) vitreous chamber depth (VCD) in 6 chicks during LIM and its recovery as a function of age.**

Open circles represent control eyes of the goggled birds, and closed circles are treated eyes before and after goggle removal (vertical dashed lines). Error bars are standard errors of the mean (SEM) across one cohort of 6 birds on each day. Red stars indicate the significant differences between eyes (paired t-tests).

Control eye data were fitted with dashed curves, and treated eye data were fitted with solid curves. MOR (a) data were from H-S measurement; exponential fits ($p<0.02$) are shown. The treated eye during LIM can also be fitted with a linear function with better F statistics, but the two fits overlay. Linear fits ($p<0.03$) in (b) to (e) are shown.

MOR and OAL were plotted for 6 chicks which also had measurements of CBL, LT, and VCD. Another cohort of 6 chicks had MOR and OAL measurements (not shown in Figure 5-1). Between the two cohorts, MOR for control eyes showed no significant difference on days 0, 4, 7, and 10; and MOR for treated eyes showed no significant differences on 0, 2, 4, 7, and 8. OAL for two cohorts were measured by two different A-scan systems, but there is no difference between systems (see A-2 Comparison between Two Ultrasound Systems in Appendix A). OAL values between the two cohorts are not significantly different on and after day 7 for both control and treated eyes; the differences before day 7 are possibly due to the individual variability.

### 5.3.2 Relative Changes in CBL and OAL and Relationship between N′ and CBL

Considering that CBL during LIM (Figure 5-1c) and LT on day 7 (Figure 5-1d) in treated eyes differ from control eyes, it is interesting to know how the front of the eye, having all components of the eye's optics, changes with OAL, and whether we can infer how the nodal point position changes with respect to the front of eye expansion.

The change in the front of the eye, specified by the change in CBL, is found to be proportional to the change in OAL (Figure 5-2a, averaged points) during LIM and its recovery for control and treated eyes. The slope for treated eyes during LIM (slope=1.3±0.1 for fit to individual points, Figure B-1 and Table B-1 in Appendix B) differs significantly from 1 but not from the other slopes; the other slopes are not significantly different from 1.0. If all points under different rearing conditions are pooled, the slope of the resulting fit is 1.12 (Figure 5-2a). Given data from Schaeffel and colleagues,[45, 53] and the method outlined in the figure caption (Figure 5-A2 in Appendix-5.6.3), the position of N′ from anterior cornea moves proportionally as CBL expands during LIM and its recovery (Figure 5-2b).These results are the bases of Assumption 4.

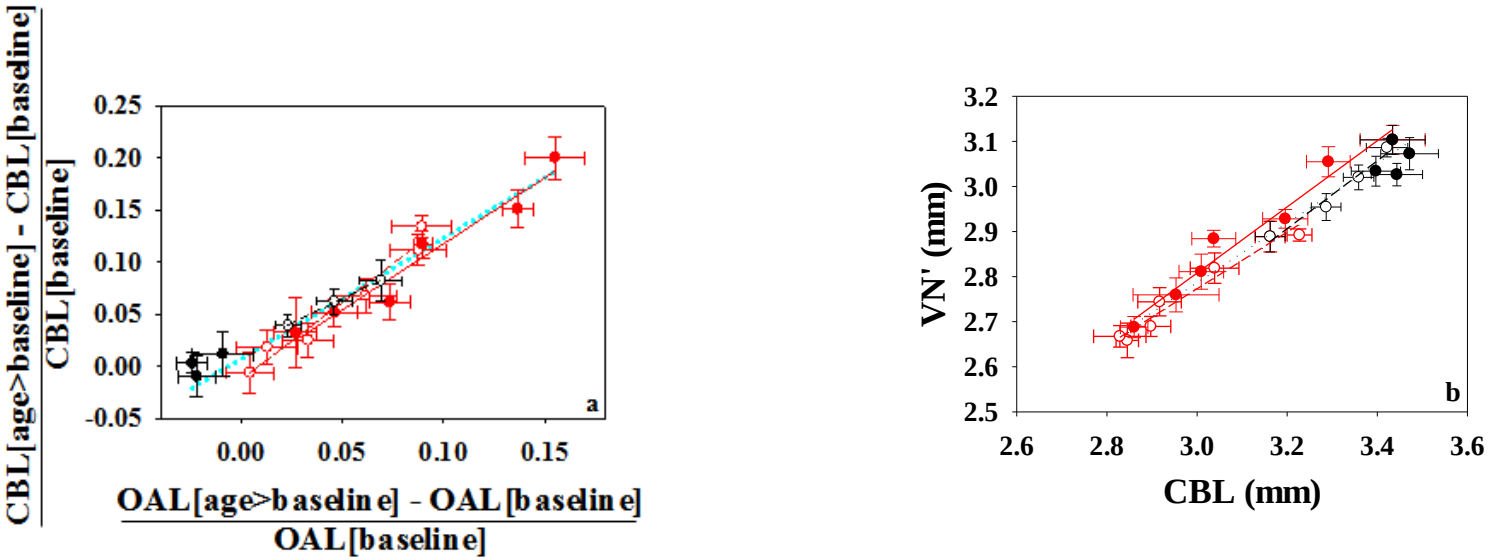


**Figure 5-2 (a) Relative change in CBL versus relative change in OAL. (b) Anterior cornea to N′ distance versus CBL.**

Open and closed circles are control and treated eyes, respectively. Red and black symbols represent data during LIM and recovery, respectively. Each point is an average across 6 birds. Error bars are SEMs.

In (a), relative change in CBL with respect to the baseline, either day 0 in LIM or day 7 in recovery varies linearly with relative change in OAL. Dashed lines are fits for control eyes (all $p<0.0001$), and solid red line is the fit for treated eyes during LIM ($p=0.006$). The fit for points for treated eyes during recovery is not significant. In (b), VN′ was calculated using the relationship of $N'R' = 0.66 \times OAL$ (see Appendix-5.6.3). Dashed lines are fits for control eyes (all $p<0.02$), and the solid red line is the fit for treated eyes during LIM ($p<0.0001$). The fit for points for treated eyes during recovery is not significant. Individual fits are not very different from the overall fit (dashed turquoise line, $p<0.0001$) with 95% confidence intervals (95% CI) overlapping with each other.

### 5.3.3 Eye Power Variation

Two cohorts of chicks had their MOR measured under the same experimental conditions. Their OAL was measured by different ultrasound systems. There is a high correlation and no difference between the two A-scan systems (Section A-2 Comparison between Two Ultrasound Systems in Appendix A); differences in the OAL values before day 7 are probably due to the variability within birds. Therefore, the two cohorts of chicks can be combined for an eye power calculation. The combined MOR (Figure 5-3a) and OAL (Figure 5-3b) change in the same ways as the individual cohorts (Figure 5-1a and b).

**Assumption 1** constrains both cardinal point positions and eye power of the treated eye to be the same as the control eye. If Equation (3-3) is used to calculate eye power with the principle point positions from the control eyes used to derive k′, the calculated eye power is inconsistent with the assumption of constant power (also see Figure 5-A1); therefore, it is not further considered.

Because the result in Assumption 1 shows that there is a change in the optical properties in the eyes with treatment, a change in either cardinal point positions or the eye power or both, we then loosen the constraint by holding the distance from the vertex to P′ (an important cardinal point) to be the same but allowed eye power to vary in the treated eye compared to the control eye (**Assumption 2)**. Under this assumption, during LIM, eye power (Figure 5-3c) in both eyes decreased (ANOVA, by day $p<0.001$, by eye $p=0.003$). Eye power in treated eyes became significantly different from the control eye on days 4 (paired t-test, $p=0.009$) and 7 (paired t-test, $p<0.001$). After goggle removal, eye power changed by eye ($p<0.001$)

and by day ($p<0.001$). Within treated eyes, eye power decreased significantly between days 7 and 8 (paired t-test, $p=0.028$) and remained significantly different from control eyes on day 8 (paired t-test, $p=0.03$). Between days 8 and 9, eye power in treated eyes did not change significantly, while eye power in the control eye continued to decrease. After day 9, eye power values in both eyes were not significantly different from each other.

**Assumption 3** assuming that the anterior cornea to N′ distance divided by OAL remains 0.66 after treatment, is based on the literature reported relationship for the distance from N′ to anterior retina and OAL (see Appendix-5.6.3 for more details). Given this assumption, during LIM, eye power (Figure 5-3d) in both eyes decreased (both $p<0.01$) (by day $p<0.001$, by eye $p=0.042$). Eye power in treated eyes became significantly different from the control eye on day 4 (t-test, $p=0.03$). After goggle removal, eye power varied by day ($p<0.001$) and by eye ($p=0.019$). Eye power in treated eyes decreased significantly between days 7 and 8 (t-tests, $p<0.001$), showing a borderline difference in power between eyes on day 8 (t-tests, $p=0.051$), then power remained relatively constant between days 8 and 9. Meanwhile, power in control eyes decreased significantly. Eye power decreased similarly in both eyes between days 9 and 10.

In **Assumption 4**, movement of N′ in the treated eye compared with the control eye is associated with the expansion of CBL or OAL in a linear relationship as found in Figure 5-2a (also see Figure B-1a). During LIM, eye power (Figure 5-3e) only showed a by day (both $p<0.001$) difference without a difference between eyes, and a borderline difference in power was found on day 4 (paired t-test, $p=0.046$). During recovery, as in the control eye, eye

power in the treated eye showed a significant decrease between days 7 and 8 (t-tests, p=0.003), but unlike the control eye, was not significantly different between days 8 and 9; however, there was no difference by eye (ANOVA).

All three models showed a decrease in eye power from 195 D to 165 D by day. If we use Assumption 3 that the P′ position remain the same between eyes (Figure 5-3c), the measurements of OAL and MOR predict an eye power change between eyes. If we let N′ position change between eyes (Figure 5-3d and e), no significant difference in eye power was found. However, this indicates that there is a change in the optical properties (either P′ or power between eyes during LIM and recovery). In addition, under all three assumptions, eye power in treated eyes decreases significantly between days 7 and 8 and then remains relatively constant between days 8 and 9.

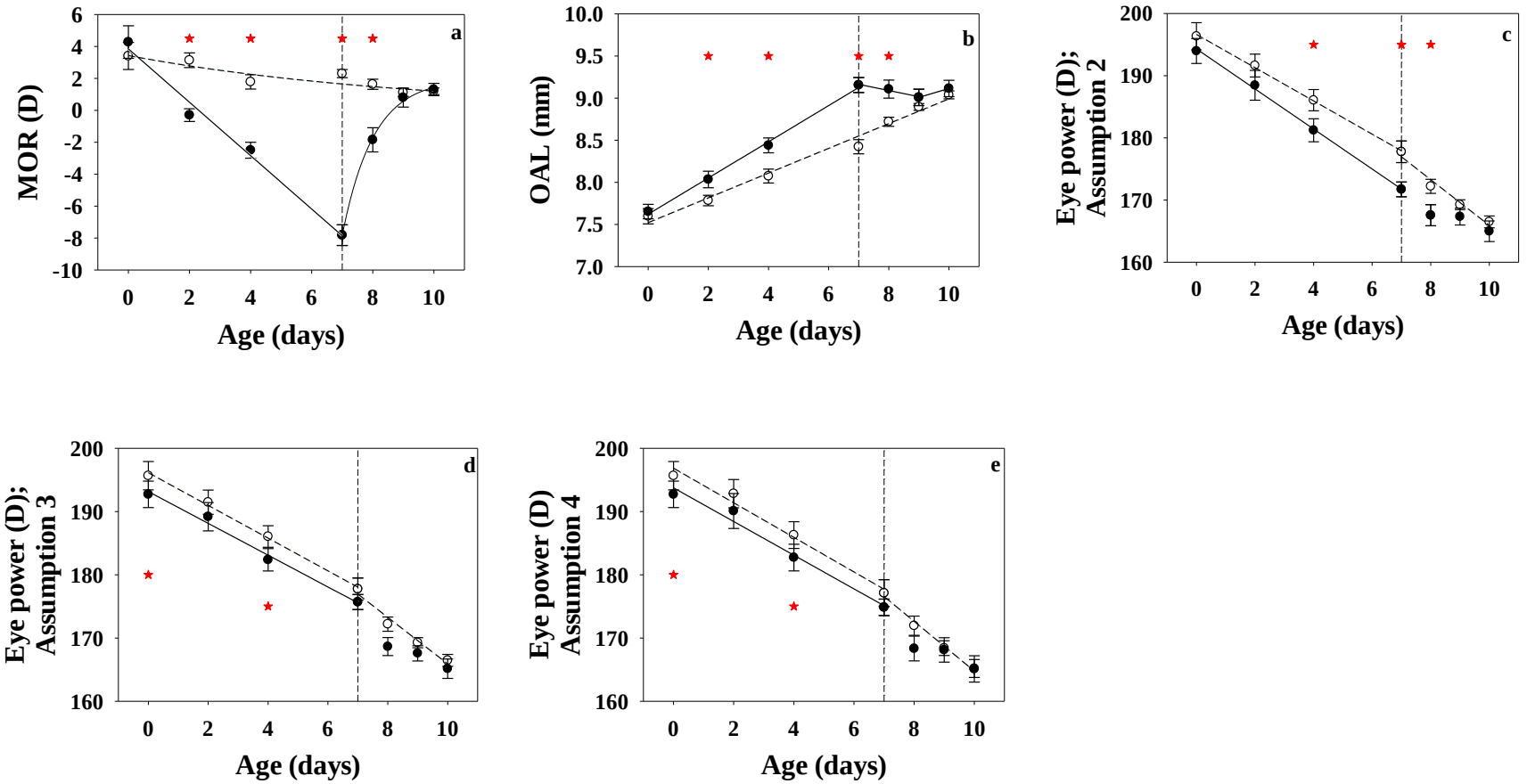


**Figure 5-3 (a) MOR, (b) OAL, and calculated eye power with (c) Assumption 2, (d) Assumption 3, and (e) Assumption 4 for 12 chicks during LIM and its recovery as a function of age.**

Control eyes of the goggled birds are the open circles, and treated eyes are the closed circles before and after goggle removal (vertical dashed lines). Error bars are SEMs across 12 birds on each day. Red stars indicate the significant differences between eyes (paired t-tests).

Here, MOR data (a) were from H-S measurement. The difference in eye power on day 0 in (d) and (e) is probably due to the combination of slightly bigger MOR and OAL in treated eyes (before treatment).

## 5.4 Discussion

### 5.4.1 Myopia Progression and its Recovery and Dimensions

The chick eye responds to an imposed negative powered goggle relatively quickly, and the difference in MOR between eyes is significant after the first day of goggling (Figure 5-1a). When MOR were fitted to exponential functions, the time for a 50% change (t50) in MOR for treated eyes (14 days) found here is longer than control eyes (t50=8 days). Treated eyes change on average by -12 (±4) D between days 0 and 7 across the 12 birds, so that 60% emmetropization to the -15 D hyperopic defocus (from initial positive MOR) is completed by day 7, while 100% recovery took place between days 7 and 9.

There are two possible reasons for the faster emmetropziation during recovery. As previous work in chicks, variation in MOR due to treatment is associated with the change in choroidal thickness.[65, 66] During emmetropization, the choroid responds rapidly, thinning in response to hyperopic defocus,[57, 66] and thickening during recovery from the induced myopic defocus pulling the retina back or pushing it forward respectively. It can thicken more than it thins, resulting in a faster recovery from induced defocus,[129] to move the retinal plane to the focal plane. It is also possible that the by eye difference in eye power contributes to the faster emmetropization during recovery (also see section 5.4.3).

More negative MOR in goggled eyes was significantly associated with longer OAL ($p=0.0001$) as previously shown.[51] As expected, once myopia was induced, axial distance (such as LT, CBL, VCD; Figure 5-1) elongated more relative to control eyes (Figure 5-1). In chicks goggled by negative lenses, axial elongation increases was accompanied by an

increase in eye volume (about 6% for -7 D lenses) while positive lenses produced a decrease in axial length with a decrease in eye volume (of about 2% for +7 D lenses).[130]

During normal development, as being observed in chicks during the first week, intraocular pressure (IOP) increases which is associated with an increase in OAL.[131] The most plausible prediction is that the chick eye expands as IOP increases,[132] as seen in the 1-1 relationship of the relative change in CBL during emmetropization, suggesting an axial expansion. However, a smaller relative change in cornea radius compared to that in OAL (Figure 4-7c) is probably because of a lower pressure seen within the cornea region (through modeling), presumably because of a greater thickness of the corneo-scleral shell in this region.[132] Considering our results did not see an increase in anterior chamber depth within the control eye (probably due to lack of accuracy for the measurement; figure not shown), this suggests an increase in the lens thickness, as seen (Figure 5-1d). Higher IOP has been associated with myopia.[133] Relative changes in CBL and OAL in treated eyes are significantly different from (larger than) the control eye ($p<0.001$), and on day 7, the significant change in CBL between treated and control eyes was 43% of the change in OAL. The rest of the change to OAL was contributed by the VCD. We do not have data for equatorial changes which are likely to differ from axial changes.[133, 134]

### 5.4.2 Anterior Part of the Eye

Unlike our results showing linear changes in CBL and VCD with age which contribute to emmetropization during normal growth in chick, others have reported a differential effect of CBL and VCD on emmetropization between the first three days and later periods.[39] During

form deprivation myopia, Wallman and Adams[58] reported that an increase in anterior chamber depth (ACD) occurs later in the course of the myopia and is considered of separate origin to the VCD change. Our results for lens-induced changes and recovery show proportional changes in anterior chamber (CBL) and VCD. The contribution of CBL to total OAL elongation is 36 to 39% throughout the entire experimental period, in both control and treated eyes. Considering OAL in the treated eye is significantly longer than in the control eye, the larger increase in CBL is a reflection of its relative increase in proportion to OAL. This confirms that the enhanced growth in the anterior part of the eye occurs with the enhanced growth in VCD,[135] resulting in significant differences in CBL and VCD with treatment. In addition, since CBL has a faster relative increase than OAL in the treated eye, on day 7 (Figure 5-2a and also Figure B-1a), a 43% contribution by CBL to the total OAL increase between treated and control eyes, which is in agreement with the report that both ACD and VCD are important to elongation.[58] Our data suggests that changes in CBL are important in both normal emmetropization and emmetropization to negative lenses, as well as recovery from LIM. The changes in CBL and LT are consistent with changes in the optics of the eye with growth and between control and treated eyes.

### 5.4.3 Possible Changes in Ocular Optics during Myopia Development and Recovery from It

Static lens power with treatment in chick has been reported,[69, 136] despite the change in size, shape or refractive index distribution. Lens power has also been reported to increase (shorter focal length) within form-deprived myopic eyes.[70] Reports on the change in the cornea during

LIM are inconsistent.[53, 136] The lack of agreement and the change in power given by calculations with Assumption 1 indicates that a change in in the optics (either a movement of the cardinal points or a change in power) is associated with myopia induction and its recovery. Therefore, the assumption was loosened by keeping P′ at the same position in both eyes (Assumption 2). An ANOVA indicated significant difference in the calculated eye power between treated and control eyes during LIM (Figure 5-3c), and on day 7, there was a lower eye power in treated eyes (Figure 5-3c), in agreement with the thicker lens observed (Figure 5-1d), in a direction opposite to the emmetropization to negative lenses as suggested above. During recovery, a significant difference in eye power between eyes continued on day 8. The significant decrease in eye power within treated eyes between days 7 and 9 but smaller than the change within control eyes resulted eye power to be not significantly different on day 9, suggesting a contribution of eye power to the rapid initial emmetropization during recovery.

Alternatively, instead of keeping cardinal points fixed, we allowed them to move. Assumption 3 incorporates an increase of anterior cornea to N′ distance in proportion to OAL expansion, and Assumption 4 incorporates a movement of N′ in proportion to CBL expansion (equivalent to assuming that the optics all expands at this rate). Assumption 3 was based on the experimentally measured N′ to anterior retina distance for normal[45] and treated eyes[53] from the literature data. The proportionality ratio was set to be 0.66, determined after fitting the values (of N′ location) with linear functions as a function of eye length (either OAL or axial length) while constraining the intercept to be zero (also see Figure 5-A2 in Appendix-

5.6.3). Alternately, the experimental change in CBL is proportional to the change in OAL suggests the front of the eye is growing at a rate related to OAL elongation; therefore, we can assume that the relative movement in N′ is the same as the relative change in CBL[137] (Assumption 4).

For Assumptions 3 and 4, after treatment, there is no significant difference between eyes except for day 4 during LIM. However, for assumption 4, the ANOVA only showed a by day difference. Previously, we calculated eye power by considering the relative movement in N′ to be the same as the relative change in CBL (similar but not identical to Assumption 4);[137] then eye power in both eyes became not significantly different from each other either during recovery. As in Assumption4, N′ moves but eye power (N′F′) remains the same as in the control eye except possibly on day 4 (paired t-tests). If we consider a simplified model having both cornea and crystalline lens as thin lenses, and a possible decrease in corneal power in treated eyes relative to control eyes, due to a bigger proportional expansion in CBL, lens power would need to increase compared to control eyes to give constant power. The hypothetically more powerful lens does not agree with a thicker lens observed in treated versus control eyes on day 7 (Figure 5-1d), unless the radii of curvature of the lens decrease significantly or the refractive index distribution changes. However, this model is still consistent within itself since a more powerful lens would shift N′ further away from the vertex, with a distance smaller than the axial elongation, resulting in a shorter N′F′ distance but a longer N′ to retina distance, agreeing with the literature measurement.[53] Alternatively, if corneal power does not change significantly between control and treated eyes, with no

significant difference in anterior chamber depth being seen on day 7, the lens power must stay the same. However, for N′ to move while lens power is unchanged and thickness changes, changes in lens radii are expected.

Verification for the assumptions of cardinal point positions or power relationships is currently not possible due to lack of additional information (radii of curvature, refractive index of the lens). Therefore, we do not know which assumption is more closely related to the reality. This information could be assessed, hopefully through two-dimension optical coherence tomography (OCT; see Chapter 6). However, all results are consistent with the optics of the eye changing during LIM and its recovery relative to the control eye.

### 5.4.4 Influence of Measurement Techniques on Eye Power Calculations

During normal growth, the influence of the F′ to anterior retina distance is considered small, and OAL and MOR come into the calculation of eye power only once during its derivation.[113] Within myopic eyes, the calculation is modified to take into account this distance, which is a function of MOR and distance N′ to the anterior retina, when deriving the optical length, so MOR comes into the equation three times (see Appendix-5.6.2) during the eye power calculation (under Assumptions 3 and 4). The accuracy and precision of the MOR measurement is therefore crucial in terms of calculating changes in eye power with treatment.

MOR can be measured by either retinoscopy or H-S techniques. A careful determination of MOR using retinoscopy has a high correlation to the H-S results but is slightly more hyperopic than H-S measurement,[42] possibly due to chromatic aberration and/or a

wavelength-dependent error called the small eye artefact,[93] in contrast to observations reported by de la Cera.[138] Before the H-S data was analyzed, we previously reported a difference in eye power between eyes during recovery under Assumption 3 and an assumption similar to Assumption 4, using retinoscopy measured MOR,[137, 139] where we assumed that reflections in retinoscopy come from the vitreous/retinal interface; and we defined OAL as the distance from anterior cornea to anterior retina. Considering that H-S MOR has better accuracy than retinoscopy,[87] we then analyzed the H-S data and have now show no change in eye power except on day 4 under Assumptions 3 and 4. The question remains whether H-S MOR and OAL have the reflection originating from the same interface, in other words, whether the reflection of the laser (633 nm) in H-S measurement originates at the vitreous/retinal interface as we assumed or potentially deeper in the retina, towards the photoreceptor layer.

### 5.5 Conclusions

Emmetropization to hyperopic defocus (LIM) is partially due to an increase in CBL; the anterior segment is also important. The distance between the corneal vertex and rear of the crystalline lens (CBL) contributes to changes in OAL in LIM. Significantly thicker lens and CBL in the treated eye was observed. During recovery, OAL and VCD decrease and LT and CBL remain relatively constant between days, while MOR magnitude decreases. Emmetropization following goggle removal is more rapid than to the goggle. Eye power

calculated based on different assumptions confirm a change in optics between treated and control eyes during LIM, either in the positions of cardinal points or in the focal length, depending on the assumptions used. Changes in curvatures, which may help to differentiate cardinal point movements from power changes, remain to be assessed. During recovery, power appears to decrease rapidly and may accelerate emmetropization. After emmetropization is complete in recovery, neither dimensions nor power differ between the two eyes.

## 5.6 Appendix

### 5.6.1 Predicted MOR in the Treated Eye

If we constrain the cardinal point positions (for example, $\overline{VP'_t} = \overline{VP'_c}$) and eye power ($F_{e_t} = F_{e_c}$) to be the same in treated eyes as in control eyes, then optical length in the treated eyes can be calculated from the positions of the principal planes in the control eyes. Therefore, the expected power is the difference between dioptric length and MOR within treated eye (from Eqn. 3-3)

$$F_{e_t} = \frac{n'}{k'_t} - MOR_t. \qquad \text{A1}$$

The resulting change in power between control and treated eyes (Figure 5-A1) is inconsistent with the initial assumption.

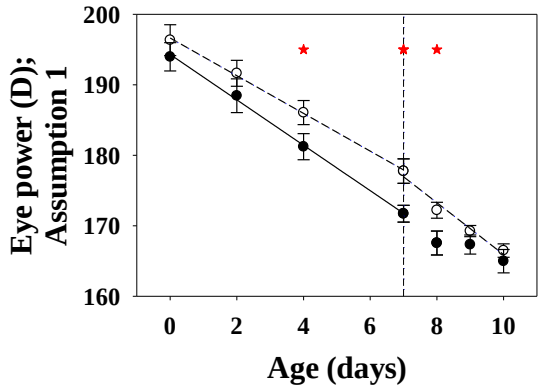


**Figure 5-A1 Comparison of eye power calculated under assumption 1 between control and treated eyes**

Closed and open circles are eye power for treated and control eyes before and after goggle removal (vertical dashed lines). Error bars are SEM across 12 birds on each day. Red stars indicate the significant differences between eyes (t-tests), suggesting that the optics in the treated eye differs from the control eye. This is contradictory to the assumption that the optics in the treated eye does not change compared to the control eye

### 5.6.2 Eye Power Calculations in Myopia Eyes

The power of the eye can be expressed as[4]

$$F_e = \frac{n'}{k'} - MOR, \qquad 3\text{-}3$$

where $n'$=1.335[43, 45] is the refractive index of the vitreous , and $k'$ can be calculated from the positions of the cardinal points

$$k' = \overline{P'R} = \overline{P'F'} + \overline{F'R}, \qquad A2$$

where the positions P, P′, F, and F′ are 1st and 2nd principal points and focal points, and R is the photoreceptor layer. Given that $\overline{P'F'} = -\overline{NF}$ and $\overline{PF} = -\overline{N'F'}$;[4] the relation between 1st and 2nd focal lengths is $f = \overline{PF}$, $f' = \overline{P'F'}$ and f′/f=n′/n, where n is the refractive index of air. Therefore,

$$k' = \frac{n'}{n} \times \left(\overline{N'R} + \overline{RF'}\right) - \overline{RF'}\,, \qquad 3\text{-}4$$

where the information of $\overline{RF'}$ can be derived from the MOR,

$$\overline{F'R} = -\frac{f' \times k'}{n' \times PO_{FAR}}. \qquad A3$$

$PO_{FAR}$ is related to MOR by the following relationship

$$\frac{1}{PO_{FAR}} = MOR\,. \qquad A4$$

From Eqn.s A3 and A4

$$\overline{RF'} = -\frac{f \times k' \times MOR}{n}, \qquad A5$$

and replaces f by negative $\overline{N'F'}$, then

$$\overline{RF'} = \frac{\overline{N'R} \times k' \times MOR}{n - k' \times MOR}. \qquad A6$$

In the low hyperopic MOR (normally smaller than 10 D, on average 6.5 D) in the normally developing eye, $\overline{RF'}$ to $\overline{N'R}$ ratio is always within 4% when the eye emmetropizes from a small hyperopic amount, meaning Eqn. A6 can be approximated to zero during the calculation of k′. However, in the high hyperopic (larger than 6.5 D) or myopic (treated) eye, the assumption that $\overline{RF'}$ is small does not hold, and $\overline{RF'}$ is about 11% of $\overline{N'R}$ of the myopic eye on day 7. Therefore, it

is important to consider the distance $\overline{RF'}$ during the derivation of k′. Substituting Eqn. A6 into Eqn. 3-4, the expression of k′ can be finally derived from the following quadratic equation

$$n(k')^2 + \left[\frac{-n^2}{MOR} - n \times \overline{N'R}\right]k' + nn' \times \frac{\overline{N'R}}{MOR} = 0. \quad \text{A7}$$

Therefore,

$$k' = \frac{-B \pm \sqrt{B^2 - 4AC}}{2A}, \quad \text{A8}$$

where $A = n$, $B = \frac{-n^2}{MOR} - n \times \overline{N'R}$, and $C = \frac{nn' \times \overline{N'R}}{MOR}$. Positive or negative sign is chosen in Eqn. A8 for negative or positive MOR value in order to get a reasonable k′ value.

Because there is no consistently reported photoreceptor layer location for chick, we use the anterior retina (R′) instead of the photoreceptor layer (R) in calculating k′ and $\overline{N'R}$.

### 5.6.3 N′ to Anterior Retina versus OAL

In Assumption (3), the same 0.66 ratio of N′ to anterior retina distance to OAL was used in both control and treated eyes for the following reasons:

(1) The relationship between N′ to anterior retina distance and eye length measured in digitized video images are not very different in normal (0.64) and experimental (0.63) birds older than day 15;[45, 53] therefore, it is possible that normal and experimental eyes have similar ratios.

(2) When N′R and OAL were measured by ultrasound for experimental birds aged 26 days,[53] a slope of 0.66 can be determined when the curve is fitted with a zero intercept. The same slope of

0.66 as found for normal birds before day 15. Therefore, it is possible that the ratio does not change with age.

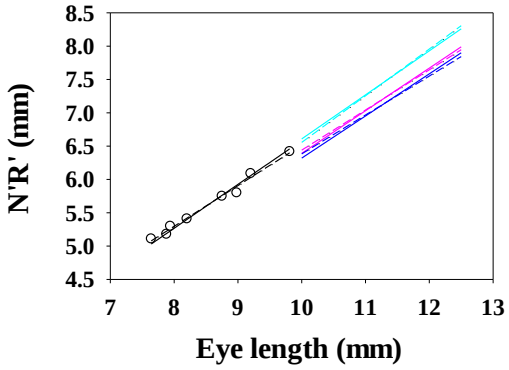


**Figure 5-A2 N′ to anterior retina (R′) distance as a function of eye length.**

Eye length is measured either by ultrasound or in digitized image. If measured by ultrasound, the eye length is from anterior cornea to anterior retina, which is OAL. If it is measured in digitized image, the value is bigger than OAL.

Open circles are N′ to anterior retina distance versus eye length (it is OAL in this case) data from Irving and colleagues[43] and Avila and McFadden[39] for normal birds before and on day 15. Data were fitted with linear functions with (black dashed line, with insignificant intercept value) and without (black solid line, $y = (0.658 \pm 0.003) \times \text{OAL}$, $p<0.0001$) intercept.

Pink dashed line is the regression taken from Schaeffel and Howland[45] for normal birds (age ranged from 14 to 86 days), $y = 0.4121 + 0.6208 \times$ eye length, where eye length is measured in a digitized image. If we set the intercept to be zero (pink solid line), the slope becomes 0.639.

Blue and turquoise dashed lines are regressions taken from Schaeffel and colleagues[53] for an experimental birds (age 26 days) with length measured in digitized video image ($y = 0.544 + 0.584 \times$ eye length) or by ultrasound ($y = -0.443 + 0.7 \times \text{OAL}$). Blue and turquoise solid lines are the fits for corresponding regression when both intercept to be zero. The blue solid line has a slope of 0.632, and the turquoise solid line has a slope of 0.661.

# Chapter 6

# Comparison of A-scan Ultrasonography and Anterior Segment Optical Coherence Tomography (AS-OCT) in the Young Awake Chick Eye

*The Visante Anterior Segment Optical Coherence Tomographer was borrowed from Dr. Luigina Sorbara from the Center of Contact Lens Research. The experiment was performed with the help of Kisilak. Kisilak provided experience with other topographers that had been tested prior to this one.*

***The author of the thesis*** *handled the animals during the experiment while Kisilak controlled the computer for image acquisition and dimensional measurement using A-scan ultrasound. The author of the thesis collected and analyzed the OCT images after discussion with Dr. Campbell, Dr. Sorbara, Dr. Natalie Hutchings, and Kisilak. The author of the thesis performed Bland-Altman Analysis and came up with possible explanations for the discrepancies between ultrasound and OCT measurements of anterior chamber depth, lens thickness and cornea to back lens distance, and discussed with Dr. Campbell. Dr. Campbell provided critical revision after the author of the thesis finished writing the first draft of the chapter.*

**ABSTRACT**

**PURPOSE:** To compare ocular biometry [anterior chamber depth (ACD; anterior cornea to anterior lens), lens thickness (LT), corneal to back of the lens (CBL)] using A-scan ultrasonography and Visante anterior segment optical coherent tomography (AS-OCT) in the chick eye.

**METHODS:** Six Ross Ross alert normal chicks were measured by A-scan ultrasound and Visante AS-OCT on days 1, 2, 3, 7, 9, and 14 between 8:00 to 11:00 am. In the AS-OCT images, physical distances were determined by dividing the optical path length by the refractive index. Bland-Altman plots and correlation analyses between methods were performed on one eye of each chick.

**RESULTS:** There was a high correlation between methods for LT ($r=0.8502$, $p<0.0001$) and CBL ($r=0.9329$, $p<0.0001$), but not for ACD ($r=0.0303$; $p=0.8649$). Measurements by AS-OCT were more precise (smaller standard deviation, SD). Bland-Altman plots showed that there were dimensional-dependent biases of opposite sign in measurements between techniques for ACD and LT. CBL showed a bias not significantly different from zero.

**CONCLUSIONS:** A high correlation between both techniques was found for LT and CBL after physical distances were calculated from the optical path lengths in AS-OCT. Measurements of CBL are very similar between the two techniques but AS-OCT is more precise. The dimensional-dependent bias in ACD and LT suggest that rotation during ultrasound measurement is most likely the major reason for the discrepancies with AS-OCT.

With this OCT instrument, limitations in depth penetration will not allow measurements of CBL elongation on birds with lens-induced myopia.

**Keywords** A-scan ultrasound • Visante anterior segment optical coherent tomography·• Chick • Ocular biometry

## 6.1 Introduction

The chick is a popular model for the study of both normal emmetropization and the development of induced refractive error because of its rapid growth changes and its independent feeding after hatching.[47] Ocular changes,[39, 43, 45] including refractive error, are measured together with image blur,[12, 42] hoping to better understand emmetropization and myopia development. A-scan ultrasonography is extensively used to measurement ocular changes, such as optical axial length (OAL; anterior cornea to anterior retina), anterior chamber depth (ACD; anterior cornea to anterior lens), lens thickness (LT), and vitreous chamber depth (VCD). An ultrasound biomicroscope[75] as well as optical low-coherence interferometry[103] have been tested within the chick eye. Procedures established for measurements within the small chick eye involve anesthesia and lid retractors because awake animals close their eyes quickly before measurements can be taken, especially newly hatched birds. However, repeated anesthesia affects the growth rate of the animals[39] and isoflurane together with lid retractors change the optical properties of the eye.[83] Avoidance of repeated anesthesia and lid retractors is best,[83] even though it makes measurements more challenging.

A typical A-scan ultrasound transducer in an ophthalmological system has a sound wave with a frequency of 10-30 MHz, which limits the resolution of finer details. The transducer is placed in front of the eye with either a soft rubber bath (immersion mode)[58, 103] or direct contact (contact mode). The former gives improved measurement within the eye. However, three different immersion instruments (including A- and B-scan ultrasound, and ultrasound biomicroscopy) failed to give adequate peaks when used on alert chicks. A minor cornea

indentation is considered the biggest disadvantage for contact A-scan ultrasonography but can be minimized after practice. Contact ultrasonography is not able to provide a measurement of corneal thickness.

In ultrasonography, time delays of various reflections are recorded. Because sound waves travel at various speeds in different media, calibration is needed to convert time delays into physical distances by multiplying by the speed of sound. Repeated measurements are required, and careful decisions are necessary to select images indicating good axial alignment. Alternatively, optical coherence tomography (OCT) provides ocular biometry measurement *in vivo*. Physical distances are obtained after dividing the measured optical path length by the refractive index of a particular element. OCT is a non-invasive technique, which does not require direct contact with the cornea. Two-dimensional images give more information. However, the available commercial systems are all designed for human eyes, and their measurement ranges do not match the small chick eye. With the anterior segment (AS) OCT (Visante AS-OCT, Carl Zeiss Meditec, Dublin, CA) for the human eye, the 3 to 6 mm image range is ideal for studying properties of the optics (cornea and crystalline lens) of the normal chick eye. The purpose of this study is to compare A-scan ultrasonography (A-scan Plus Connect ultrasound, Accutome, Malvern, PA) with AS-OCT in the anterior chamber of awake chick eyes. Bland-Altman analysis was applied to evaluate precision and to compare the measurements using the two techniques.

## 6.2 Methods

A total of six Ross Ross chicks (Gallus gallusdomesticus) of mixed sex were obtained from a local hatchery (Maple Leaf Poultry, New Hamburg, ON, Canada) on the day of hatching. All chicks developed naturally under a fluorescent light cycle of 14-hour light/10-hour dark during the experiment. Ocular dimensional measurements were performed on days 1, 2, 3, 7, 9, and 14 to ensure measurement values across a relatively large range. Measurements were performed in the morning between 8:00 and 11:00 am, approximately during the same time of the day to avoid the influence of the diurnal variation.[40] Each animal was handled by the same person during measurements. Both ultrasound and AS-OCT measurements were performed on alert chicks. The experiment received ethics approval from the University of Waterloo Animal Care Committee.

The A-scan Plus Connect ultrasound biometry has a 10 MHz frequency transducer and offers a stated clinical accuracy of 0.1 mm for length in human and electronic resolution of 0.016 mm. During the measurement, the contact mode was used, and five scans were obtained during each measurement. A customized program was developed to show a scaled-up view of the complex of reflections originating from the rear of the retina, the choroid, and the sclera complex of the eye.

The Visante AS-OCT is a time-domain instrument with a central wavelength of 1310 nm. Several image scans were obtained for each individual eye. We adjusted the fixation angle to ensure the OCT images were aligned with respect to the geometric axis of the anterior eye.

Both Raw Image Mode (Figure 6-1a) and Raw Image High Resolution Mode (Figure 6-1b) were used to save images. Images were aligned with respect to the geometric axis of the anterior eye. Images with best efforts for alignment along the optical axis (within a 10 degree tilt) were analyzed. Image analysis was performed in Image J. Axial optical path lengths were converted to physical distances with literature refractive indices for different ocular media. The refractive index for the cornea and aqueous were taken to be 1.369 and 1.335.[43] An average refractive index for the chick crystalline lens of 1.396 was used.[45]

A single eye of each bird was analyzed. The eye with more OCT images indicating good alignment was analyzed, and the ultrasound data for the same eye was used. Pearson's correlation coefficient (r) was used to quantify correlations between the two methods. The Bland-Altman plot was employed to indicate the differences between the measured values from the two techniques plotted against the averages. The 95% limits of agreement were defined as mean $\pm$1.96 standard deviations (SD) of the differences between the techniques.

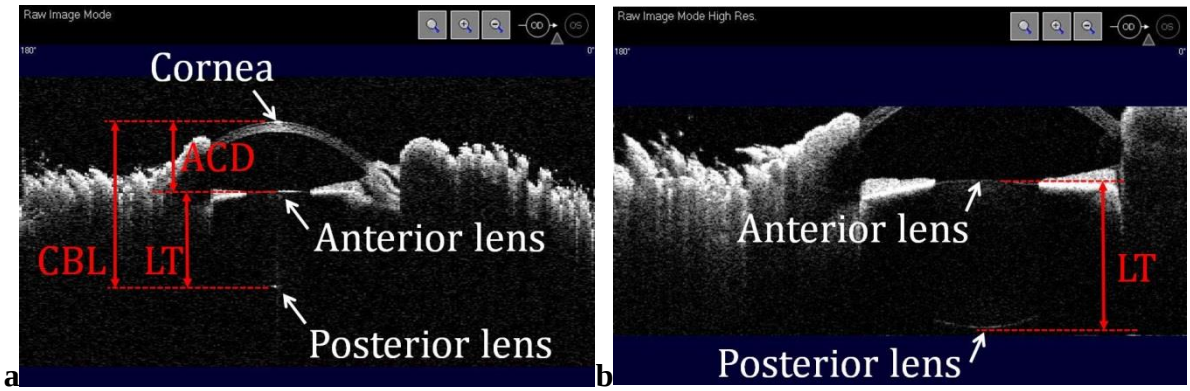


**Figure 6-1 Visante AS-OCT images with good alignment showing the optical path length under (a) Raw Image Mode (16mm×6mm), and (b) Raw Image High Resolution Mode (10mm×3mm).**

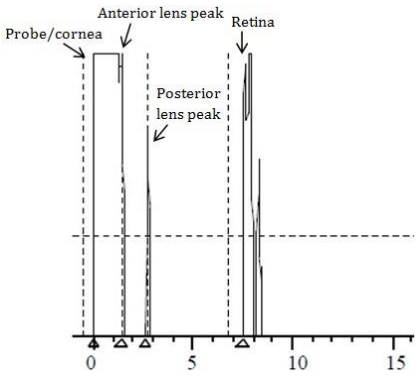


**Figure 6-2 An example of the best A-scan output. Horizontal axis has units of millimeters (mm).**

### 6.3 Results

The results of the pairwise comparisons and the correlations between A-scan ultrasound and Visante AS-OCT for ACD, LT and CBL, including the means of the standard deviations (SD), mean differences, Pearson correlation factors (r), and 95% confidence intervals (CI) for the correlations, are show in Table 6-1 and Table 6-2. In general, the Visante AS-OCT gives a smaller standard deviation (SD) compared with the A-scan ultrasound; however, the SD is only significantly lower during ACD measurement but not for LT or CBL measurement. Pairwise correlations between instruments for LT and CBL were highly significant (both $p<0.0001$) but not for ACD ($p=0.8649$).

**Table 6-1 Comparison of standard deviations (SDs) between ultrasound and Visante AS-OCT.**

| Dimension (mm) | Technique | Mean of SDs (SD of SDs)(mm) | t-test (p value) |
|---|---|---|---|
| **ACD** | Ultrasonography | 0.067 (0.033) | 0.003 |
| | Visante AS-OCT | 0.045 (0.020) | |
| **LT** | Ultrasonography | 0.083 (0.039) | 0.430 |
| | Visante AS-OCT | 0.073 (0.042) | |
| **CBL** | Ultrasonography | 0.108 (0.049) | 0.970 |

**Table 6-2 Pairwise comparisons and correlations between measurements with ultrasound and Visante AS-OCT.**

| Dimensions (mm) | Pearson correlation coefficient (r) | Correlation slope with SE | Slope 95% CI | Correlation p value | Mean Bias(mm) (SD) | Bias 95% CI |
|---|---|---|---|---|---|---|
| ACD | 0.0303 | 0.1 (0.4) | -0.7410 to 0.8773 | 0.8649 | -0.04 (0.15) | -0.0964 to 0.0104 |
| LT | 0.8502 | 0.57** (0.06) | 0.4496 to 0.6970 | <0.0001 | 0.06* (0.15) | 0.0082 to 0.1124 |
| CBL | 0.9329 | 1.04** (0.07) | 0.8981 to 1.1881 | <0.0001 | 0.01 (0.11) | -0.0255 to 0.0541 |

The bias is the difference between ultrasound measured value and the Visante OCT measured value.

* represents that the 95% CI for the bias does not include zero.

** represents that the significant correlation between techniques.

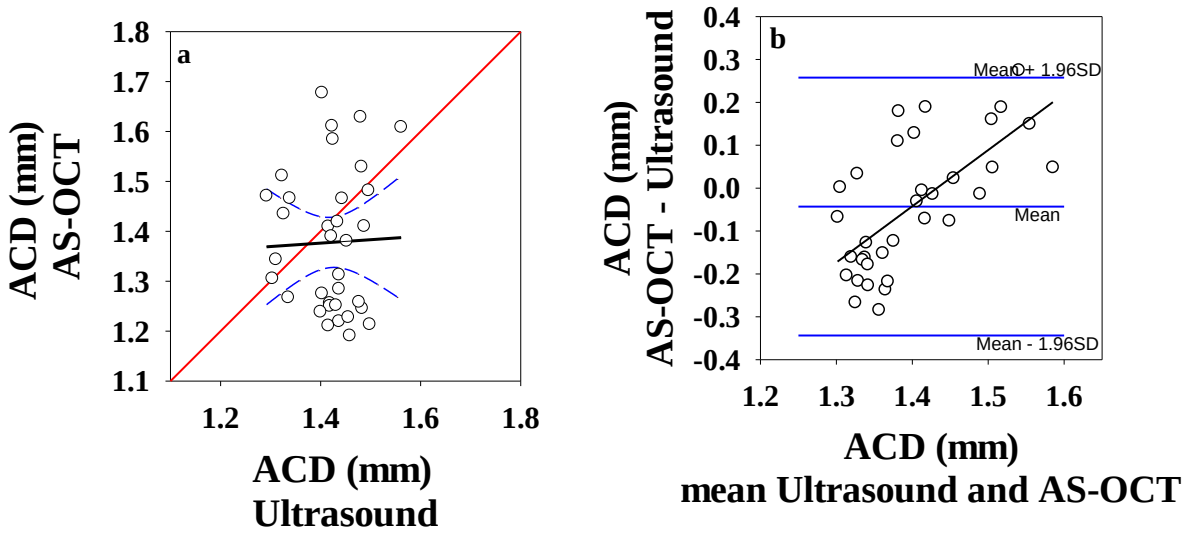


**Figure 6-3 Comparison of anterior chamber depth: (a) Correlation data between A-scan ultrasonography and Visante AS-OCT; (b) Bland-Altman plot.**

In (a), the long red line is the 1-1 line; blue dashed curves indicate the 95% CI. The correlation between ACD measured by Visante AS-OCT and measured by ultrasound, representing by the black solid line, is not significant.

In (b), the blue solid horizontal line in the middle represents the mean of the bias, and the other blue lines indicate the 95% CI. The black solid line is the fit to the bias (Visante AS-OCT minus Ultrasound) versus the mean ($p < 0.0001$).

There is no significant correlation between the two techniques ($r=0.0303$, $p=0.8649$, Figure 6-3a) for ACD. The difference in ACD between the techniques was not significantly different from zero (paired t-test: $p=0.112$; mean bias is not significant different from zero). However, the Bland-Altman plot (Figure 6-3b) showed that there is a dimensional dependence of the

difference between methods (r = 0.6699, p<0.0001, slope = 1.3099 ± 0.2567, Figure 6-3b). The difference between methods (Visante AS-OCT minus ultrasound) is more positive as the ACD increases.

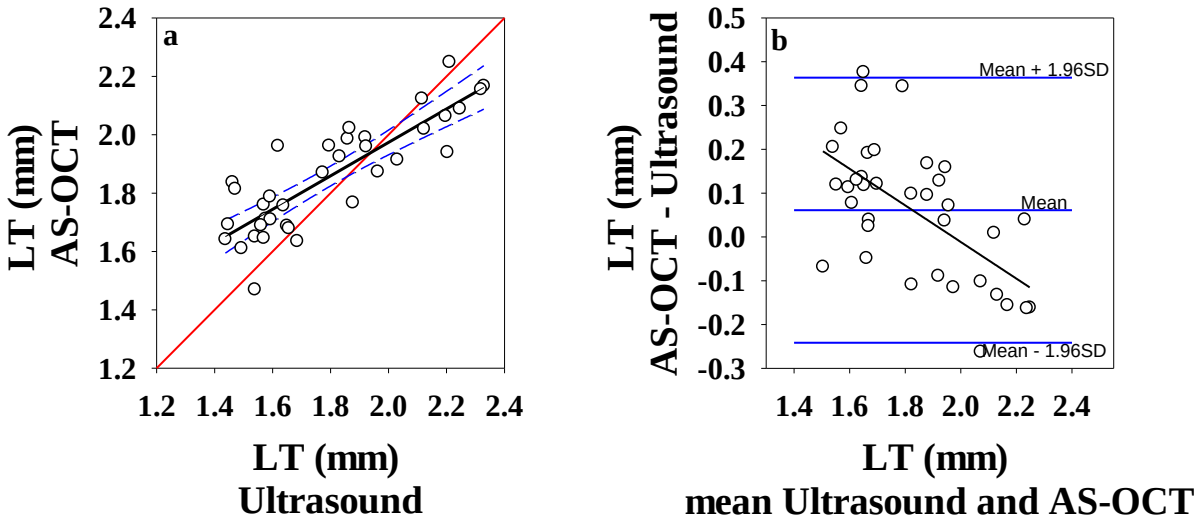


**Figure 6-4 Comparison of lens thickness: (a) Correlation data between A-scan ultrasonography and Visante AS-OCT; (b) Bland-Altman plot.**

In (a), the long red line is the 1-1 line; blue dashed curves indicate the 95% CI. The black solid line is the correlation between LT measured by Visante AS-OCT and measured by ultrasound (p <0.0001).

In (b), the blue solid horizontal line in the middle represents the mean of the bias, and the other blue lines indicate the 95% CI. The black solid line is the fit to the bias (Visante AS-OCT minus Ultrasound) versus the mean (p <0.0001).

The same analysis was performed for LT measurements. Figure 6-4a showed that there is a high correlation between methods (r=0.8502, p<0.0001). No significant difference in LT

between methods was found (Table 6-2). However, the linear regression showed that there is a proportional bias as well as a fixed bias between the two methods (95% CI for the slope is 0.04496 to 0.6970 and for the intercept is 0.6019 to 1.0514). The Bland-Altman plot (Figure 6-4b) illustrates that the Visante AS-OCT has an overall larger value compared to ultrasound, and this difference is significant different from zero (t-test, p=0.02). Interestingly, the difference becomes smaller as the measured LT increases ($r = 0.6092$, $p < 0.0001$, slope = -0.4193±0.0930, Figure 6-4b), opposite to the observation for ACD.

For the CBL measurement, there is a strong correlation between methods ($r=0.9329$, $p<0.0001$, Figure 6-5a). The difference between methods is not significant different from zero ($p=0.471$). Also, the linear regression showed there is neither proportional bias (95% CI for the slope is 0.8981 to 1.1881) nor fixed bias (95% CI for the intercept -0.5950 to 0.3450) between methods. Additionally, the Bland-Altman plot (Figure 6-5b) shows there is no bias between the two methods (0.0143 ± 0.1143). The two methods can be used interchangeably based on the above analysis for CBL.

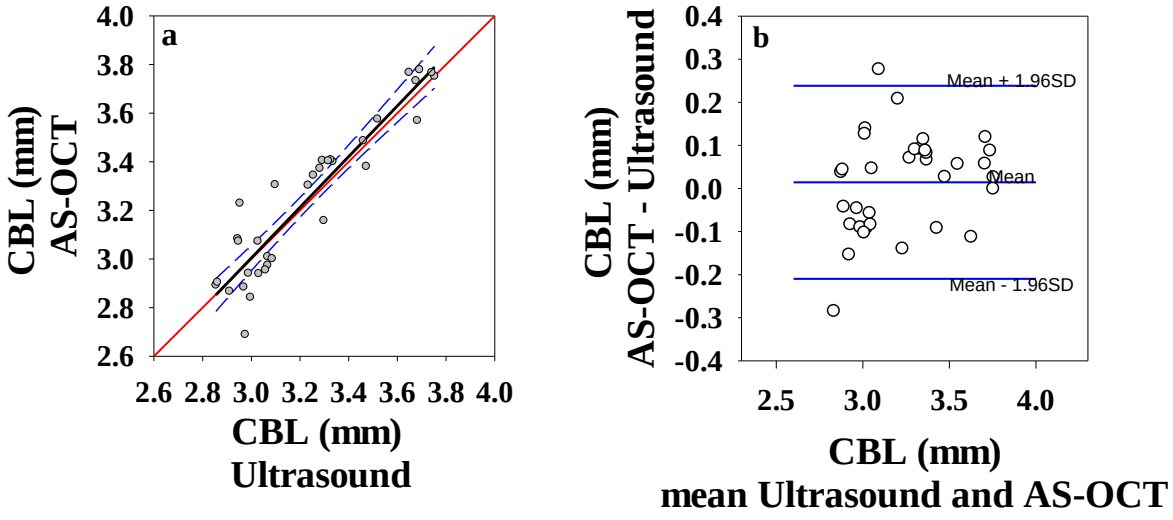


**Figure 6-5 Comparison of CBL measurements: (a) Correlation data between A-scan ultrasonography and Visante AS-OCT; (b) Bland-Altman plot.**

In (a), the long red line is the 1-1 line; blue dashed curves indicate the 95% CI. The black solid line is the correlation between CBL measured by Visante AS-OCT and measured by ultrasound ($p < 0.0001$).

In (b), the blue solid horizontal line in the middle represents the mean of the bias, and the other blue lines indicate the 95% CI. There is no significant dimensional dependence of the difference between techniques.

### 6.4 Discussion

A-scan ultrasonography is a well-established technique for *in vivo* biometric measurement in the eye. Anterior segment OCT has also been used, particularly in the human eye to measure angle anatomy in glaucoma diagnosis.[140] This study made comparison between the A-scan ultrasonography (Accutome, Malvern, PA) and AS-OCT (Visante, Carl Zeiss Meditec, Dublin, CA) in anterior chamber measurements of ACD, LT, and CBL. The results show a

difference in measuring ACD and LT by different techniques, but the measurements of CBL are interchangeable between ultrasound and Vistante AS-OCT. Similar comparison between the ultrasound and OCT (for example with IOLMaster and Lenstar) have been carried out on human eyes, because OCT is a less invasive and possibly more accurate technique[94] for determining intraocular lens parameters than ultrasound.[96, 99-101]

*In vivo* measurements of ocular dimensions designed for human and rodent do not have the right range for chicks because ocular structures are different sizes. The chick is an important animal model for myopia research. Therefore, a comparison between optical and ultrasound techniques in chick is important. Here, we saw a significant increased precision in ACD measurement with OCT but no correlation with ultrasound. Different studies have confirmed that, unlike our results in chick, the human ACD measured with ultrasound is significantly smaller than ACD obtained with optical biometry,[99-101, 141] but whether there is a correlation between the two techniques remains controversial.[101] In chicks, we see a correlation in CBL but not a consistent result of corneal indentation (explained below). Because CBL is the sum of the ACD and LT, the fact that CBL measurement is interchangeable between techniques provides insight into the discrepancies seen in ACD and LT measurements.

Firstly, cornea indentation has been commonly held responsible for the smaller ACD measured by contact A-scan ultrasound. However, we don't see this result with a slightly positive bias in ultrasound. On the other hand, the difference between techniques in CBL measurements should be similar to (in the same direction as) that in ACD but it is not. Most

importantly, there is a dimensional-dependent bias within ACD or LT (as shown in Figure 6-3b and Figure 6-4b).

Secondly, in human measurements, decentration and misalignment with the visual axis during contact A-scan ultrasound measurement are attributed as another cause for the difference between measurements.[99] The results in the current study suggest that rotation are larger sources of differences between techniques than any corneal compression. The Visante OCT used here uses two-dimensional images to visualize alignment during the measurement, and a series of measurements are acquired within one second after good alignment is seen. Thus rotation is likely to occur more often in ultrasound giving a larger ACD and smaller LT than the actual values (explanation given by Figure 6-6). As long as the rotational misalignment is small, the effect on CBL is not large because the posterior surface of the crystalline lens is considered spherical within a small region. Therefore, at small angles of incidence, there would be no accumulated effect of misalignment in CBL because the misalignment has opposite effects on ACD and LT, as seen (Figure 6-3b and Figure 6-4b). As the eye gets bigger with age, alignment becomes relatively easier, and any misalignment gets smaller. As the eye grows, the radii of curvature of both the anterior and posterior lens surfaces increase, given the same angle of tilt, the measured ACD and LT within ultrasound gets closer to the actual values. Therefore, the difference between ACD and LT (Visante AS-OCT minus ultrasound) gets smaller until the relative impact of misalignment is relatively small. On later days when misalignment is smaller, the ACD measured by Visante AS-OCT is larger than by ultrasound, consistent with a remaining effect of corneal indentation in

ultrasound. On later days, the measured LT by Visante AS-OCT is smaller than that by ultrasound.

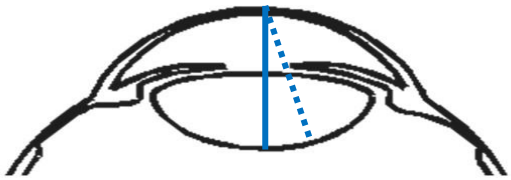

**Figure 6-6 Diagram indicating a tilt in A-scan ultrasonography.**

The long dashed line indicates the correct perpendicular alignment. The dotted line indicates misalignment with a slight rotation, presumably occurred during the ultrasound measurement, causing the ACD value to be slightly bigger and the LT value to be slightly smaller in the ultrasound measurement than in the OCT measurement.

This particular OCT system has the following advantages for use in the chick eye. Firstly, the two-dimensional video provided by the Visante AS-OCT system allows the operator to visualize the alignment and save images for the best alignment. Another optical device, Lenstar, also an OCT has been tested in the chick eye.[103] The system will only save images when it automatically decides that they are aligned.[103] The stringent alignment requirements make the measurement in the chick eye difficult without anesthesia. It's unfortunate that the Lenstar cannot be used with awake chicks as it would, in principle, be possible to obtain the radii of curvatures of both the anterior and posterior surfaces of the cornea and the crystalline lens. Secondly, the Visante AS-OCT system can save raw images with optical path lengths

(instead of the processed images which use built-in human refractive indices), then physical distances were obtained using refractive indices reported within literature[43, 45] for the chick eye. This feature is not available in Lenstar,[103] and using an incorrect (for example, higher) average lens refractive index for chick leads to a smaller LT measured by Lenstar.[103]

In the mouse eye, for a different OCT system, the OCT technique can be extended to obtain an axial length measurement if the reference arm is set to approximately the mid-position in the crystalline lens so that both anterior and posterior lens surfaces appear superimposed.[102] Similar techniques have the potential to be applied to the chick eye measurement; however, the scan depth which gives a clear lens posterior surface (3mm depth; see Figure 6-1b) does not have enough depth to measure the vitreous chamber depth in normal or myopic chick eyes. Swept source OCT systems allow resolution to be maintained over a larger measurement depth. A swept source system recently built by Professor Bizheva and tested by us on the chick eye showed promise for measuring along the full axial length of the chick eye.

## 6.5 Conclusions

Alignment during ultrasound measurements within alert chicks is important, because rotation causes larger ACD and smaller LT in young chicks and the opposite bias as the eye grows longer (due to slight corneal compression). Measurement of ocular dimensions using the Visante AS-OCT can be a powerful alternative to ultrasound. The two-dimensional image

not only provides visualization during alignment but also suggests the possibility of obtaining *in vivo* radii of curvature data in the chick eye, given the flexibility of substituting appropriate refractive indices for further image processing.

# Chapter 7
# Conclusions

## 7.1 General Discussion

A calculation of *in vivo* eye power during normal growth using two simplifying assumptions and longitudinal data for ocular defocus (spherical equivalent refraction or mean ocular refraction, MOR) and optical axial length (OAL) was developed, showing good agreements with literature data determined via either invasive measurements or more complex calculations. The calculated eye power from MOR and OAL showed eye power decreases with age during normal emmetropization (Figure 3-2d), in agreement with previous eye power measurements[39, 43] and with the observed increase in corneal radius (Figure 4-3a), decrease in lens power (Figure 4-5) and increase in the anterior segment (specified as cornea to back lens distance, CBL; Figure 5-1c).

By definition, MOR is the dioptric distance from where the distance light is focused to the photoreceptor layer; it is unlikely that eye growth is regulated by a distance. Instead, it is more plausible to discuss regulation in terms of equivalent angular blur (EB) due to defocus on the retina, physical information that can be sampled by the retina. The results here showed a strong support of active emmetropization by the three linear relationships with retinal blur due to defocus (EB): of OAL (Figure 4-2c), corneal radius (Figure 4-4a) and lens power (Figure 4-6d) during emmetropization. In addition, emmetropization appears to be driven by values of angular blur which are above the level of the cone photoreceptor resolution during emmetropization, reaching a level where the radius of angular blur is similar to cone spacing

at the completion of emmetropization. In this thesis, EB due to defocus is defined as an absolute value. The limitation of the proposed above mechanism during normal emmetropiization is that it does not fully explain what is seen during recovery from the induced myopic defocus. During recovery, we still need to plot the changes in ocular parameters versus retinal blur to determine if the same relationships hold. In addition, if EB had started at a larger value due to the myopic defocus and decreased to a level that is very close to the cone spacing, the treated eye should have ended up with mild myopia, instead of the mild hyperopia, as seen (Figure 5-1a). This process might involve a homeostatic mechanism[65] as the treated eye eventually becomes very similar to the control eye.

During emmetropization and after emmetroipzation is complete, linear relationships were found between the rate of change in OAL with rates of change in both corneal radius (Figure 4-4c) and lens power (Figure 4-6f), which suggest either a passive linking of the growth changes or a similar molecular signaling for all three parameters. In addition, the relative change in anterior segment (specified as CBL; Figure 5-2a or Figure B-1a) is very similar to the relative change in OAL, but both are bigger than the relative change in corneal radius (Figure 4-7c). For the normally growing eye, the relative change in lens power (Figure 4-7a) is the not significantly different from the relative change in K′, calculated from the OAL. The relative change in the corneal power (Figure 4-7b) is slower than in K′. The proportionalities between eye length and CBL, and lens power and K′ suggest the possibility of uniform expansion of the anterior segment at the same rate as the OAL. However, the corneal radius

changes more slowly than uniform expansion during emmetropization, accounting for the rapid decrease in MOR.

If signaling molecules originating at the retina are involved in coordinating component growth during emmetropization, the refractive index profile of the crystalline lens might be influenced by the signaling molecules. The slower rate of corneal growth might be due to the presence of a lower level of signaling molecules during growth, since it is farther away from the retina.

To explore how optical properties change within myopic eyes, the approximate eye power calculation during normal growth needed to be modified, requiring an additional assumption about the cardinal point position or power. The assumption that ametropia resulting from the application of the lens is completely axial in origin (no change in cardinal position nor eye power) was disproven. A modification of the *in vivo* eye power calculation for use in eyes developing lens-induced myopia or recovering from it was then developed, with one assumption needed for the nodal point position. Different assumptions have been tested, and the results are all consistent with a change in the optics, either in the positions of cardinal points or in the focal length, depending on the assumptions used (Figure 5-3), but more information is required to determine which assumption is closer to the reality. A preliminary comparison of dimensional measurements of the anterior segment between optical coherence tomography (OCT) and ultrasonography was performed, and the results suggest the possibility of measuring the longitudinal variation in the curvatures and thicknesses of optical

components of the eye in treated and normal eyes as a function of age. This may give insight into which optical components and optical properties change with treatment.

### 7.2 Conclusions

The end point of emmetropization can be defined as when the rate of change in MOR becomes almost zero and when angular retinal blur (EB) are stable. MOR and linear retinal blur would then change slowly as the eye grows uniformly. Under this definition, emmetropization of normal growth in the chick eye ends at around day 30 to 35. During emmetropization, concurrent variations in eye power and length combine to produce the smaller, more rapid changes in MOR, primarily due to a slower decrease in corneal power than predicted by uniform expansion. Emmetropization appears to be driven by an active reduction of EB to a value close to cone resolution. In chick, during emmetropization, rates of change in optical axial length (OAL), corneal radius and lens power are changing linearly with EB. Also, proportional changes in the rates of change in corneal radius and lens power with respect to the rate of change in OAL are possibly due to a similar molecular signaling. After emmetropization is complete, that the subsequent change in linear retinal blur and MOR while angular blur stays constant is consistent with a slow, almost uniform expansion of the posterior chamber and cornea with the lens, continuing to reduce in power proportional to the increase in eye length. However, after the age when normal emmetropization is complete, an emmetropization response to additional imposed defocus blur has been observed.

Myopia development occurs when normal emmetropization breaks down, usually involving at least some axial elongation. Emmetropization due to hyperopic defocus is partially due to a change in VCD, but the anterior segment also changes. Eye power has been calculated under several assumptions, together with dimensional measurements, to discuss any possible "additional mechanism" (differences between treated eyes and control eyes). There is a change in the optical properties with a change in cardinal point positions or eye power. Based on the biometry data for normal eyes, two-dimensional OCT is a promising alternative to ultrasound to provide visualization for measurement of anterior segment change between myopic and normal eyes. Also, it is possible to apply the two-dimensional OCT to obtain surface radii in order to determine changes in optical properties during myopia development.

### 7.3 Future Work

Future interesting studies would involve:

(1) Calculation of angular and linear blurs within myopic chick eyes based on pupil radius data to study if/how EB drives the emmetropization to hyperopic defocus and its recovery. It might be helpful to increase the experimental period of LIM to approximately day 14, when almost 100% induced myopia is established,[42] so that more measurement points may be obtained during recovery.

(2) Application of the two-dimensional optical imaging technique for *in vivo* measurement of surface radii to determine which optical parameters change. Correction of optical path length images is required first. For example, using Visante OCT, the corneal anterior radius can be easily obtained. For lens radii, the full image of the crystalline lens needs to be obtained under both Raw Image High Resolution Mode (to obtain a full scan of the lens) and Raw Image Mode (to provide a reference position for optical path length correction). Good alignment of the eyes of awake chicks is needed for accurate measurements.

(3) A test of whether the linear relationships between OAL, corneal radius and lens power also exist during lens-induced myopia and its recovery.

(4) Series of experiments on lens-induced myopia and its recovery to increase the sample population and track individual eyes. Because eye power calculations are highly associated with the accuracy and precision of the MOR measurement, it would be beneficial to include more birds to reduce its standard deviation. Also, more frequent measurement points between days 0 and 10 might make it possible to detect any eye power difference during LIM. Therefore, performing another one or two trials of the experiment of LIM and its recovery under exact same experimental conditions could be helpful. Tracking whether birds with higher initial refractive errors emmetropize more rapidly would also be interesting.

(5) Exploration of signaling molecules and receptors in cornea and chick lens that might be related to optical axial length alternation. The retina has the capacity to extract information from retinal blur and create signals controlling the development of other ocular

components. Dopamine, a signaling substance released by the retina, is a possible candidate for controlling emmetropization because it can diffuse freely within the eye.[117] Evidence of dopamine effects on lens growth has been found within the fish eye[142] but not yet in the chick. If confirmed, considering the reciprocal nature between dopamine and melatonin, which affects ocular growth during diurnal variation and were found within both retina and cornea, it would be interesting to see if corneal and lens powers show diurnal variation.

# Appendix A

## A-scan Ultrasound Measurement Selection

The ACCUTOME A-scan recorded five measurements for each eye. A perfect ultrasound A-scan measurement for the human eye contains five high-amplitude spikes including a corneal peak, anterior and the posterior the lens peaks, a steeply rising retinal peak and a good resolution of the separate retinal and sclera peaks; a similar output should be obtained for the chick eye (Figure A-1). Because the measurement is done in the small awake chick eye, A-scan outputs indicating some degree of misalignment are considered not ideal. Therefore, the A-scan measurement selection protocols are discussed here, so that the best A-scan measurements can be carefully selected from the five scans of optical-axial-length measurements for each eye recorded in individual bird. The sets of values for each eye are then averaged for further analysis (experiment in Chapter 5). In a later experiment (Chapter 6), measurements not satisfying the following criteria are deleted, and new scans are redone.

It is worth mentioning that the gain setting before talking about the alignment, because setting the correct gain enables the determination of various retinal spikes for the study of diurnal variation. Generally, the gain of the ultrasound machine should be set to emphasize these peaks while avoiding over-saturation that would cause less resolution and would smear retina and scleral spikes together. However, due to the relatively high gain set for some scans in individual chicks, spikes are plateaus, thus retinal and scleral spikes are undistinguishable. Fortunately, the gain setting is somewhat forgiving when it comes to the determination of optical axial length (OAL). OAL is defined as the distance from anterior cornea to anterior retina, so once the A-scan

output shows a good alignment during the measurement, the determination of the OAL value only requires the locations of corneal and retinal spikes. When using the contact mode, the cornea surface is considered as the 0 mm location as where the probe is located, and the front of the retina is indicated by the start of the retinal spike; therefore, the main goal of the A-scan output selection is to exclude outputs indicating misalignment or missing information, hoping to increase the precision of the OAL measurement.

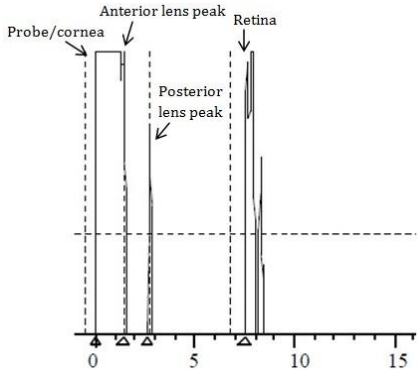


**Figure A-1 An example for an ideal scan output.**

### A-1 Misaligned Scan Measurements

Because the contact mode is used, all OAL values were double checked against other scans to remove values indicating obvious cornea compression. Measurements that have the following characteristics were not included.

- **Misalignment demonstrated by the present of jags, humps, or steps on the ascending edge of the retinal spike when the perpendicularity to the area centralis is not achieved.**

  In human eyes, if the probe is off-axis, the retina will be measured at a spot other than the central macula, often resulting in a shorter than true axial length. When looking at the retina spike, make sure that it is at a 90° angle (perpendicular) and rising straight up without a step, notch or curve at the base. When scaling up the measurement, there is a very small peak before the sharp increase for the retinal spike (Figure A-2). A similar error will likely be seen in chick if the beam is not perpendicular to the retina.

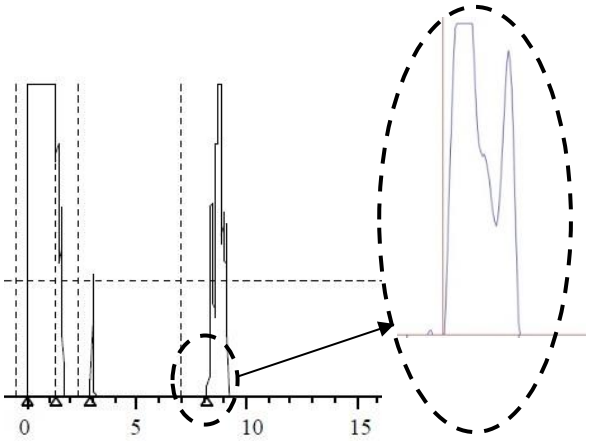


**Figure A-2 An example output indicates the failure of perpendicularly alignment of the ultrasound beam to the area centralis surface.**

- **Misalignment demonstrated by only one spike at the "retinal position".**

  On one hand, a common clinical explanation for the missing spike is that there is only a retinal spike as a consequence of the misalignment of the ultrasound beam intersecting

the optic nerve. Considering that there is no sclera at the optic nerve, the ultrasound beam is passing through the nerve cord with only short amplitude echoes present (the ultrasound beam is striking blood vessels within the nerve cord). On the other hand, the missing spike could be the retinal spike caused by the difference between the refractive indices for the vitreous (n=1.335, Avila and McFadden)[39] and the retina (n=1.351, Avila and McFadden)[39] or the sclera ($n \approx n_{cornea}$=1.369,[39] because similar to cornea, the sclera consists mainly of compact fibrous tissue).[143] The bigger refractive index difference between vitreous and the sclera suggests a stronger reflection at the retina/sclera interface.

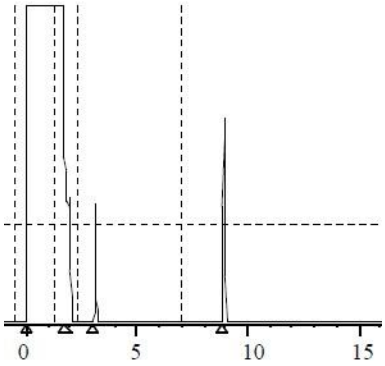


**Figure A-3 An sample output indicates one "retinal" spike.**

- If the presenting "OAL" value is relatively larger than the value given by other scans, the missing spike is probably the retinal spike. In this case, the diagram should be excluded. Because the choroid thickness for the chick eye is between 0.2-0.3mm, if the presumed

retinal spike has a width larger than 0.3mm, the diagram can be reasonably used to obtain OAL. Even though this kind of misalignment presumably leads to a slightly bigger optical-axial-length value as the eye is not perfectly spherical, the error is much smaller compared to other operational factors, such as cornea compression.

- **Misalignment demonstrated by the decreased amplitude of the posterior lens spike.**

  This misalignment (shown as Figure A-4) occurs when the ultrasound beam is aligned at an angle through the lens rather than though its center, meaning the beam is not aligned along the visual axis. As most chickens present a posterior lens peak higher than the set baseline, any measurement with lens peak not exceeding the baseline was excluded. The effect of this kind of misalignment is not as big as the previous two cases.

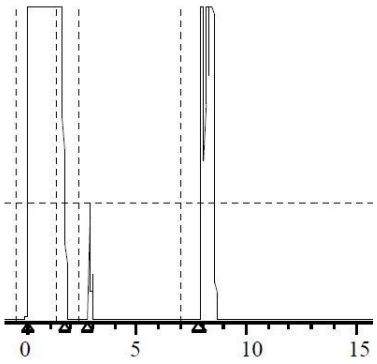


**Figure A-4 An sample measurement for decreased lens peak amplitude.**

## A-2 Comparison between Two Ultrasound Systems

Seven chicks had their OAL measured by two ultrasound systems, A-scan Plus Connect ultrasonography (Accutome, Malvern, PA) and an older ultrasound system that we had used previously (Oculometer 4000, Radionics Medical Inc, Scarborough, Ontario), during an experiment of lens-induced myopia (LIM) and its recovery.

There are strong correlations between the surface positions given by the two ultrasound systems within control eyes, treated eyes and when all eyes are considered (Figure A-5a). Bland-Altman analyses show the difference in OAL between two systems is not significantly different from zero (Figure A-5b). Therefore, it is possible to pool the data from two sets of birds, having their OAL measured by two different ultrasound systems. Across all eyes, the ACCUTOME A-scan gives slightly more precise measurement than Oculometer 4000 with a smaller standard deviation.

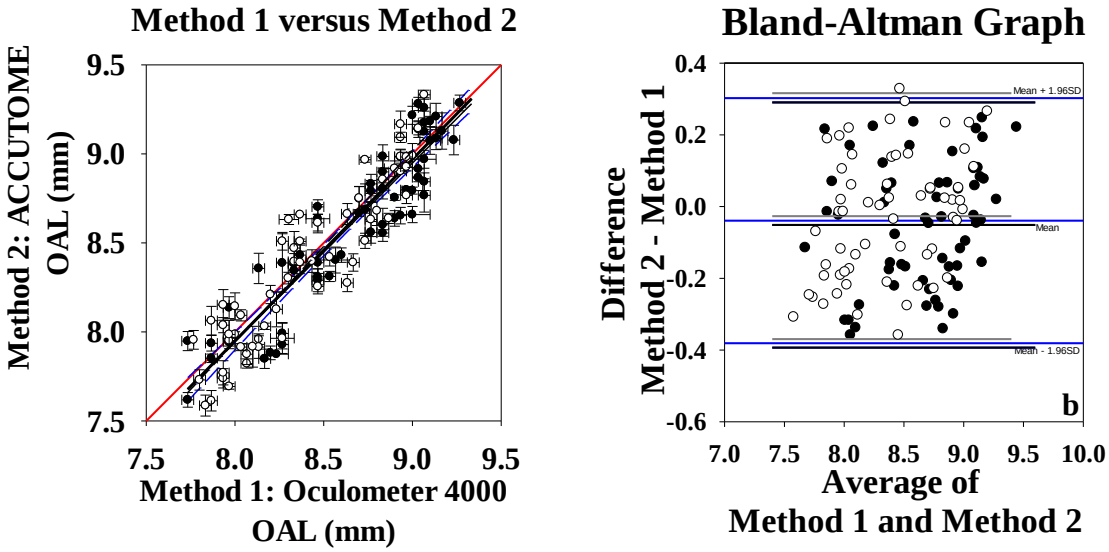


**Figure A-5 (a) Correlation data between OAL by Oculometer 4000 (Method 1) and ACCUTOME A-scan (Method 2); (b) Bland-Altman plot.**

Each spot represents the average of each eye (control eyes: open circles, grey lines; treated eyes: closed circle, black lines; all eyes comparison: blue lines) from each bird on each day. In (a), slopes are not significantly different from 1.0 (red line).

Paired t-tests show no significant difference between measurements within control or treated eyes on days 0, 1, 2, 3, 4, 6, 7, 8, 9, and 10.

In (b), the blue solid horizontal line in the middle represents the mean of the bias for all eyes, and the other blue lines indicate the 95% confidence interval (CI). The black and grey solid horizontal lines in the middle represent the mean of the bias and the other black and grey indicate the 95% CI for the treated and control eyes, respectively.

**Table A-1 Pairwise comparisons between ACCUTOME A-scan and Oculometer 4000.**

| | # of data pair | Technique | Mean of SE | SD of SE |
|---|---|---|---|---|
| **OD** | 60 | ACCUTOME A-scan | 0.0516 | 0.0302 |
| | | Oculometer 4000 | 0.1216 | 0.6715 |
| **OS** | 60 | ACCUTOME A-scan | 0.0490 | 0.0255 |
| | | Oculometer 4000 | 0.0280 | 0.0153 |
| **All eyes** | 120 | ACCUTOME A-scan | 0.0503 | 0.0279 |
| | | Oculometer 4000 | 0.0748 | 0.4753 |

# Appendix B

## Additional Figures & Explanations for Chapter 5

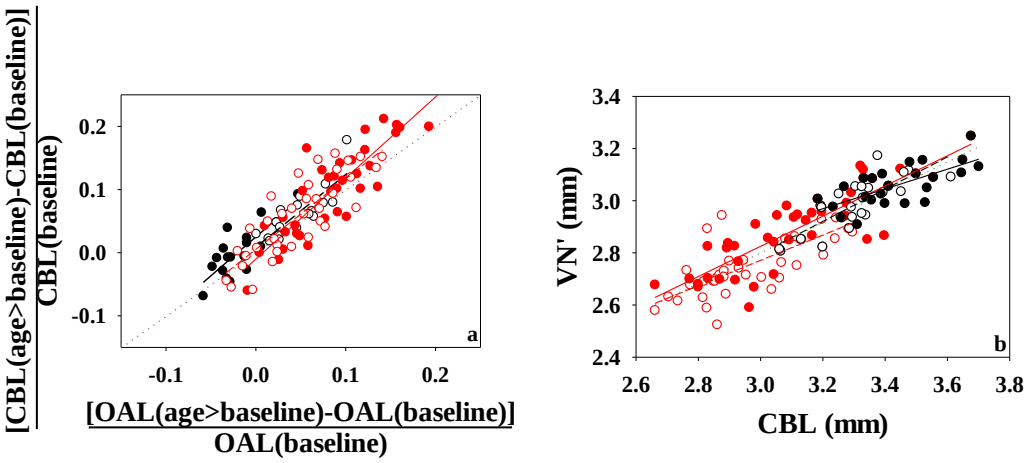


**Figure B-1 (a) Relative change in CBL versus relative change in OAL, relative to their values on baseline day (day 0 for LIM, day 7 for recovery), (b) anterior cornea (V) to N′ distance versus CBL, for treated and control eyes.**

This figure shows the individual points for Figure 5-2. Because there are only three averaged measurement time points during recovery (Figure 5-2), the fit to the recovering eye is not significant. To obtain the relationship during recovery, measurements for individual birds were considered and are shown here.

Control eyes of the goggled birds are the open circles, and treated eyes are the closed circles. Red symbols are for LIM, and black symbols are for recovery. Control eye data are fitted with dashed lines, and treated eye data are fitted with solid lines (see Table B-1 or Table B-2 for slopes).

In (a), pink dotted line is the 1-1 line, solid red line is the fit to LIM. In (b), the turquoise line is the overall fit to all data points. In (b), values of the VN′ distance were calculated from $0.34\times OAL$[39, 43, 45, 53] (also see discussion in Appendix-5.6.3). Except for the fit for treated eyes during recovery, which differs slightly from the overall fit, the other fits are not significantly different from the overall fit.

**Table B-1 Slope of fits in Figure B-1a.**

| Slopes ± SEM | Treated eyes | Control eyes |
|---|---|---|
| **LIM** | 1.3±0.1 | 1.1±0.1* |
| **Recovery** | 1.2±0.2* | 1.2±0.2* |

All linear regression fits were highly significant ($p<0.0001$). * Slope is not different from 1.0.

The slope for treated eyes during LIM is different from 1.0 but not different from the other three slopes.

The intercepts are not different from 0.0, except for treated eyes during recovery (95% confidence interval for the intercept is 0.010 to 0.041, which is considered close to zero).

**Table B-2 Slope and intercept of fits in Figure B-1b.**

| | Treated eyes | | Control eyes | |
|---|---|---|---|---|
| | **Slopes ± SEM** | **Intercepts ± SEM** | **Slopes ± SEM** | **Intercepts ± SEM** |
| **LIM** | 0.58±0.06 | 1.1±0.2 | 0.49±0.07 | 1.3±0.2 |
| **Recovery** | 0.38±0.08 | 1.8±0.3 | 0.62±0.10 | 0.9±0.3 |

All linear regression fits were highly significant, $p<0.002$.

The fit to the overall points has a slope of (0.58±0.03) and an intercept of (1.06±0.09). 95% CI of slope and intercept the fit to overall points overlaps with the 95% CI of the individual fits.

We used a relationship of $VN' = 0.58 \times CBL + 1.06$ ($p<0.0001$; turquoise line in Figure B-1b) for Assumption 4 in Chapter 5.

We used a relationship of $VN' = 0.58 \times CBL + 1.06$ to derive the distance from N′ to anterior retina for Assumption 4 in Chapter 5. For some birds, measured by Oculometer 4000 during an

earlier experiment, the CBL measurement is not available, the CBL data is inferred from its relationship to OAL because

$$\frac{\mathrm{CBL[age > baseline]} - \mathrm{CBL[baseline]}}{\mathrm{CBL[baseline]}} \cong \mathrm{slope} \times \frac{\mathrm{OAL[age > baseline]} - \mathrm{OAL[baseline]}}{\mathrm{OAL[baseline]}},$$

where $\mathrm{OAL[baseline]}$ is the average OAL on day 0 for LIM and day 7 for recovery.

## Reference


1. Flitcroft DI. The complex interactions of retinal, optical and environmental factors in myopia aetiology. *Prog.Retin.Eye Res.* 2012;31:622-660.

2. Spaide RF, Ohno-Matsui K, Yannuzzi LA. *Pathologic myopia.* New York, NY: Springer New York; 2014. 383 pp.

3. Smith EL,3rd, Campbell MC, Irving E. Does peripheral retinal input explain the promising myopia control effects of corneal reshaping therapy (CRT or ortho-K) & multifocal soft contact lenses? *Ophthalmic Physiol.Opt.* 2013;33:379-384.

4. Bennett AG, Rabbetts RB. *Clinical visual optics.* Boston: Butterworth Heinemann; 1998. .

5. Troilo D. Neonatal eye growth and emmetropisation - A literature review. *Eye* 1992;6:154-160.

6. Atkinson J, Anker S, Bobier W, et al. Normal emmetropization in infants with spectacle correction for hyperopia. *Invest.Ophthalmol.Vis.Sci.* 2000;41:3726-3731.

7. Iribarren R, Morgan IG, Chan YH, Lin X, Saw SM. Changes in lens power in singapore chinese children during refractive development. *Invest.Ophthalmol.Vis.Sci.* 2012;53:5124-5130.

8. Norton TT. Animal models of myopia: Learning how vision controls the size of the eye. *ILAR J.* 1999;40:59-77.

9. Pennie FC, Wood IC, Olsen C, White S, Charman WN. A longitudinal study of the biometric and refractive changes in full-term infants during the first year of life. *Vision Res.* 2001;41:2799-2810.

10. Saunders KJ, Woodhouse JM, Westall CA. Emmetropisation in human infancy: Rate of change is related to initial refractive error. *Vision Res.* 1995;35:1325-1328.

11. Brown NP, Koretz JF, Bron AJ. The development and maintenance of emmetropia. *Eye (Lond)* 1999;13 ( Pt 1):83-92.

12. Hunter JJ, Campbell MC, Kisilak ML, Irving EL. Blur on the retina due to higher-order aberrations: Comparison of eye growth models to experimental data. *J.Vis.* 2009;9:12.1-20.

13. Mutti DO, Mitchell GL, Jones LA, et al. Axial growth and changes in lenticular and corneal power during emmetropization in infants. *Invest.Ophthalmol.Vis.Sci.* 2005;46:3074-3080.

14. Rabin J, Van Sluyters RC, Malach R. Emmetropization: A vision-dependent phenomenon. *Invest.Ophthalmol.Vis.Sci.* 1981;20:561-564.

15. Sivak J. The cause(s) of myopia and the efforts that have been made to prevent it. *Clin Exp Optom* 2012;95(6):572-582.

16. Kurtz D, Hyman L, Gwiazda JE, et al. Role of parental myopia in the progression of myopia and its interaction with treatment in COMET children. *Invest.Ophthalmol.Vis.Sci.* 2007;48:562-570.

17. Jones LA, Mitchell GL, Mutti DO, Hayes JR, Moeschberger ML, Zadnik K. Comparison of ocular component growth curves among refractive error groups in children. *Invest.Ophthalmol.Vis.Sci.* 2005;46:2317-2327.

18. Lam DS, Fan DS, Lam RF, et al. The effect of parental history of myopia on children's eye size and growth: Results of a longitudinal study. *Invest.Ophthalmol.Vis.Sci.* 2008;49:873-876.

19. Ip JM, Saw SM, Rose KA, et al. Role of near work in myopia: Findings in a sample of australian school children. *Invest.Ophthalmol.Vis.Sci.* 2008;49:2903-2910.

20. Mutti DO, Mitchell GL, Moeschberger ML, Jones LA, Zadnik K. Parental myopia, near work, school achievement, and children's refractive error. *Invest.Ophthalmol.Vis.Sci.* 2002;43:3633-3640.

21. Saw SM, Chua WH, Hong CY, et al. Nearwork in early-onset myopia. *Invest.Ophthalmol.Vis.Sci.* 2002;43:332-339.

22. Congdon N, Wang Y, Song Y, et al. Visual disability, visual function, and myopia among rural chinese secondary school children: The xichang pediatric refractive error study (X-PRES)--report 1. *Invest.Ophthalmol.Vis.Sci.* 2008;49:2888-2894.

23. Lu B, Congdon N, Liu X, et al. Associations between near work, outdoor activity, and myopia among adolescent students in rural china: The xichang pediatric refractive error study report no. 2. *Arch.Ophthalmol.* 2009;127:769-775.

24. French AN, Morgan IG, Mitchell P, Rose KA. Risk factors for incident myopia in australian schoolchildren: The sydney adolescent vascular and eye study. *Ophthalmology* 2013;120:2100-2108.

25. Guo Y, Liu LJ, Xu L, et al. Myopic shift and outdoor activity among primary school children: One-year follow-up study in beijing. *PLoS One* 2013;8:e75260.

26. Wu PC, Tsai CL, Wu HL, Yang YH, Kuo HK. Outdoor activity during class recess reduces myopia onset and progression in school children. *Ophthalmology* 2013;120:1080-1085.

27. Schmid KL, Leyden K, Chiu YH, et al. Assessment of daily light and ultraviolet exposure in young adults. *Optom.Vis.Sci.* 2013;90:148-155.

28. Rose KA, Morgan IG, Ip J, et al. Outdoor activity reduces the prevalence of myopia in children. *Ophthalmology* 2008;115:1279-1285.

29. Rose KA, Morgan IG, Smith W, Burlutsky G, Mitchell P, Saw SM. Myopia, lifestyle, and schooling in students of chinese ethnicity in singapore and sydney. *Arch.Ophthalmol.* 2008;126:527-530.

30. Iribarren R, Morgan IG, Hashemi H, et al. Lens power in a population-based cross-sectional sample of adults aged 40 to 64 years in the shahroud eye study. *Invest.Ophthalmol.Vis.Sci.* 2014;55:1031-1039.

31. Iyamu E, Iyamu J, Obiakor CI. The role of axial length-corneal radius of curvature ratio in refractive state categorization in a nigerian population. *ISRN Ophthalmol.* 2011;2011:138941.

32. Llorente L, Barbero S, Cano D, Dorronsoro C, Marcos S. Myopic versus hyperopic eyes: Axial length, corneal shape and optical aberrations. *J.Vis.* 2004;4:288-298.

33. Scheiman M, Li D, Gwiazda JE, et al. Longitudinal changes in corneal power and axial length in the correction of myopia evaluation trial (COMET) cohort. *IOVS* 2014;374:E-Abstract 3602.

34. Ojaimi E, Rose KA, Morgan IG, et al. Distribution of ocular biometric parameters and refraction in a population-based study of australian children. *Invest.Ophthalmol.Vis.Sci.* 2005;46:2748-2754.

35. Grosvenor T, Scott R. Role of the axial length/corneal radius ratio in determining the refractive state of the eye. *Optom.Vis.Sci.* 1994;71:573-579.

36. Shih YF, Chiang TH, Lin LL. Lens thickness changes among schoolchildren in taiwan. *Invest.Ophthalmol.Vis.Sci.* 2009;50:2637-2644.

37. Zadnik K, Mutti DO, Fusaro RE, Adams AJ. Longitudinal evidence of crystalline lens thinning in children. *Invest.Ophthalmol.Vis.Sci.* 1995;36:1581-1587.

38. Wallman J, Adams JI, Trachtman JN. The eyes of young chickens grow toward emmetropia. *Invest.Ophthalmol.Vis.Sci.* 1981;20:557-561.

39. Avila NV, McFadden SA. A detailed paraxial schematic eye for the white leghorn chick. *J.Comp.Physiol.A.Neuroethol Sens.Neural Behav.Physiol.* 2010;196:825-840.

40. Campbell MC, Bunghardt K, Kisilak ML, Irving EL. Diurnal rhythms of spherical refractive error, optical axial length, and power in the chick. *Invest.Ophthalmol.Vis.Sci.* 2012;53:6245-6253.

41. Hunter JJ, Campbell MC, Kisilak ML, Irving EL. Blur on the retina due to higher-order aberrations: Comparison of eye growth models to experimental data. *J.Vis.* 2009;9:12.1-20.

42. Kisilak ML, Campbell MC, Hunter JJ, Irving EL, Huang L. Aberrations of chick eyes during normal growth and lens induction of myopia. *J.Comp.Physiol.A.Neuroethol Sens.Neural Behav.Physiol.* 2006;192:845-855.

43. Irving EL, Sivak JG, Curry TA, Callender MG. Chick eye optics: Zero to fourteen days. *J.Comp.Physiol.A.* 1996;179:185-194.

44. Rohrer B, Schaeffel F, Zrenner E. Longitudinal chromatic aberration and emmetropization: Results from the chicken eye. *J.Physiol.* 1992;449:363-376.

45. Schaeffel F, Howland HC. Visual optics in normal and ametropic chickens. *Clin Vision Sci* 1988;3(2):83-98.

46. Hocking PM, Guggenheim JA. The chick as an animal model of eye disease. *Drug Discovery Today: Disease Models*.

47. Irving EL. Optically induced ametropia in young chickens. *PhD Thesis, University of Waterloo, Waterloo* 1993.

48. Fujikado T, Kawasaki Y, Suzuki A, Ohmi G, Tano Y. Retinal function with lens-induced myopia compared with form-deprivation myopia in chicks. *Graefes Arch.Clin.Exp.Ophthalmol.* 1997;235:320-324.

49. Morgan IG, Ashby RS, Nickla DL. Form deprivation and lens-induced myopia: Are they different? *Ophthalmic Physiol.Opt.* 2013;33:355-361.

50. Feldkaemper M, Schaeffel F. An updated view on the role of dopamine in myopia. *Exp.Eye Res.* 2013;114:106-119.

51. Irving EL, Sivak JG, Callender MG. Refractive plasticity of the developing chick eye. *Ophthalmic Physiol.Opt.* 1992;12:448-456.

52. Kisilak M,L., Hunter J,J., Huang ,Lan, Campbell M,C.W., Irving E,L. In chicks wearing high powered negative lenses, spherical refraction is compensated and oblique astigmatism is induced. *Journal of Modern Optics* 2008;55(4-5):611-623.

53. Schaeffel F, Glasser A, Howland HC. Accommodation, refractive error and eye growth in chickens. *Vision Res.* 1988;28:639-657.

54. Irving EL, Callender MG, Sivak JG. Inducing myopia, hyperopia, and astigmatism in chicks. *Optom.Vis.Sci.* 1991;68:364-368.

55. Irving EL, Callender MG, Sivak JG. Inducing ametropias in hatchling chicks by defocus—Aperture effects and cylindrical lenses. *Vision Res.* 1995;35:1165-1174.

56. Schaeffel F, Howland HC. Mathematical model of emmetropization in the chicken. *J.Opt.Soc.Am.A* 1988;5:2080-2086.

57. Wildsoet C, Wallman J. Choroidal and scleral mechanisms of compensation for spectacle lenses in chicks. *Vision Res.* 1995;35:1175-1194.

58. Wallman J, Adams JI. Developmental aspects of experimental myopia in chicks: Susceptibility, recovery and relation to emmetropization. *Vision Res.* 1987;27:1139-1163.

59. Schmid KL, Wildsoet CF. Effects on the compensatory responses to positive and negative lenses of intermittent lens wear and ciliary nerve section in chicks. *Vision Res.* 1996;36:1023-1036.

60. Troilo D, Gottlieb MD, Wallman J. Visual deprivation causes myopia in chicks with optic nerve section. *Curr.Eye Res.* 1987;6:993-999.

61. Troilo D, Wallman J. The regulation of eye growth and refractive state: An experimental study of emmetropization. *Vision Res.* 1991;31:1237-1250.

62. Schaeffel F, Glasser A, Howland HC. Accommodation, refractive error and eye growth in chickens. *Vision Res.* 1988;28:639-657.

63. Pickett-Seltner RL, Sivak JG, Pasternak JJ. Experimentally induced myopia in chicks: Morphometric and biochemical analysis during the first 14 days after hatching. *Vision Res.* 1988;28:323-328.

64. Zhu X, McBrien NA, Smith EL,3rd, Troilo D, Wallman J. Eyes in various species can shorten to compensate for myopic defocus. *Invest.Ophthalmol.Vis.Sci.* 2013;54:2634-2644.

65. Wallman J, Winawer J. Homeostasis of eye growth and the question of myopia. *Neuron* 2004;43:447-468.

66. Wallman J, Wildsoet C, Xu A, et al. Moving the retina: Choroidal modulation of refractive state. *Vision Res.* 1995;35:37-50.

67. Read SA, Collins MJ, Sander BP. Human optical axial length and defocus. *Invest.Ophthalmol.Vis.Sci.* 2010;51:6262-6269.

68. Sivak JG, Mandelman T. Chromatic dispersion of the ocular media. *Vision Res.* 1982;22:997-1003.

69. Sivak JG, Ryall LA, Weerheim J, Campbell MC. Optical constancy of the chick lens during pre- and post-hatching ocular development. *Invest.Ophthalmol.Vis.Sci.* 1989;30:967-974.

70. Choh V, Sivak JG. Lenticular accommodation in relation to ametropia: The chick model. *J.Vis.* 2005;5:165-176.

71. Breslin KM, O'Donoghue L, Saunders KJ. A prospective study of spherical refractive error and ocular components among northern irish schoolchildren (the NICER study). *Invest.Ophthalmol.Vis.Sci.* 2013;54:4843-4850.

72. Koretz JF, Cook CA. Aging of the optics of the human eye: Lens refraction models and principal plane locations. *Optom.Vis.Sci.* 2001;78:396-404.

73. Mutti DO, Zadnik K, Fusaro RE, Friedman NE, Sholtz RI, Adams AJ. Optical and structural development of the crystalline lens in childhood. *Invest.Ophthalmol.Vis.Sci.* 1998;39:120-133.

74. Sivak JG, Moore S.E., Irving EL, Callender MGE. Experimental ametropia in chicks: Axial vs corneal contributions and response to non-emmetrpoic initial refractive error. *IOVS* 2000:ARVO Abstract.

75. Choh V, Sivak JG, Irving EL, Wong W. Ultrasound biomicroscopy of the anterior segment of the enucleated chicken eye during accommodation. *Ophthalmic Physiol.Opt.* 2002;22:401-408.

76. Choh V, Sivak JG, Meriney SD. A physiological model to measure effects of age on lenticular accommodation and spherical aberration in chickens. *Invest.Ophthalmol.Vis.Sci.* 2002;43:92-98.

77. de la Cera EG, Rodriguez G, Marcos S. Longitudinal changes of optical aberrations in normal and form-deprived myopic chick eyes. *Vision Res.* 2006;46:579-589.

78. Gottlieb MD, Fugate-Wentzek LA, Wallman J. Different visual deprivations produce different ametropias and different eye shapes. *Invest.Ophthalmol.Vis.Sci.* 1987;28:1225-1235.

79. Guggenheim JA, Erichsen JT, Hocking PM, Wright NF, Black R. Similar genetic susceptibility to form-deprivation myopia in three strains of chicken. *Vision Res.* 2002;42:2747-2756.

80. Troilo D, Wallman J. Changes in corneal curvature during accommodation in chicks. *Vision Res.* 1987;27:241-247.

81. Zhu X, Lin T, Stone RA, Laties AM. Sex differences in chick eye growth and experimental myopia. *Exp.Eye Res.* 1995;61:173-179.

82. Birkenfeld J, de Castro A, Ortiz S, Pascual D, Marcos S. Contribution of the gradient refractive index and shape to the crystalline lens spherical aberration and astigmatism. *Vision Res.* 2013;86:27-34.

83. Kisilak ML, Bunghardt K, Choh V, Irving EL, Campbell MCW. Isoflurane and lid retractors affect the optics of the chick eye. 2013;253:E-Abstract 1918.

84. Tian Y, Wildsoet CF. Diurnal fluctuations and developmental changes in ocular dimensions and optical aberrations in young chicks. *Invest.Ophthalmol.Vis.Sci.* 2006;47:4168-4178.

85. Bassnett S, Winzenburger PA. Morphometric analysis of fibre cell growth in the developing chicken lens. *Exp.Eye Res.* 2003;76:291-302.

86. de Castro A. Reconstruction of the gradient refractive index of the crystalline lens with optimization methods. *PhD Thesis, University of Valladolid, Spain* 2012.

87. Kisilak ML. Optical aberrations in growing eyes and in eyes with lens-induced myopia. *MSc Thesis, University of Waterloo, Waterloo* 2005.

88. Liang J, Williams DR. Aberrations and retinal image quality of the normal human eye. *J.Opt.Soc.Am.A Opt.Image Sci.Vis.* 1997;14:2873-2883.

89. Thibos LN, Hong X, Bradley A, Cheng X. Statistical variation of aberration structure and image quality in a normal population of healthy eyes. *J.Opt.Soc.Am.A Opt.Image Sci.Vis.* 2002;19:2329-2348.

90. Thibos LN, Applegate RA, Schwiegerling JT, Webb R, VSIA Standards Taskforce Members. Vision science and its applications. Standards for reporting the optical aberrations of eyes. *J.Refract.Surg.* 2002;18:S652-60.

91. Cubalchini R. Modal wave-front estimation from phase derivative measurements. *J.Opt.Soc.Am.* 1979;69:972-977.

92. Applegate RA, Ballentine C, Gross H, Sarver EJ, Sarver CA. Visual acuity as a function of zernike mode and level of root mean square error. *Optom.Vis.Sci.* 2003;80:97-105.

93. Glickstein M, Millodot M. Retinoscopy and eye size. *Science* 1970;168:605-606.

94. Fujimoto JG, Pitris C, Boppart SA, Brezinski ME. Optical coherence tomography: An emerging technology for biomedical imaging and optical biopsy. *Neoplasia* 2000;2:9-25.

95. Schmucker C, Schaeffel F. In vivo biometry in the mouse eye with low coherence interferometry. *Vision Res.* 2004;44:2445-2456.

96. Drexler W, Findl O, Menapace R, et al. Partial coherence interferometry: A novel approach to biometry in cataract surgery. *Am.J.Ophthalmol.* 1998;126:524-534.

97. Jasvinder S, Khang TF, Sarinder KK, Loo VP, Subrayan V. Agreement analysis of LENSTAR with other techniques of biometry. *Eye (Lond)* 2011;25:717-724.

98. Quinn GE, Francis EL, Nipper KS, et al. Highly precise eye length measurements in children aged 3 through 12 years. *Arch.Ophthalmol.* 2003;121:985-990.

99. Wissa AR, Wahba SS, Roshdy MM. Agreement and relationship between ultrasonic and partial coherence interferometry measurements of axial length and anterior chamber depth. *Clin.Ophthalmol.* 2012;6:193-198.

100. Lam AK, Chan R, Pang PC. The repeatability and accuracy of axial length and anterior chamber depth measurements from the IOLMaster. *Ophthalmic Physiol.Opt.* 2001;21:477-483.

101. Nemeth J, Fekete O, Pesztenlehrer N. Optical and ultrasound measurement of axial length and anterior chamber depth for intraocular lens power calculation. *J.Cataract Refract.Surg.* 2003;29:85-88.

102. Park H, Qazi Y, Tan C, et al. Assessment of axial length measurements in mouse eyes. *Optom.Vis.Sci.* 2012;89:296-303.

103. Penha AM, Burkhardt E, Schaeffel F, Feldkaemper MP. Ultrasonography and optical low-coherence interferometry compared in the chicken eye. *Optom.Vis.Sci.* 2012;89:916-921.

104. Zhou X, Xie J, Shen M, et al. Biometric measurement of the mouse eye using optical coherence tomography with focal plane advancement. *Vision Res.* 2008;48:1137-1143.

105. Fredrick DR. Myopia. *BMJ* 2002;324:1195-1199.

106. Morgan I, Rose K. How genetic is school myopia? *Prog.Retin.Eye Res.* 2005;24:1-38.

107. Iribarren R, Rozema JJ, Schaeffel F, Morgan IG. Calculation of crystalline lens power in chickens with a customized version of bennett's equation. *Vision Res.* 2014;96:33-38.

108. Morgan IG, Rose KA, Ellwein LB, Refractive Error Study in Children Survey Group. Is emmetropia the natural endpoint for human refractive development? an analysis of population-based data from the refractive error study in children (RESC). *Acta Ophthalmol.* 2010;88:877-884.

109. Kisilak ML, Bunghardt K, Hunter JJ, Irving EL, Campbell MC. Longitudinal in vivo imaging of cones in the alert chicken. *Optom.Vis.Sci.* 2012;89:644-651.

110. Rozema JJ, Atchison DA, Kasthurirangan S, Pope JM, Tassignon MJ. Methods to estimate the size and shape of the unaccommodated crystalline lens in vivo. *Invest.Ophthalmol.Vis.Sci.* 2012;53:2533-2540.

111. Schmid K, Wildsoet C. Breed- and gender-dependent differences in eye growth and form deprivation responses in chick. *J.Comp.Physiol.A.* 1996;178:551-561.

112. Troilo D, Li T, Glasser A, Howland HC. Differences in eye growth and the response to visual deprivation in different strains of chicken. *Vision Res.* 1995;35:1211-1216.

113. Shao Z, Irving EL, Kisilak ML, Campbell MCW. Calculation of total eye power and retinal blur during normal emmetropization in the chick eye. Unpublished manuscript.

114. Zadnik K, Mutti DO, Friedman NE, Adams AJ. Initial cross-sectional results from the orinda longitudinal study of myopia. *Optom.Vis.Sci.* 1993;70:750-758.

115. Gordon RA, Donzis PB. Refractive development of the human eye. *Arch.Ophthalmol.* 1985;103:785-789.

116. Rada JA, Wiechmann AF. Melatonin receptors in chick ocular tissues: Implications for a role of melatonin in ocular growth regulation. *Invest.Ophthalmol.Vis.Sci.* 2006;47:25-33.

117. Kroger RH. Optical plasticity in fish lenses. *Prog.Retin.Eye Res.* 2013;34:78-88.

118. Mutti DO, Hayes JR, Mitchell GL, et al. Refractive error, axial length, and relative peripheral refractive error before and after the onset of myopia. *Invest.Ophthalmol.Vis.Sci.* 2007;48:2510-2519.

119. Ishii K, Iwata H, Oshika T. Quantitative evaluation of changes in eyeball shape in emmetropization and myopic changes based on elliptic fourier descriptors. *Invest.Ophthalmol.Vis.Sci.* 2011;52:8585-8591.

120. Kroger RH, Hirt B, Wagner HJ. Effects of retinal dopamine depletion on the growth of the fish eye. *J.Comp.Physiol.A.* 1999;184:403-412.

121. Kroger RH, Campbell MC, Fernald RD. The development of the crystalline lens is sensitive to visual input in the african cichlid fish, haplochromis burtoni. *Vision Res.* 2001;41:549-559.

122. Mayer DL, Hansen RM, Moore BD, Kim S, Fulton AB. Cycloplegic refractions in healthy children aged 1 through 48 months. *Arch.Ophthalmol.* 2001;119:1625-1628.

123. McFadden SA, Howlett MH, Mertz JR. Retinoic acid signals the direction of ocular elongation in the guinea pig eye. *Vision Res.* 2004;44:643-653.

124. Hung LF, Crawford ML, Smith EL. Spectacle lenses alter eye growth and the refractive status of young monkeys. *Nat.Med.* 1995;1:761-765.

125. Shen W, Sivak JG. Eyes of a lower vertebrate are susceptible to the visual environment. *Investigative Ophthalmology & Visual Science JID - 7703701* 1101.

126. Rada JA, Shelton S, Norton TT. The sclera and myopia. *Exp.Eye Res.* 2006;82:185-200.

127. Mutti DO, Mitchell GL, Sinnott LT, et al. Corneal and crystalline lens dimensions before and after myopia onset. *Optom.Vis.Sci.* 2012;89:251-262.

128. Shao Z, Irving EL, Kisilak ML, Campbell MCW. Both changes in eye power and optical eye length contribute to emmetropization of refractive error in early, normal development of chick eyes. *IOVS* 2012;352:ARVO E-Abstract 3445.

129. Nickla DL, Wallman J. The multifunctional choroid. *Prog.Retin.Eye Res.* 2010;29:144-168.

130. Tepelus TC, Vazquez D, Seidemann A, Uttenweiler D, Schaeffel F. Effects of lenses with different power profiles on eye shape in chickens. *Vision Res.* 2012;54:12-19.

131. Schmid KL, Hills T, Abbott M, Humphries M, Pyne K, Wildsoet CF. Relationship between intraocular pressure and eye growth in chick. *Ophthalmic Physiol.Opt.* 2003;23:25-33.

132. Genest R, Chandrashekar N, Irving EL. Finite element model of the chick eye to study myopia. *J Med Biol Eng* 2012;33(2):215-220.

133. Genest R, Chandrashekar N, Irving E. The effect of intraocular pressure on chick eye geometry and its application to myopia. *Acta Bioeng.Biomech.* 2012;14:3-8.

134. Ritchey ER, Zelinka CP, Tang J, Liu J, Fischer AJ. The combination of IGF1 and FGF2 and the induction of excessive ocular growth and extreme myopia. *Exp.Eye Res.* 2012;99:1-16.

135. Wildsoet CF, Pettigrew JD. Kainic acid-induced eye enlargement in chickens: Differential effects on anterior and posterior segments. *Invest.Ophthalmol.Vis.Sci.* 1988;29:311-319.

136. Sivak JG, Barrie DL, Callender MG, Doughty MJ, Seltner RL, West JA. Optical causes of experimental myopia. *Ciba found.Symp.* 1990;155:160-72; discussion 172-7.

137. Shao Z, Bunghardt K, Kisilak ML, Campbell MCW. Eye dimensions during lens induced myopia (LIM) and recovery in the chick. *IOVS* 2014;374:ARVO E-Abstract 3606.

138. de la Cera EG. Optical quality and role of the ocular aberrations in animal models of myopia. *PhD Thesis, Instituto De Optica, Consejo Superior De Investigaciones Cientifica (CSIC), Spain* 2007.

139. Shao Z, Bunghardt K, Kisilak ML, Irving EL, Campbell MCW. Contributions of eye power and optical eye length to emmetropization during lens induced myopia and recovery in the chick eye. *IOVS* 2013;253:ARVO E-Abstract 1914.

140. Sharma R, Sharma A, Arora T, et al. Application of anterior segment optical coherence tomography in glaucoma. *Surv.Ophthalmol.* 2014;59:311-327.

141. Reddy AR, Pande MV, Finn P, El-Gogary H. Comparative estimation of anterior chamber depth by ultrasonography, orbscan II, and IOLMaster. *J.Cataract Refract.Surg.* 2004;30:1268-1271.

142. Schartau JM, Kroger RH, Sjogreen B. Dopamine induces optical changes in the cichlid fish lens. *PLoS One* 2010;5:e10402.

143. Fine I, Loewinger E, Weinreb A, Weinberger D. Optical properties of the sclera. *Phys.Med.Biol.* 1985;30:565-571.

# Copyrighted Materials

**Permission to use Human Eye Schematic (Figure 1-4).**

From: Zheng Shao z8shao@uwaterloo.ca
To Kisilak kisilak@gmail.com

Dear Miss Kisilak,

May I use the Human Eye Schematic you originally created, in my master thesis entitled *"Optical Changes during Normal Emmetropization, Lens-induced Myopia and its Recovery in the Young Chick Eye"*, but with further modification (as shown in the Figure 1-4 of my thesis; please see the attached Figure)? Thank you in advance!

Best regards,
Zheng Shao

From: Kisilak kisilak@gmail.com
To: Zheng Shao z8shao@uwaterloo.ca

Hello,

Yes, you have my permission to use the figure in your thesis.

Marsha Kisilak

**Permission to use figure by Irving and colleagues (1996); Figure 2-1 and Figure 3-1.**



**SPRINGER LICENSE**
**TERMS AND CONDITIONS**

Dec 23, 2014

This is a License Agreement between Zheng Shao ("You") and Springer ("Springer") provided by Copyright Clearance Center ("CCC"). The license consists of your order details, the terms and conditions provided by Springer, and the payment terms and conditions.

| | |
|---|---|
| License Number | 3534921198685 |
| License date | Dec 23, 2014 |
| Licensed content publisher | Springer |
| Licensed content publication | Journal of Comparative Physiology A: Neuroethology, Sensory, Neural, and Behavioral Physiology |
| Licensed content title | Chick eye optics: zero to fourteen days |
| Licensed content author | E. L. Irving |
| Licensed content date | Jan 1, 1996 |
| Volume number | 179 |
| Issue number | 2 |
| Type of Use | Book/Textbook |
| Requestor type | Publisher |
| Publisher | Open University |
| Portion | Figures |
| Format | Print + e-rights |
| Number of figures | 1 |
| Print run | 1 |
| Author of this Springer article | No |
| Order reference number | None |
| Original figure numbers | Figure 6 the first diagram |
| Title of new book | Optical Changes during Normal Emmetropization, Lens-induced Myopia and its Recovery in the Young Chick Eye |
| Author of new book | Zheng Shao |
| Expected publication date of new book | Jan 2015 |
| Estimated size of new book (pages) | 185 |
| Billing Type | Credit Card |
| Credit card info | Visa ending in 4600 |
| Credit card expiration | 05/2016 |
| Total | 20.04 CAD |

Terms and Conditions

Introduction
The publisher for this copyrighted material is Springer Science + Business Media. By clicking "accept" in connection with completing this licensing transaction, you agree that the following terms and conditions apply to this transaction (along with the Billing and Payment terms and conditions established by Copyright Clearance Center, Inc. ("CCC"), at the time that you opened your Rightslink account and that are available at any time at http://myaccount.copyright.com).

Limited License
Springer Science + Business Media hereby grants to you a non-exclusive license to use this material, for the use as indicated in your inquiry. Licenses are for one-time use only with a maximum distribution equal to the number that you identified in the licensing process.

This License includes use in an electronic form, provided it's password protected, on intranet, or CD-Rom/DVD or E-book/E-Journal. For any other electronic use, please contact Springer at (permissions.dordrecht@springer.com or permissions.heidelberg@springer.com)

Although Springer holds copyright to the material and is entitled to negotiate on rights, this license is only valid, subject to a courtesy information to the author (address is given with the article/chapter) and provided it concerns original material which does not carry references to other sources (if material in question appears with credit to another source, authorization from that source is required as well).

Permission is valid upon payment of the fee as indicated in the licensing process.

Geographic Rights: Scope
Licenses may be exercised anywhere in the world.

Altering/Modifying Material: Not Permitted
Figures and illustrations may be altered minimally to serve your work. Any other abbreviations, additions, deletions and/or any other alterations shall be made only with prior written authorization of the author(s) and/or Springer Science + Business Media. (Please contact Springer at (permissions.dordrecht@springer.com or permissions.heidelberg@springer.com)

Reservation of Rights
Springer Science + Business Media reserves all rights not specifically granted in the combination of (i) the license details provided by you and accepted in the course of this licensing transaction, (ii) these terms and conditions and (iii) CCC's Billing and Payment terms and conditions.

License Contingent on Payment
While you may exercise the rights licensed immediately upon issuance of the license at the end of the licensing process for the transaction, provided that you have disclosed complete and accurate details of your proposed use, no license is finally effective unless and until full payment is received from you (either by Springer Science + Business Media or by CCC) as provided in CCC's Billing and Payment terms and conditions. If full payment is not received by Due Date, then any license preliminarily granted shall be deemed automatically revoked and shall be void as if never granted. Further, in the event that you breach any of these terms and conditions or any of CCC's Billing and Payment terms and conditions, the license is

automatically revoked and shall be void as if never granted. Use of materials as described in a revoked license, as well as any use of the materials beyond the scope of an unrevoked license, may constitute copyright infringement and Springer Science + Business Media reserves the right to take any and all action to protect its copyright in the materials.

Copyright Notice: Disclaimer
You must include the following copyright and permission notice in connection with any reproduction of the licensed material:

*"Springer and the original publisher /journal title, volume, year of publication, page, chapter/article title, name(s) of author(s), figure number(s), original copyright notice) is given to the publication in which the material was originally published, by adding:" With kind permission from Springer Science and Business Media"*

In case of use of a graph or illustration, the caption of the graph or illustration must be included, as it is indicated in the original publication.

Warranties: None

Example 1: Springer Science + Business Media makes no representations or warranties with respect to the licensed material.

Example 2: Springer Science + Business Media makes no representations or warranties with respect to the licensed material and adopts on its own behalf the limitations and disclaimers established by CCC on its behalf in its Billing and Payment terms and conditions for this licensing transaction.

Indemnity
You hereby indemnify and agree to hold harmless Springer Science + Business Media and CCC, and their respective officers, directors, employees and agents, from and against any and all claims arising out of your use of the licensed material other than as specifically authorized pursuant to this license.

No Transfer of License
This license is personal to you and may not be sublicensed, assigned, or transferred by you to any other person without Springer Science + Business Media's written permission.

No Amendment Except in Writing
This license may not be amended except in a writing signed by both parties (or, in the case of Springer Science + Business Media, by CCC on Springer Science + Business Media's behalf).

Objection to Contrary Terms
Springer Science + Business Media hereby objects to any terms contained in any purchase order, acknowledgment, check endorsement or other writing prepared by you, which terms are inconsistent with these terms and conditions or CCC's Billing and Payment terms and conditions. These terms and conditions, together with CCC's Billing and Payment terms and conditions (which are incorporated herein), comprise the entire agreement between you and Springer Science + Business Media (and CCC) concerning this licensing transaction. In the event of any conflict between your obligations established by these terms and conditions and those established by CCC's Billing and Payment terms and conditions, these terms and

conditions shall control.

Jurisdiction
All disputes that may arise in connection with this present License, or the breach thereof, shall be settled exclusively by arbitration, to be held in The Netherlands, in accordance with Dutch law, and to be conducted under the Rules of the 'Netherlands Arbitrage Instituut' (Netherlands Institute of Arbitration).***OR:***

All disputes that may arise in connection with this present License, or the breach thereof, shall be settled exclusively by arbitration, to be held in the Federal Republic of Germany, in accordance with German law.

**Other conditions:**

v1.0

**Questions? customercare@copyright.com or +1-855-239-3415 (toll free in the US) or +1-978-646-2777.**

**Gratis licenses (referencing $0 in the Total field) are free. Please retain this printable license for your reference. No payment is required.**

**Permission to use figure by Kisilak et al. (2006); Figure 2-2.**



**SPRINGER LICENSE**
**TERMS AND CONDITIONS**

Dec 23, 2014

This is a License Agreement between Zheng Shao ("You") and Springer ("Springer") provided by Copyright Clearance Center ("CCC"). The license consists of your order details, the terms and conditions provided by Springer, and the payment terms and conditions.

| | |
|---|---|
| License Number | 3534921082845 |
| License date | Dec 23, 2014 |
| Licensed content publisher | Springer |
| Licensed content publication | Journal of Comparative Physiology A: Neuroethology, Sensory, Neural, and Behavioral Physiology |
| Licensed content title | Aberrations of chick eyes during normal growth and lens induction of myopia |
| Licensed content author | Marsha L. Kisilak |
| Licensed content date | Jan 1, 2006 |
| Volume number | 192 |
| Issue number | 8 |
| Type of Use | Book/Textbook |
| Requestor type | Publisher |
| Publisher | Open University |
| Portion | Figures |
| Format | Print + e-rights |
| Number of figures | 1 |
| Print run | 1 |
| Author of this Springer article | No |
| Order reference number | None |
| Original figure numbers | Figure 1 |
| Title of new book | Optical Changes during Normal Emmetropization, Lens-induced Myopia and its Recovery in the Young Chick Eye |
| Author of new book | Zheng Shao |
| Expected publication date of new book | Jan 2015 |
| Estimated size of new book (pages) | 185 |
| Billing Type | Credit Card |
| Credit card info | Visa ending in 4600 |
| Credit card expiration | 05/2016 |
| Total | 20.04 CAD |

Terms and Conditions

Introduction
The publisher for this copyrighted material is Springer Science + Business Media. By clicking "accept" in connection with completing this licensing transaction, you agree that the following terms and conditions apply to this transaction (along with the Billing and Payment terms and conditions established by Copyright Clearance Center, Inc. ("CCC"), at the time that you opened your Rightslink account and that are available at any time at http://myaccount.copyright.com).

Limited License
Springer Science + Business Media hereby grants to you a non-exclusive license to use this material, for the use as indicated in your inquiry. Licenses are for one-time use only with a maximum distribution equal to the number that you identified in the licensing process.

This License includes use in an electronic form, provided it's password protected, on intranet, or CD-Rom/DVD or E-book/E-Journal. For any other electronic use, please contact Springer at (permissions.dordrecht@springer.com or permissions.heidelberg@springer.com)

Although Springer holds copyright to the material and is entitled to negotiate on rights, this license is only valid, subject to a courtesy information to the author (address is given with the article/chapter) and provided it concerns original material which does not carry references to other sources (if material in question appears with credit to another source, authorization from that source is required as well).

Permission is valid upon payment of the fee as indicated in the licensing process.

Geographic Rights: Scope
Licenses may be exercised anywhere in the world.

Altering/Modifying Material: Not Permitted
Figures and illustrations may be altered minimally to serve your work. Any other abbreviations, additions, deletions and/or any other alterations shall be made only with prior written authorization of the author(s) and/or Springer Science + Business Media. (Please contact Springer at (permissions.dordrecht@springer.com or permissions.heidelberg@springer.com)

Reservation of Rights
Springer Science + Business Media reserves all rights not specifically granted in the combination of (i) the license details provided by you and accepted in the course of this licensing transaction, (ii) these terms and conditions and (iii) CCC's Billing and Payment terms and conditions.

License Contingent on Payment
While you may exercise the rights licensed immediately upon issuance of the license at the end of the licensing process for the transaction, provided that you have disclosed complete and accurate details of your proposed use, no license is finally effective unless and until full payment is received from you (either by Springer Science + Business Media or by CCC) as provided in CCC's Billing and Payment terms and conditions. If full payment is not received by Due Date, then any license preliminarily granted shall be deemed automatically revoked and shall be void as if never granted. Further, in the event that you breach any of these terms and conditions or any of CCC's Billing and Payment terms and conditions, the license is

automatically revoked and shall be void as if never granted. Use of materials as described in a revoked license, as well as any use of the materials beyond the scope of an unrevoked license, may constitute copyright infringement and Springer Science + Business Media reserves the right to take any and all action to protect its copyright in the materials.

Copyright Notice: Disclaimer
You must include the following copyright and permission notice in connection with any reproduction of the licensed material:

*"Springer and the original publisher /journal title, volume, year of publication, page, chapter/article title, name(s) of author(s), figure number(s), original copyright notice) is given to the publication in which the material was originally published, by adding:" With kind permission from Springer Science and Business Media"*

In case of use of a graph or illustration, the caption of the graph or illustration must be included, as it is indicated in the original publication.

Warranties: None

Example 1: Springer Science + Business Media makes no representations or warranties with respect to the licensed material.

Example 2: Springer Science + Business Media makes no representations or warranties with respect to the licensed material and adopts on its own behalf the limitations and disclaimers established by CCC on its behalf in its Billing and Payment terms and conditions for this licensing transaction.

Indemnity
You hereby indemnify and agree to hold harmless Springer Science + Business Media and CCC, and their respective officers, directors, employees and agents, from and against any and all claims arising out of your use of the licensed material other than as specifically authorized pursuant to this license.

No Transfer of License
This license is personal to you and may not be sublicensed, assigned, or transferred by you to any other person without Springer Science + Business Media's written permission.

No Amendment Except in Writing
This license may not be amended except in a writing signed by both parties (or, in the case of Springer Science + Business Media, by CCC on Springer Science + Business Media's behalf).

Objection to Contrary Terms
Springer Science + Business Media hereby objects to any terms contained in any purchase order, acknowledgment, check endorsement or other writing prepared by you, which terms are inconsistent with these terms and conditions or CCC's Billing and Payment terms and conditions. These terms and conditions, together with CCC's Billing and Payment terms and conditions (which are incorporated herein), comprise the entire agreement between you and Springer Science + Business Media (and CCC) concerning this licensing transaction. In the event of any conflict between your obligations established by these terms and conditions and those established by CCC's Billing and Payment terms and conditions, these terms and

conditions shall control.

Jurisdiction
All disputes that may arise in connection with this present License, or the breach thereof, shall be settled exclusively by arbitration, to be held in The Netherlands, in accordance with Dutch law, and to be conducted under the Rules of the 'Netherlands Arbitrage Instituut' (Netherlands Institute of Arbitration).***OR:***

All disputes that may arise in connection with this present License, or the breach thereof, shall be settled exclusively by arbitration, to be held in the Federal Republic of Germany, in accordance with German law.

**Other conditions:**

v1.0

**Questions? customercare@copyright.com or +1-855-239-3415 (toll free in the US) or +1-978-646-2777.**

**Gratis licenses (referencing $0 in the Total field) are free. Please retain this printable license for your reference. No payment is required.**